④

RADC-TR-89-270
Final Technical Report
December 1989

AD-A218 547

MEASUREMENT OF LOCALIZED DEEP LEVELS AND WAFER NON-UNIFORMITIES AT III-V SEMICONDUCTOR HETEROJUNCTIONS

University of Southern California

Stephen R. Forrest

DTIC
S ELECTE
MAR 0 1 1990
B D

Rome Air Development Center
Air Force Systems Command
Griffiss Air Force Base, NY 13441-5700

90 02 27 010

This report has been reviewed by the RADC Public Affairs Division (PA) and is releasable to the National Technical Information Service (NTIS). At NTIS it will be releasable to the general public, including foreign nations.

RADC-TR-89-270 has been reviewed and is approved for public release.
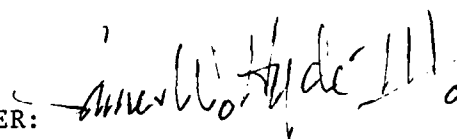
APPROVED:

J. P. LORENZO
Project Engineer

APPROVED:

HAROLD ROTH
Director of Solid State Sciences

FOR THE COMMANDER:

JAMES W. HYDE III
Directorate of Plans & Programs

REPORT DOCUMENTATION PAGE

Form Approved
OMB No. 0704-0188

1a. REPORT SECURITY CLASSIFICATION UNCLASSIFIED	1b. RESTRICTIVE MARKINGS N/A

2a. SECURITY CLASSIFICATION AUTHORITY N/A	3. DISTRIBUTION/AVAILABILITY OF REPORT Approved for public release;
2b. DECLASSIFICATION/DOWNGRADING SCHEDULE N/A	distribution unlimited.

4. PERFORMING ORGANIZATION REPORT NUMBER(S) N/A	5. MONITORING ORGANIZATION REPORT NUMBER(S) RADC-TR-89-270

6a. NAME OF PERFORMING ORGANIZATION University of Southern California	6b. OFFICE SYMBOL (If applicable)	7a. NAME OF MONITORING ORGANIZATION Rome Air Development Center (ESOC)

6c. ADDRESS (City, State, and ZIP Code) Departments of Electrical Engineering/ Electrophysics and Materials Science Los Angeles CA 90089-0241	7b. ADDRESS (City, State, and ZIP Code) Hanscom AFB MA 01731-5000

8a. NAME OF FUNDING/SPONSORING ORGANIZATION Rome Air Development Center	8b. OFFICE SYMBOL (If applicable) ESOC	9. PROCUREMENT INSTRUMENT IDENTIFICATION NUMBER F19628-86-K-0002

8c. ADDRESS (City, State, and ZIP Code)	10. SOURCE OF FUNDING NUMBERS			
	PROGRAM ELEMENT NO.	PROJECT NO.	TASK NO.	WORK UNIT ACCESSION NO.
Hanscom AFB MA 01731-5000	61101F	LDFP	09	C7

11. TITLE (Include Security Classification)
MEASUREMENT OF LOCALIZED DEEP LEVELS AND WAFER
NON-UNIFORMITIES AT III-V SEMICONDUCTOR HETEROJUNCTIONS

12. PERSONAL AUTHOR(S)
Stephen R. Forrest

13a. TYPE OF REPORT Final	13b. TIME COVERED FROM Dec 86 TO Sep 88	14. DATE OF REPORT (Year, Month, Day) December 1989	15. PAGE COUNT 102

16. SUPPLEMENTARY NOTATION

This effort was funded totally by the Laboratory Director's fund.

17.	COSATI CODES		18. SUBJECT TERMS (Continue on reverse if necessary and identify by block number)
FIELD	GROUP	SUB-GROUP	
20	12		III-V Heterojunctions Organic interfaces
17	05		Indium phosphide Charge transport

19. ABSTRACT (Continue on reverse if necessary and identify by block number)

Reported are the results of a two year program in which organic thin films were used to non-destructively study the properties of inorganic semiconductor epitaxial materials. The organic films can be applied to the substrate in vacuum in a non-destructive manner such that many bulk and surface properties of the semiconductor under study can be easily obtained. Once the characterization process is complete, the thin films can be removed without damage to the semiconductor substrate. This allows for the correlation of the fundamental materials properties of the semiconductor to the performance of devices fabricated on the same wafer.

20. DISTRIBUTION/AVAILABILITY OF ABSTRACT ☒ UNCLASSIFIED/UNLIMITED ☐ SAME AS RPT. ☐ DTIC USERS	21. ABSTRACT SECURITY CLASSIFICATION UNCLASSIFIED	
22a. NAME OF RESPONSIBLE INDIVIDUAL Joseph P. Lorenzo	22b. TELEPHONE (Include Area Code) (617) 377-3598	22c. OFFICE SYMBOL RADC (ESOC)

DD Form 1473, JUN 86   Previous editions are obsolete.

MEASUREMENT OF LOCALLIZED DEEP LEVELS AND WAFER NON-UNIFORMITIES AT III-V SEMICONDUCTOR HETEROJUNCTIONS

Stephen R. Forrest
Departments of Electrical Engineering/Electrophysics
and Materials Science
University of Southern California
Los Angeles, CA   90089-0241

Abstract

We report the results of a two year program in which organic thin films were used to non-destructively study the properties of inorganic semiconductor epitaxial materials. The organic films can be applied to the substrate in vacuum in a non-destructive manner such that many bulk and surface properties of the semiconductor under study can be easily obtained. Once the characterization process is complete, the thin films can be removed without damage to the semiconductor substrate. This allows for the correlation of the fundamental materials properties of the semiconductor to the performance of devices fabricated on the same wafer.

Among the most important results of this work are the following: (i) A complete model of charge transport across the organic-on-inorganic semiconductor heterojuntion (OI HJ) was developed. This lead directly to the measurement, for the first time, of energy band offsets between a crystalline molecular organic semiconductor and an inorganic semiconductor. Furthermore, this theory allowed for the clear interpretation of admittance data used in analyzing the surface state spectra of semiconductor wafers. (ii) A very accurate means for the determination of inorganic semiconductor heterojunction offsets by capacitance-voltage techniques was developed. This extension of earlier developed methods makes C-V measurements the

most reliable manner of offset measurement since it can separately determine the contributions of surface states and the HJ dipole. This technique was applied to the study of $In_{0.53}Ga_{0.47}As/InP$ which was expedited by the use of organic thin film contacts. (iii) The organic technique was employed to study $Hg_{0.7}Cd_{0.3}Te/CdTe$ HJ's via our accurate C-V method. Results surprisingly indicate that these materials form a Type II heterojunction with a valence band offset energy of 110 ± 20 meV.

TABLE OF CONTENTS

I.   Introduction

The purpose of this two year investigation has been to expand the use of organic thin films as a diagnostic tool for the study of InGaAs/InP and related heterojunctions (HJs). This work builds on past experience in using such organic materials for the investigation of several III-V and Group IV semiconductors. However, in this program, considerable attention was used in understanding the fundamental nature of the organic-inorganic (OI) semiconductor contact to allow for more confident interpretation of data used to determine the surface properties of the underlying semiconductors. In general, most of the major tasks set forward in the proposed program were accomplished, and in addition, several interesting new areas of study were pursued which yielded unexpected results.

In particular, the following goals were accomplished during the course of this program:

1) A detailed theoretical understanding of the transport properties of charge across the OI HJ was developed. To this end, a general theory concerning the bias dependence of the quasi-Fermi levels and carrier velocities across the OI HJ was derived, and was found to provide a simple, clear explanation of the admittance spectra for OI diodes used in determining the defect state density spectrum at the semiconductor surface. Thus, the OI technique was further developed in its ability to act as an in-process monitor of the effects that exposure of the semiconductor surface to various chemical agents or process conditions have on the ultimate state of that surface. A second result of this analysis was the finding that the carrier

4

velocities across the organic thin film are unexpectedly high. In related research, direct measurements of these theoretical findings were verified, and indicated that the OI HJ has considerable promise for high frequency optoelectronic device applications, as well as being a structure useful for high frequency analysis of semiconductor properties.

Furthermore, this study has led directly to the measurement of the valence-band offset energy between the organic, 3,4,9,10 perylenetetracarboxylic dianhydride (PTCDA), and p-Si. To our knowledge, this is the first time that the band discontinuity energy between a crystalline molecular organic semiconductor and an inorganic semiconductor has been accomplished. We find that this interface is nearly ideal with a negligible contribution of defect states to the overall offset potential. This finding is most significant in that it appears to open the way to the realization of a very broad range of OI HJ devices which might find general optoelectronic applications.

2) Following on these theoretical results, we investigated the non-destructive nature of several organic compounds when deposited onto Si surfaces. Here, we found that some perylene and naphthaline-based compounds can indeed be used to obtain the as-prepared surface state density at the semiconductor surface. However, other compounds such as the metal-phthalocyanines (metal-Pc's) actively undergo surface reactions with the semiconductor surface. While this effect makes these latter compounds ineffective for the study of intrinsic surface defects, we conclude that the metal-Pc's provide a unique tool for

5

studying metal/semiconductor surface reactions, since the Pc's can be used to introduce trace concentrations of metal atoms to the semiconductor surfaces. Thus, the metal-Pc's, used in combination with other analytical techniques including the OI-HJ surface study technique, may prove to be an important means for understanding the mechanisms surrounding Schottky barrier formation on III-V compound semiconductor surfaces.

3) Full software tools for studying the distribution of various wafer parameters (such as epitaxial layer thickness, doping density, defect charge at surfaces and at heterojunctions, etc.) have been developed. Several InGaAs/InP heterojunction wafers grown in our liquid phase epitaxial growth system were mapped using this software, and this process was useful in gaining an understanding of the dynamics of growth. Some of this software has been transferred for use at RADC as part of our collaborative effort.

4) A method for the very accurate determination of band discontinuity energies was developed and applied, along with the OI technique, to the measurement of the band offset energies of InGaAs/InP heterojunctions. This work has resulted in what we believe to be the most accurate method for determining HJ band offset energies. Its major strength lies in the fact that it is the only method which measures the band offset energies while removing the effects of interface state charge from this measurement.

5) To obtain carrier concentration profiles very deeply into the bulk of samples with thick epitaxial layers, we have combined the OI diagnostic technique with the taper-etching of samples. For the

6

particular samples studied using tapered surfaces, we used a n-$Hg_{0.7}Cd_{0.3}Te$/p-$Hg_{0.7}Cd_{0.3}Te$/P-CdTe wafer where the total epitaxial layer thickness was nearly 10 μm. The entire composite profile was made through both n and p-type material. We were able to successfully profile all layers and we obtained, for the first time by capacitance-voltage methods, a measurement of the band offset energy at the HgCdTe/CdTe HJ interface. Here, our methods for very accurate determination of offset energies was applied to this materials system.

Several manuscripts have been published or have been submitted for publication as a result of this two-year program. Reprints of those papers which have been published are included in Appendix A. The substance of papers which have been accepted, or are awaiting a publication decision, are included in the body of this report. The titles and authors of all publications are listed below:

1) F. F. So and S. R. Forrest, "Dependence of the electrical characteristics of organic-on-inorganic semiconductor contact barrier diodes on organic thin-film composition", J. Appl. Phys., 63, 442 (1988).

2) S. R. Forrest and F. F. So, "Organic-on-Inorganic semiconductor heterojunctions: Energy-band discontinuities, quasi-Fermi levels, and carrier velocities", J. Appl. Phys., 64, 399 (1988).

3) F. F. So and S. R. Forrest, "Measurement of the valence-band discontinuities for molecular organic semiconductor/inorganic semiconductor heterojunctions", Appl. Phys. Lett., 52, 1341 (1988).

4) F. F. So and S. R. Forrest, "Growth characteristics of organic-on-inorganic semiconductor heterostructures", Proc. SPIE, 944, 117 (1988).

5) S. J. Chang, L. Y. Leu, and S. R. Forrest and C. E. Jones, "Determination of the free carrier concentration profiles and valence band discontinuity energy of $Hg_{0.7}Cd_{0.3}Te$/CdTe heterojunctions using organic thin films", Appl. Phys. Lett. (March, 1989).

6) L. Y. Leu and S. R. Forrest, "Accurate determination of heterojunction band discontinuity energies in the presence of interface traps using capacitance-voltage techniques", submitted to Appl. Phys. Lett. (1988).

This report is organized as follows: in Sec. II we discuss the theory and applications of the OI technique, and give details of sample preparation and organic material purification methods. In Sec. III we highlight the most important aspects of the theory regarding charge transport across OI barriers, and its application to the study of semiconductor surfaces. In Sec. IV, the method for highly accurate measurement of inorganic HJ offset energies in the presence of interface charge is detailed, and is applied to the study of InGaAs/InP heterojunctions. Sec V is concerned with obtaining very deep profiles through both p and n-type layers. Here, the study of an HgCdTe/CdTe multilayer sample is discussed, as well as our results on the measurement of HgCdTe/CdTe valence band offset energies by the techniques described in Sec. IV. In Sec. V we present conclusions and directions for future research.

II. OI device fabrication and theory

a. Sample preparation

To obtain high-quality, stable, reproducible diodes it is imperative to purify organic materials prior to their use in devices. The compounds with which we are most often concerned[1] are PTCDA, *N,N'*-dimethyl-3,4,9,10-perylenetetracarboxylic diimide (DIME-PTCDI), 3,4,7,8-naphtahlenetetracarboxylic dianhydride (NTCDA) and the phthalocyanines (Pc's) including CuPc and metal free Pc (or H_2Pc).

The methods available for purification are limited due to the relative insolubility of these organic semiconductors. For obtaining high purity, therefore, gradient vacuum sublimation appears to give the best quality product. To purify PTCDA, a few grams of commercially available powder are placed at the sealed end of a Pyrex tube. Quartz wool is then packed down on top of the PTCDA to keep it from spreading uncontrollably throughout the tube as vacuum is applied. The tube is evacuated to less than 10^{-4} torr, and with the pump on, it is inserted into the open end of a standard diffusion furnace. The sample is brought to 425-450°C (for PTCDA) and remains at that temperature for the duration of the purification process. This temperature is adjusted for other materials to be somewhat less than their specific vacuum sublimation temperatures. After the sublimation proceeds for about 16 hr., the tube is cooled while the vacuum pump remains on. The walls of tube show bands of material of different colors. Only the region nearest the hot end is of interest. In the case of PTCDA, the band nearest the hot end consists of a dark, reddish crystalline substance that exhibits

9

elemental analysis and spectroscopic properties expected for PTCDA. Recovered product is about 10-20% by weight of the starting material.

We found that gradient sublimation is a method that requires a great deal of time and yields a small amount of pure material. A more convenient and efficient means of producing usable PTCDA may sometimes be necessary. One such method is continuous extraction using a Soxhlet apparatus with hot 2-methoxyethylether (diglyme) under a dr, N_2 atmosphere. The impurities are removed in the extraction process, leaving PTCDA that after drying in vacuo gives high-quality organic contacts usable in wafer-diagnostic applications.

Once the organic material is purified the first step in the fabrication of OI diodes (Fig. 1) is to clean the semiconductor substrate. For most semiconductor materials, a thorough solvent cleaning is employed, followed by an oxide-removing etch, such as exposure of the sample to an HF solution. However, in some materials, particularly InP and related compounds, it has been found that the contact barrier can be significantly enhanced by exposure of the surface to an oxidant such as HNO_3 or H_2O_2 following the solvent surface-cleaning procedure. A summary of surface preparation conditions used for several semiconductor materials is given in Table 1.

Immediately following surface cleaning, the sample is inserted into a standard vacuum apparatus, and brought to a pressure lower than 10^{-5} torr. A full-surface ohmic contact is then deposited onto the bottom substrate surface. Next, 1000-2000 A of the organic
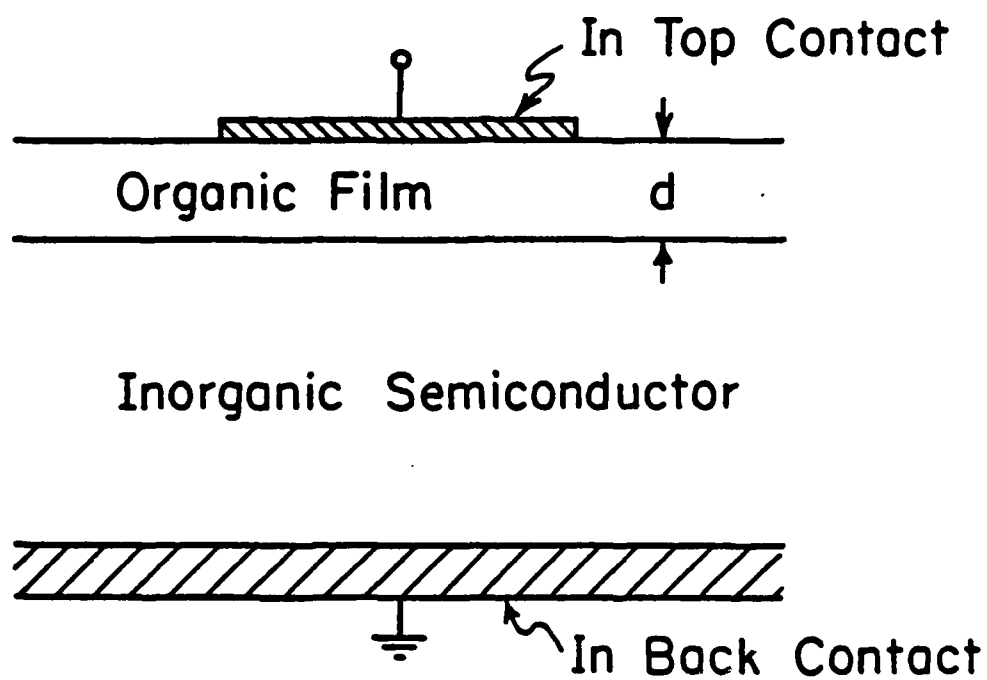
In Top Contact

Organic Film   d

Inorganic Semiconductor

In Back Contact

Fig. 1

Table I

Surface-cleaning sequence for selected semiconductors[a]

Semiconductor[c]	1:4 HF:H$_2$O (30 s)	HNO$_3$(conc.) (10 s)	30%H$_2$O$_2$ (30s)
Si	X		
GaAs	X		X
InP	X	X	
In$_{0.53}$Ga$_{0.47}$As	X		X[b]

[a]Surface treatments all follow a thorough detergent and solvent cleaning. All acid exposure steps were followed by a 5 min rinse in deionized water. Samples were inserted in a vacuum system for organic film deposition immediately following the last water rinse and blow dry.

[b]Exposure to 30% H$_2$O$_2$ for 2 min for this sample.

[c]CuInSe$_2$ and CdTe undergo solvent clean only.

material is deposited onto the precleaned top wafer surface at vacuum levels similar to those employed for deposition of the metallic contact. Deposition sources consisting of two chambers separated by baffles, such as those employed for silicon oxide deposition are convenient for use in the sublimation of crystalline organic materials. The thickness of the organic film is monitored during deposition, with a standard oscillating crystal monitor, on the basis that the density of PTCDA is 1.7 g/cm^3. Details of the deposition and synthesis of other organic compounds used in these studies are reported in the literature[2-4]; hence we concern ourselves here only with the details of formation of the archetype PTCDA-based diodes. After the organic film has been deposited, an ohmic top metal contact pad 3000-4000 A thick is deposited onto the thin film surface through a shadow mask. Ohmic contact metals made to the various organic compounds used in this study are listed in Table II.

Electrical measurements are made by contacting the diodes using a standard wafer probe station; soft Au wire probes are used to avoid damage to the devices. Alternatively, eutectic thermal compression bonds have been made to In contact dots on chips premounted on TO-18 headers. This latter arrangement is particularly useful when the samples are subjected to variable temperature measurements during which the mechanical contact used in the probe station may be unreliable. After the measurements are complete, the organic film and top ohmic contacts can be removed by immersion in a dilute aqueous base solution (e.g. $KOH:H_2O$ or positive photoresist developer) followed by a thorough rinse in deionized water.

Table II

Ohmic Contact Metallization for Various
Organic Materials

Organic Material	Ohmic Contact
PTCDA	In, Ti, ITO
NTCDA	In
CuPc	Au
H_2Pc	In

b. Theory of the OI heterojunction diode

In order to understand the electrical properties of the OI heterojunction, it is necessary to study the crystal structure of these organic materials. For example, PTCDA is a monoclinic crystal that forms infinite stacks of planar, uniformly spaced molecules in which the atoms of one molecule are located directly above adjacent molecules[5], as shown in Fig. 2. The most important aspect of the crystal structure of PTCDA is its extremely small interplanar spacing of 3.21 A, which is even smaller than that of graphite (3.37 A). Thus, the π-orbitals overlap to the extent that carriers moving along the stacking axis are highly delocalized. However, no such orbital overlap occurs in the stacking plane thus inhibiting transport in this direction. This gives rise to a significant anisotropy of electrical conductivity when measured with respect to the crystalline axes. Typical anisotropies range from 10-1000.

Anistropy can also be caused by the presence of grain boundaries in the organic films. The deposited organic films are polycrystalline, with a grain size on the order of several thousand angstroms[5]. Carriers moving in the vertical direction are not likely to cross the grain boundaries if the organic film is thin enough (<2000 A). On the other hand carriers moving along any in-plane direction will be trapped at the grain boundaries and therefore the mobility is drastically reduced, resulting in additional anisotropy in conductivity. To gain an appreciation of the mechanisms active in OI diode current transport, we examine the band diagram of the organic-inorganic heterointerface shown in Fig. 3. This diagram has
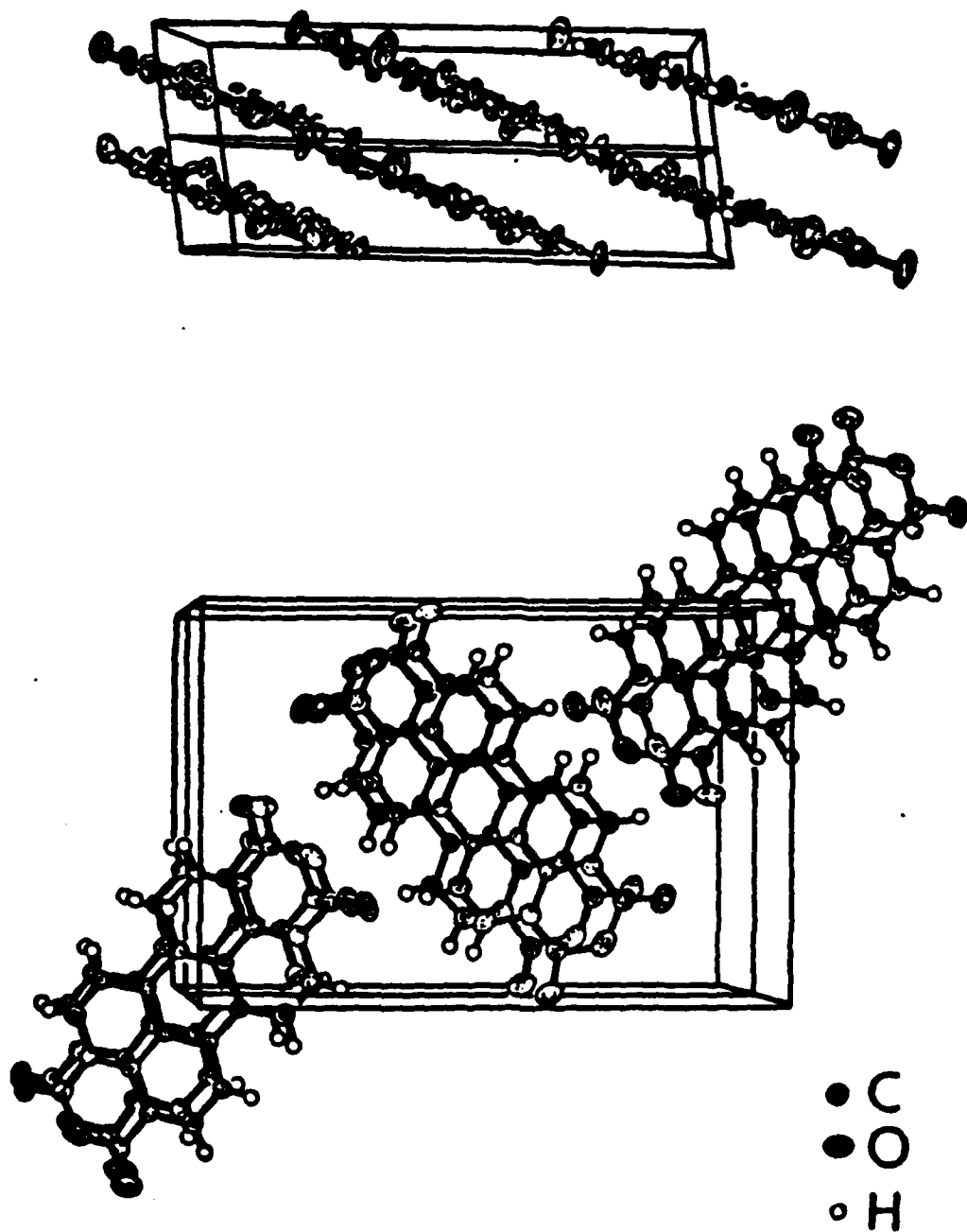
3, 4, 9, 10 Perylenetetracarboxylic Dianhydride
(PTCDA) (Unit Cell)

- Crystalline Aromatic Dianhydride
- Stable
- Deposited in vacuum

Fig. 2

16

been constructed by inference from several properties of the organic material as well as from analysis of OI diode performance characteristics. In this diagram, we show the contact between PTCDA and an n-type semiconductor with band gap energy E_g. The PTCDA "band gap" of 2.2 eV extends from the top of the highest occupied molecular orbital (HOMO) to the lowest unoccupied molecular orbital (LUMO). This material differs markedly from a conventional, inorganic semiconductor such as Si in that the total bandwidth (from the bottom of the HOMO to the top of the LUMO) is only 0.9 eV larger than the band gap, as inferred from spectroscopic data (see inset, Fig. 3). Additional tightly bound bands exist at higher energies beyond the top of the LUMO band, and there can be futher energy gaps interfacial layer of thickness δ_{ss} and densities of the defect states D_{ss} and D_{so}.

The predominant mechanism for carrier transport across this heterojunction-like interface is thermionic emission. In this case, the current density is given by[2,6]:

$$J_T = J_0[\exp(\beta V_D) - 1], \tag{1}$$

where J_T is the total current density; J_0 is the saturation current density; $\beta = q/kT$ (q is the electronic charge, k is Boltzmann's constant, and T is the absolute temperature); and V_D is the voltage dropped across the inorganic semiconductor substrate. The saturation current (See Sec. III) is $J_0 \propto \exp(-\beta\phi_B)$, where ϕ_B is the energy barrier between the organic and inorganic materials, and is a result of their different bulk electrostatic potentials. In effect, this barrier height is similar to the conduction band discontinuity energy
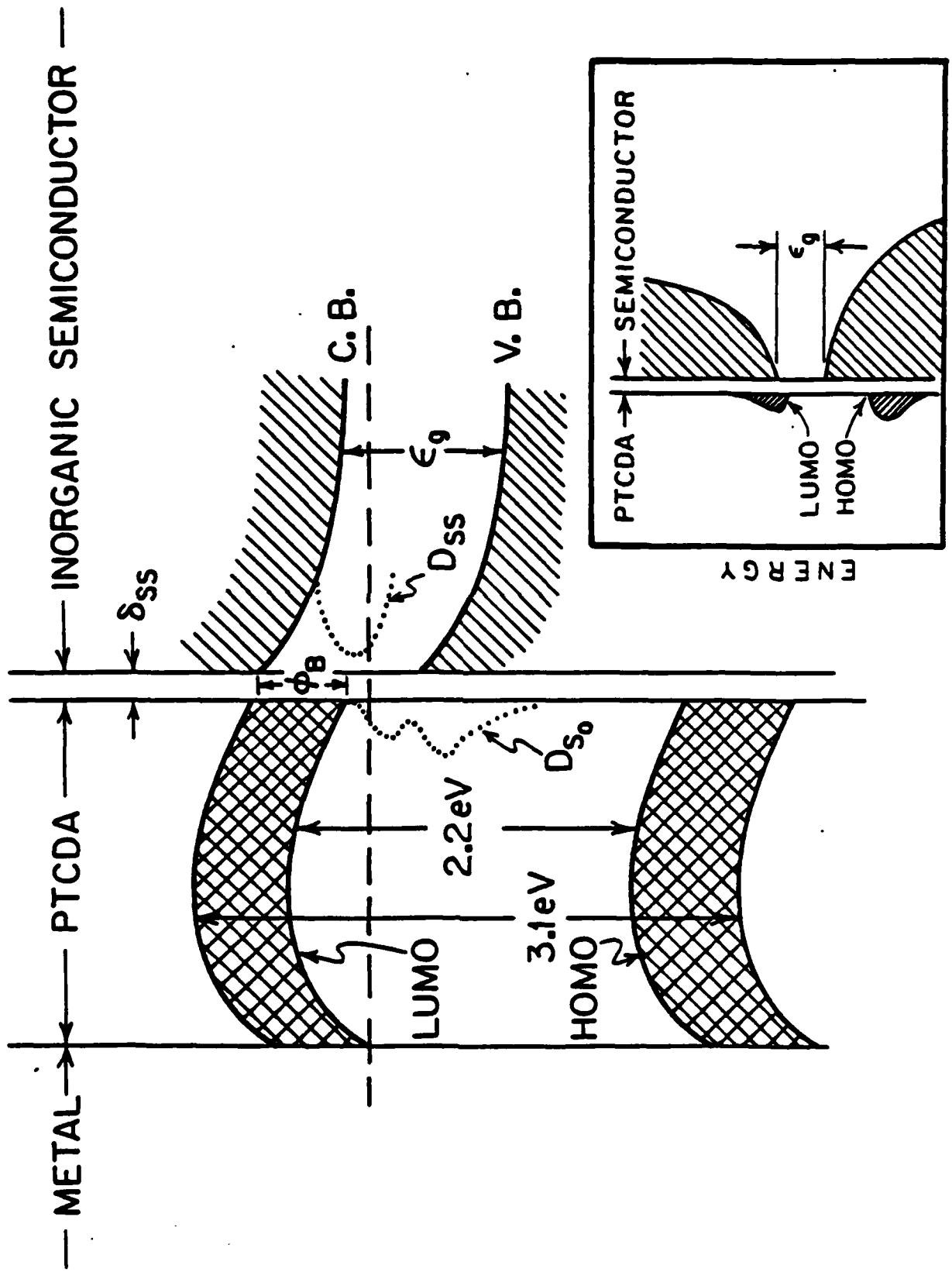
17

Fig. 3

18

at an inorganic/semiconductor heterojunction. The constant of proportionality in this expression for the saturation current is determined by the density of states in the inorganic layer[6]. Note that the saturation current is strongly reduced as the barrier energy is increased. It is the large values of ϕ_B and small value of J_0 that account for the low reverse-biased leakage currents commonly observed in OI devices.

From Eq. (1), and from the theory discussed more fully in the next section, it is apparent that a measurement of the saturation current as a function of temperature will give its activation energy. In this work, we directly measured the heterojunction offsets between PTCDA and p-Si. A plot[7] of $\log(J_s)$ as a function of $1/T$ is shown in Fig. 4. A schematic cross-sectional drawing of an organic-on-inorganic semiconductor heterojunction device is shown in the inset. A least square fit to the data, as indicated by the straight line, gives ϕ_{Bp} = 0.56 ± 0.02 eV. The valence band discontinuity energy, ΔE_v, for this isotype heterojunction is obtained from

$$\Delta E_v = \phi_{Bp} + \delta_s - \delta_0 \qquad (2)$$

where δ_s and δ_0 are the differences between the Fermi-level and the valence band maximum in the inorganic and organic bulk semiconductors. Taking the p-Si hole concentration of 5×10^{14} cm^{-3}, a hole concentration[2] of 5×10^{14} cm^{-3} for PTCDA, and assuming the effective hole mass (m^*) in PTCDA is equal to the free electron mass, we obtain ΔE_v = (0.48 ± 0.2)eV for a PTCDA/p-Si heterojunction. Also, $\Delta E_c = \Delta E_g - \Delta E_v$ = 0.6 eV where ΔE_g is the difference in band gap energies between PTCDA and Si.

In/PTCDA/p−Si

(b)

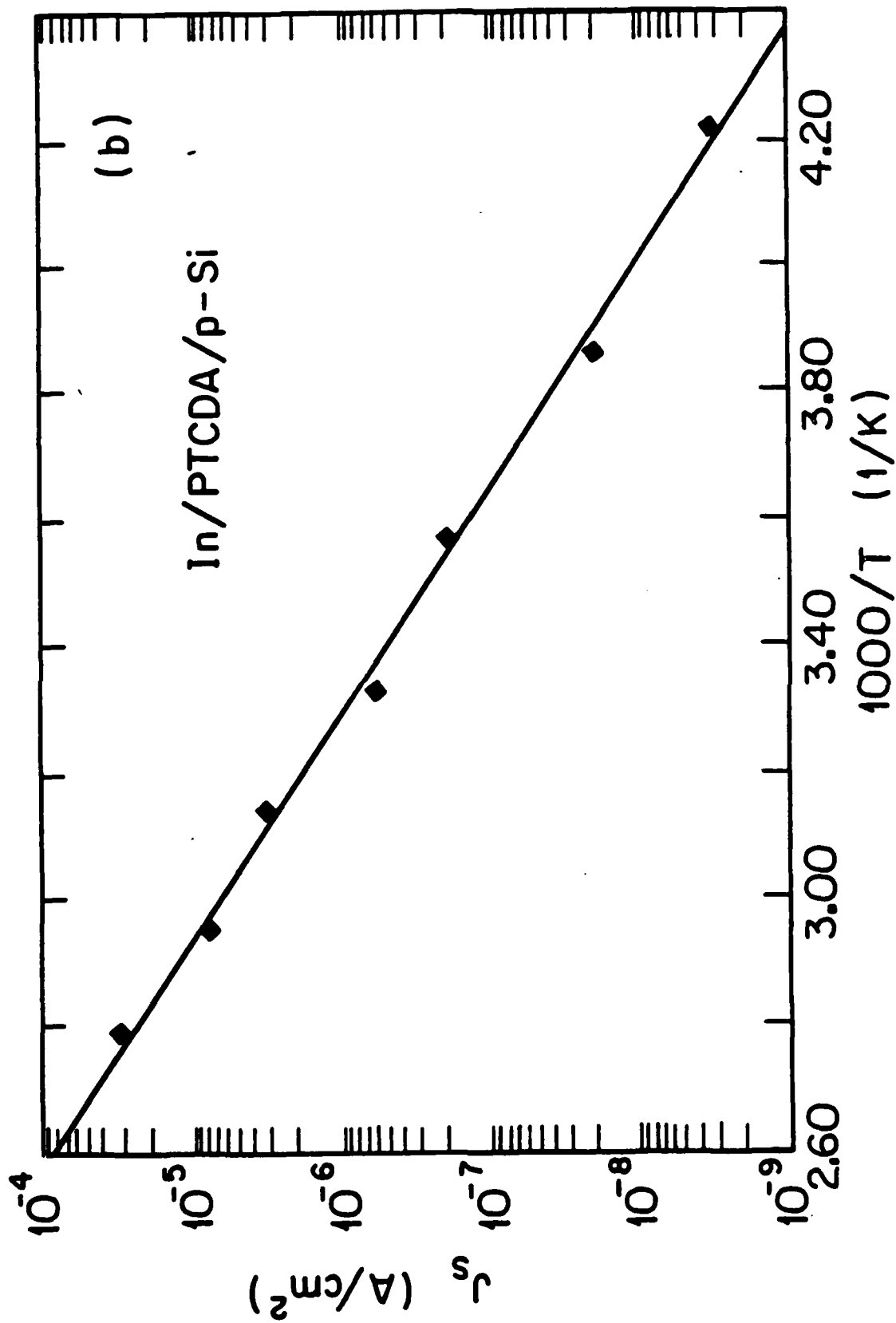J_S (A/cm^2)

1000/T (1/K)

Fig. 4

20

We have also measured ΔE_V directly by internal photoemission spectroscopy. In this experiment, a PTCDA/p-Si heterostructure was illuminated through the Si substrate using a chopped light source, such that light with energy greater than 1.1 eV is filtered by the substrate. Further attenuation of short wavelength light was achieved by inserting a second Si wafer between the sample and the light source. The short circuit photocurrent was then measured as a function of photon energy. Fig. 5(a) shows a photoemission spectrum where a peak is found at $h\nu = 0.57$ eV. The results can be interpreted as follows: At $h\nu < 0.57$ eV, holes in the organic film are emitted over the OI energy barrier. This photoemission current is expected to follow: $I_{ph} \propto (h\nu - \Delta E_V)^2$. Fig. 5(b) shows a plot of the square root of photocurrent versus $h\nu$ for the data taken on the long wavelength side of the emission peak. A least squares fit to these data gives $\Delta E_V = (0.50 \pm 0.1)$ eV--a value which agrees with that obtained from the forward I-V characteristics.

Note that at $h\nu > 0.57$ eV, I_{ph} drops rapidly to zero. This can be understood using the band diagram shown in the inset of Fig. 5(a). For PTCDA, the total bandwidth (BW), which is the sum of highest occupied molecular orbital (HOMO) and lowest unoccupied molecular orbital (LUMO) bandwidths, is only 0.9 eV. Thus, transition "b" beyond the BW is forbidden, resulting in a drop in I_{ph} for high energy photons.

Equation 1 is constrained by the requirement that the total applied voltage (V_a) be given by:

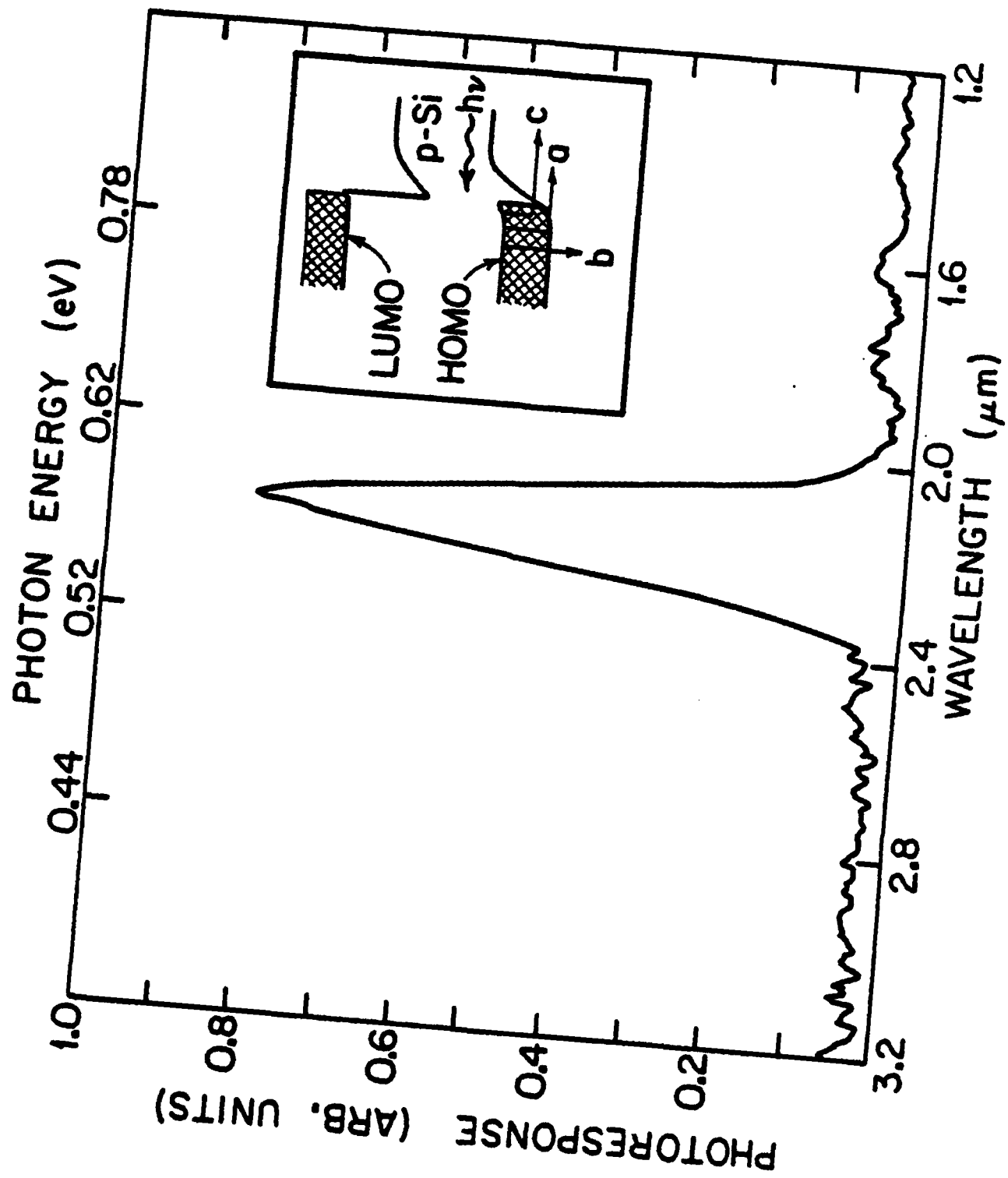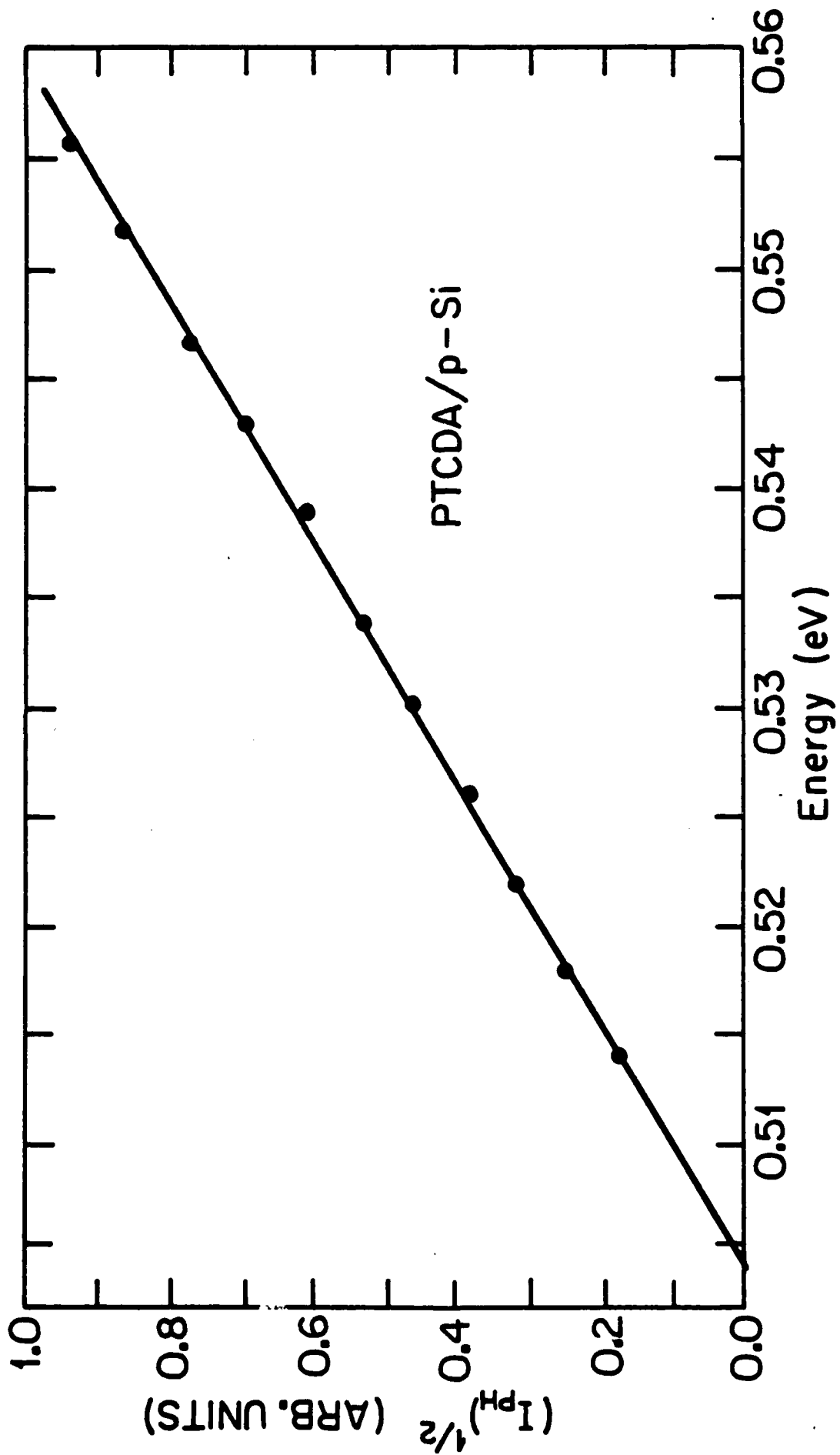$$V_a = V_0 + V_{SS} + V_D = V_0 + V_D', \qquad (3)$$

Fig. 5 a

PTCDA/p-Si

Energy (eV)

$(I_{PH})^{1/2}$ (ARB. UNITS)

Fig. 5b

23

where V_o is the voltage across the organic thin film, and V_{ss} is the voltage across the interface region. We define n via:

$$V_{ss} = (n - 1)V_D. \qquad (4)$$

Equation 1 can then be rewritten in a somewhat more convenient form:

$$J_T = J_0(\exp(\beta V_D/n) - 1). \qquad (5)$$

Transport of charge across the organic layer is limited, at least at high current, by space charge injection from the ohmic metal contact. In this regime, it can be shown that:

$$J_T = -9/8\kappa_i\mu_p V^2_o/d^3, \qquad (6)$$

where κ_i is the permittivity of the organic material, d its thickness, and μ_p the mobility of holes. Simultaneous solution of Eq. 5 and 6 can thus be used to calculate the foward and reverse current characteristics of the OI diode, provided that the correct values for n, d, and other variables are used. Figure 6 shows both the measured and calculated forward current characteristics for several PTCDA-Si diodes in which the PTCDA layer thickness was varied. The dark current rises exponentially at low voltage, which is consistent with Eq. 5, whereas at higher voltage $J_T \sim V_o^2$ (Eq. 6). The reverse current is determined solely by thermionic emission and other bulk semiconductor properties. The reverse breakdown voltage is comparable to that expected for ideal p-n junction diodes fabricated using only the underlying semiconductor substrate. This high breakdown voltage, which is the key to the utility of the OI structure for wafer diagnostics, results from the fact that the OI heterointerface is far from the diode contacts. In Schottky diodes, however, low-voltage breakdown occurs due to the high density of
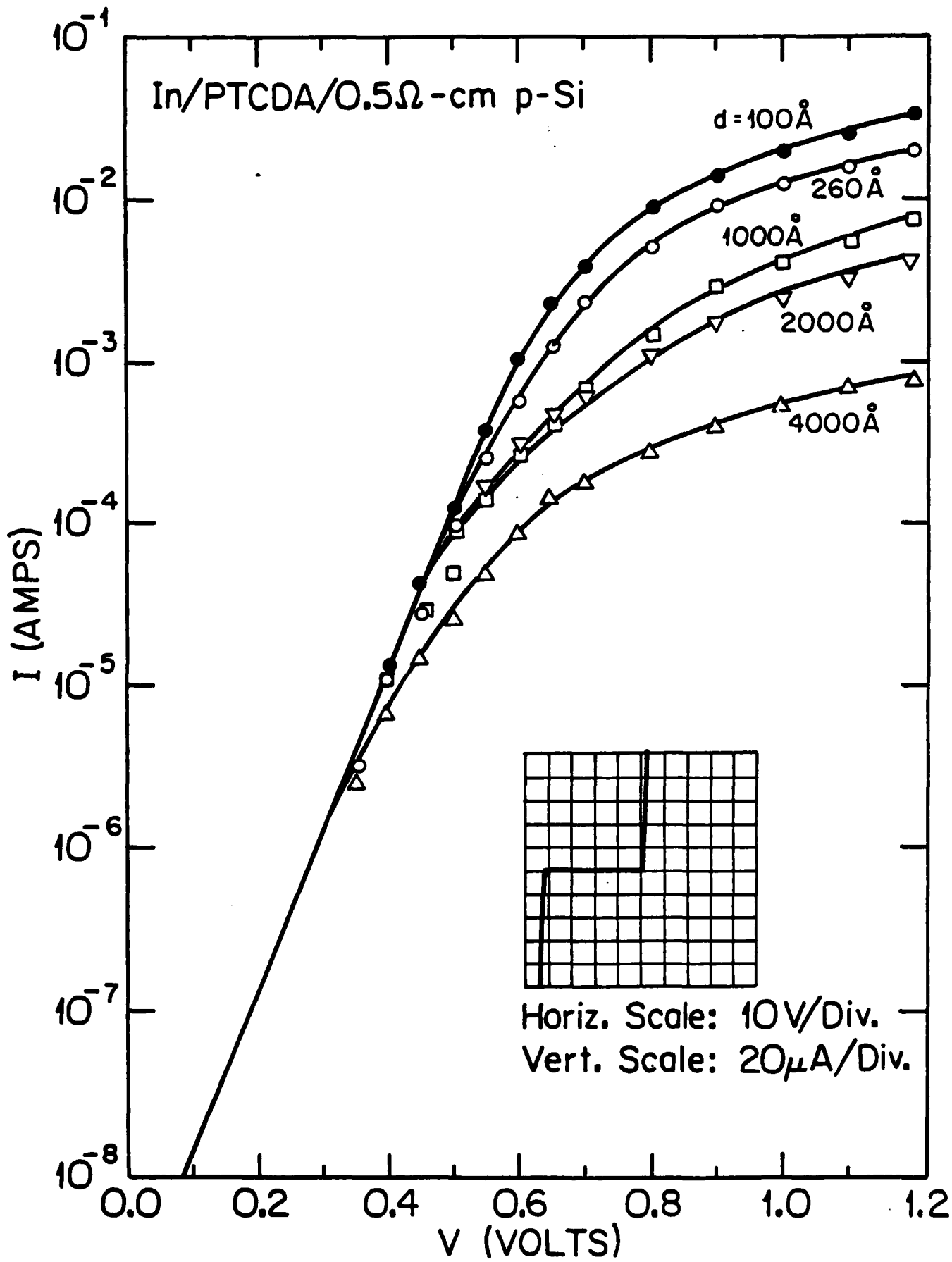
24

Fig. 6

25

electric field lines at the contact edges. As suggested in the treatment given above, the metal-organic interface in the OI diode is not the current-limiting interface. Due to the large anisotropy of conductivity of the organic material, current is confined to the region under the contact pad. There is no significant current spreading under the contact pad, which indicates that the field lines are parallel to each other and perpendicular to the wafer surface. This low field concentration thus avoids low-voltage, edge-related breakdown in the OI diodes.

Data for wafer diagnostic applications is obtained via standard capacitance-voltage (C-V) analysis. In the absence of surface or interface states in the OI diode, the capacitance is related to the apparent free carrier concentration, $n^*(x^*)$, in the underlying semiconductor wafer according to the familiar relationship[8]:

$$n^*(x^*) = (2/q\kappa_S A^2)dV_D(d(1/C^2_D)$$ (7)

Here C_D is the capacitance due to the depletion of the semiconductor substrate material, A is the ohmic contact area, and κ_S is the permittivity of the semiconductor. Furthermore, the apparent distance from the OI interface at which the free carrier concentration is determined using Eq. 7 is given by:

$$x^* = \kappa_S A/C_D.$$ (8)

Thus, by measuring C_D as a function of voltage, one can also obtain the free carrier concentration as a function of depth from the wafer surface. Indeed, the higher the applied voltage, the deeper the profile can be extended into the semiconductor bulk, which makes OI diode anlysis extremely useful for obtaining n^* versus x^* data. For

example, for uniformly doped semiconductors, the relationship between x^* and voltage is:

$$x^{*2} = 2\kappa_s(V_D + \phi_B)/qn^*(x^*) \qquad (9)$$

For a typical Schottky barrier diode, generally less than 10 V can be applied in the reverse-biased direction; however, voltages more than ten times this value can be applied to similar OI structures. This fact suggests that the free carrier concentration profile can be extended three to four times deeper into the semiconductor bulk in these latter diodes. This capability makes the OI diode very attractive for wafer diagnostic applications.

Note that Eq. 7 and 8 depend on C_D and V_D, which are not directly measurable quantities. However, Eq. 3 and 5 make it apparent that under reverse bias, where the current is small and far from being space-charge-limited, the amount of the total voltage dropped across the organic film (V_0) is very small compared with V_D. Therefore we can assume that $V_a \sim V_D$. Furthermore, it can be shown that at moderate measurement frequencies ($f \leq 1$ MHz) the effect of the capacitance due to the organic film is negligible compared with C_D. In this case, Eq. 7 and 8 can be simplified by replacing V_D and C_D with V_a and C_T, respectively, where C_T is the total OI diode capacitance.

The depth resolution of the C-V method is limited to a few Debye lengths, L_D, where

$$L_D^2 = \kappa_s kT/[q^2_A n^*(x^*)]. \qquad (10)$$

Thus, for a semiconductor substrate with a net free carrier concentration of 1×10^{15} cm^{-3}, a typical depth resolution is roughly

1000 A, and that number decreases with increasing carrier concentration. The spatial resolution is limited, in principle, only by the width of the depletion region at breakdown, which is usually on the order of a few micrometers. In practice, however, the spatial resolution is limited by the minimum diameter of contact that can be easily probed.

Although OI analysis follows traditional C-V measurement techniques, the strengths of the method are that (a) it allows nondestructive application and removal of the OI contact, (b) very large reverse biases can be applied without evidence for early reverse breakdown phenomena, and (c) high spatial and depth resolution are inherent in this technique.

c. Applications of the OI diode to wafer diagnostics
i) Depth profiling of free carrier concentration and epitaxial layer thickness

Figure 7 shows a typical profile of the free carrier concentration of a heteroepitaxial wafer consisting of thin layers of InGaAsP and InGaAs grown on an InP wafer substrate. All epitaxial layers shown are lightly n-type, and the substrate is S-doped to approximately 10^{18} cm^{-3}. The growth of the layers was accomplished by liquid phase epitaxy (LPE). There are several features immediately apparent in this profile that provide information about the properties of the grown layers. For example, the data indicate a background doping level of approximately 4 x 10^{15} cm^{-3} in the bulk of the InGaAs layer. The spike features result from the energy band
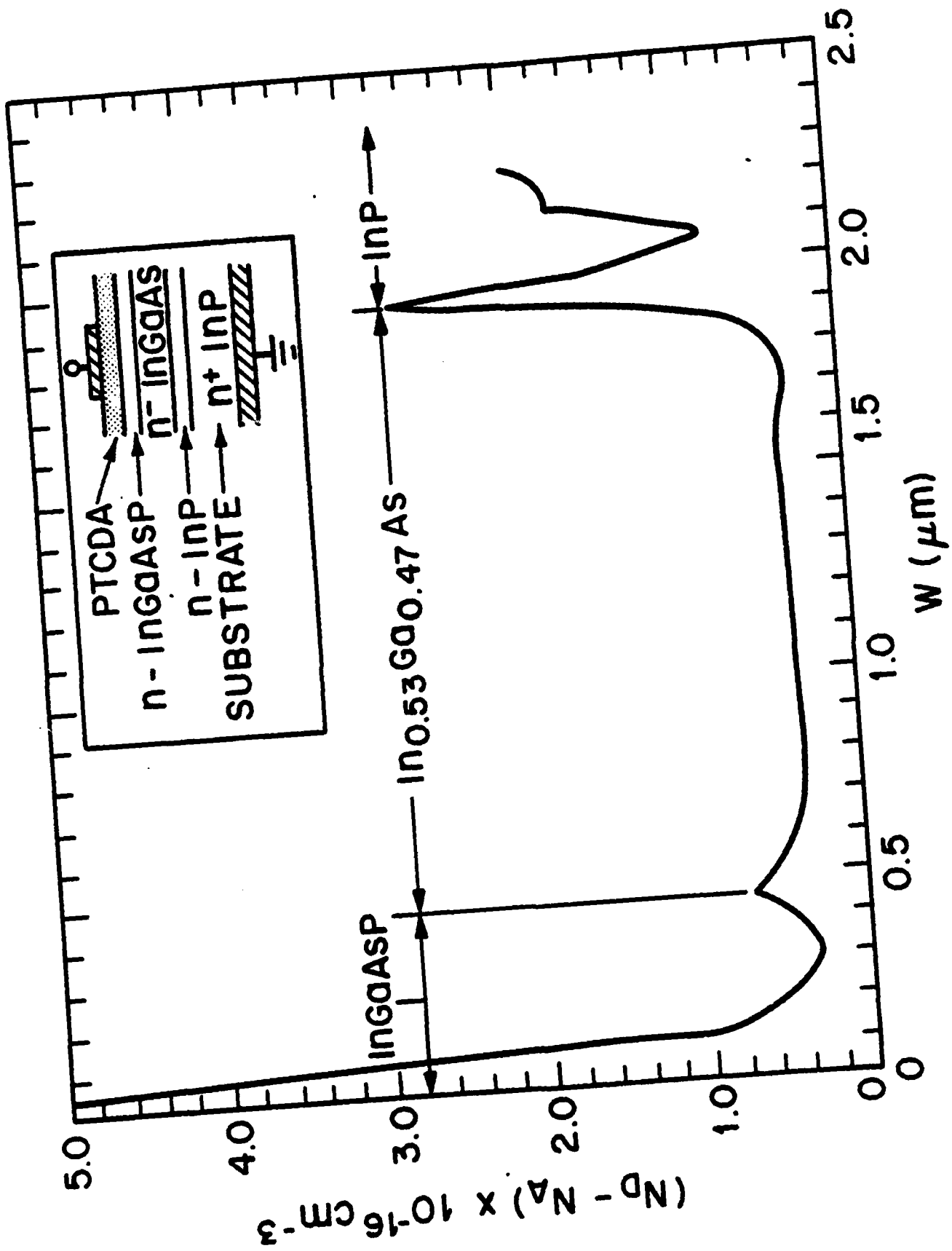
Fig. 7

29

discontinuities arising at the heterojunctions between semiconductors of differing compositions. These features can be analyzed to determine the size of the energy discontinuity, as is shown below. Here, however, we only note that the spike peaks indicate the positions of the InP-InGaAs and InGaAs-InGaAsP interfaces. Using this information, we infer that the thickness of the InGaAsP layer is 0.45 μm and that of the InGaAs layer is 1.50 μm. Thus the discontinuities in energy bands, or even free carrier concentration, that arise at interfaces between two grown layers can be resolved from C-V data to accurately indicate the thickness of these layers.

Finally, the free carrier concentration appears to increase very rapidly near the wafer surface (i.e. as x > 0). A detailed study of the conductance properties of the wafer in the near-surface region, which is accessed at low applied voltage, can yield quantitative information as to the energy and densities of defect levels at semiconductor surfaces[9].

Once the free carrier concentration has been determined at several different locations around a wafer surface via a measurement of the C-V characteristics of a matrix of OI diodes, it is possible to construct "contour maps" delineating the spatial distribution of the various wafer properties accessible by these methods. Figure 8 is such a map of the thickness of an InGaAs layer grown via LPE. The thickness of the layer was determined from the depth at which the free carrier concentration increased abruptly from its value in the grown layer ($\sim 1 \times 10^{15}$ cm^{-3}) due to the existence of charge accumulation at the InGaAs/InP heterointerface (see Fig. 7). This
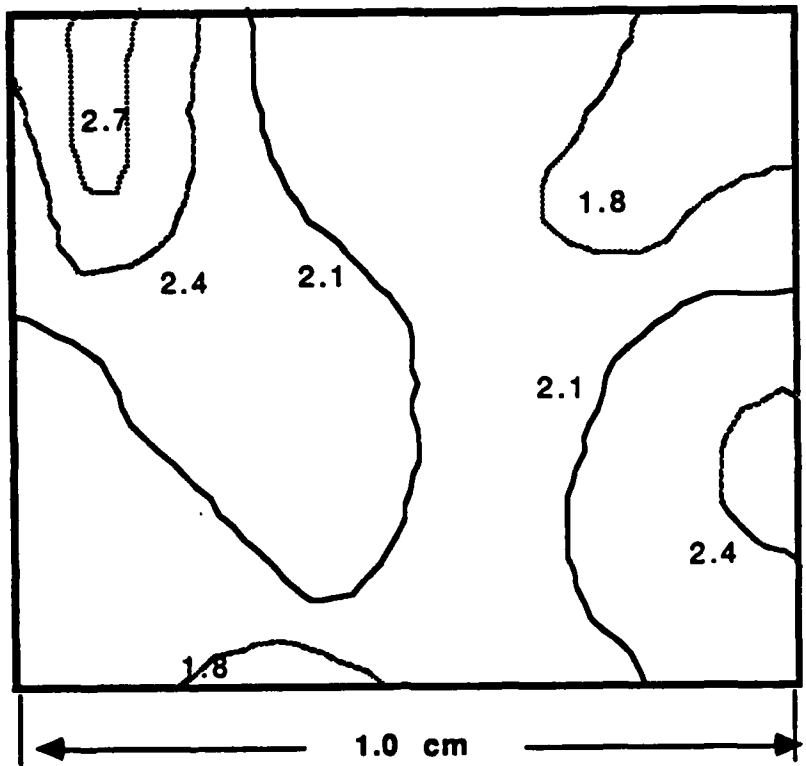
InGaAs Layer Thickness

(Contour Units = Microns)

Fig. 8

31

map indicates a thin region at the periphery of the wafer, becoming considerably thicker near the center. Understanding of the geometry of the growth reactor can lead to a consistent picture of the source of these nonuniformities. We speculate that these growth inhomogenities are a result of small thermal gradients which occur across the diameter of the growth furnace.

It is apparent that these contour maps contain a wealth of diagnostic information about the wafer, and the dynamics of the conditions under which it was grown. Furthermore, if the organic layer is removed after such information is obtained, it is possible to fabricate the semiconductor devices for which the material was originally grown. The finished device performance can then be directly correlated with the detailed materials data. Such studies result in a rapid and in-depth understanding of the materials, which can then be used to obtain a higher ultimate device yield.

As noted previously, the spikes in the free carrier concentration profiles in the region of heterojunctions can be figure analyzed to determine the energy discontinuity, which is due to the energy dipole resulting from the semiconductor-semiconductor contact. The source of this heterojunction feature can be understood in terms of the energy band diagram of an InP/InGaAs heterojunction shown in the inset of Fig. 9. The increase in conduction-band electron energy on the large band gap side of the heterointerface results in the depletion of carriers from this region, as evidenced by a dip in the measured free carrier concentration ($n^*(x^*)$) shown in Fig. 9. This depletion is balanced on the small band gap side by charge

Ñ(X) (×10⁻¹⁶ cm⁻³)

$\tilde{n}(X)$ ($\times 10^{-16}$ cm^{-3})

X (microns)

Fig. 9

InGaAsP (E$_g$ =0.95eV)

InP

N$_Q$

N$_B$

X$_i$

PTCDA — InGaAsP — InP

ΔE_c δ_B E_F

δ_Q ΔE_v E$_{gB}$

E_{gQ}

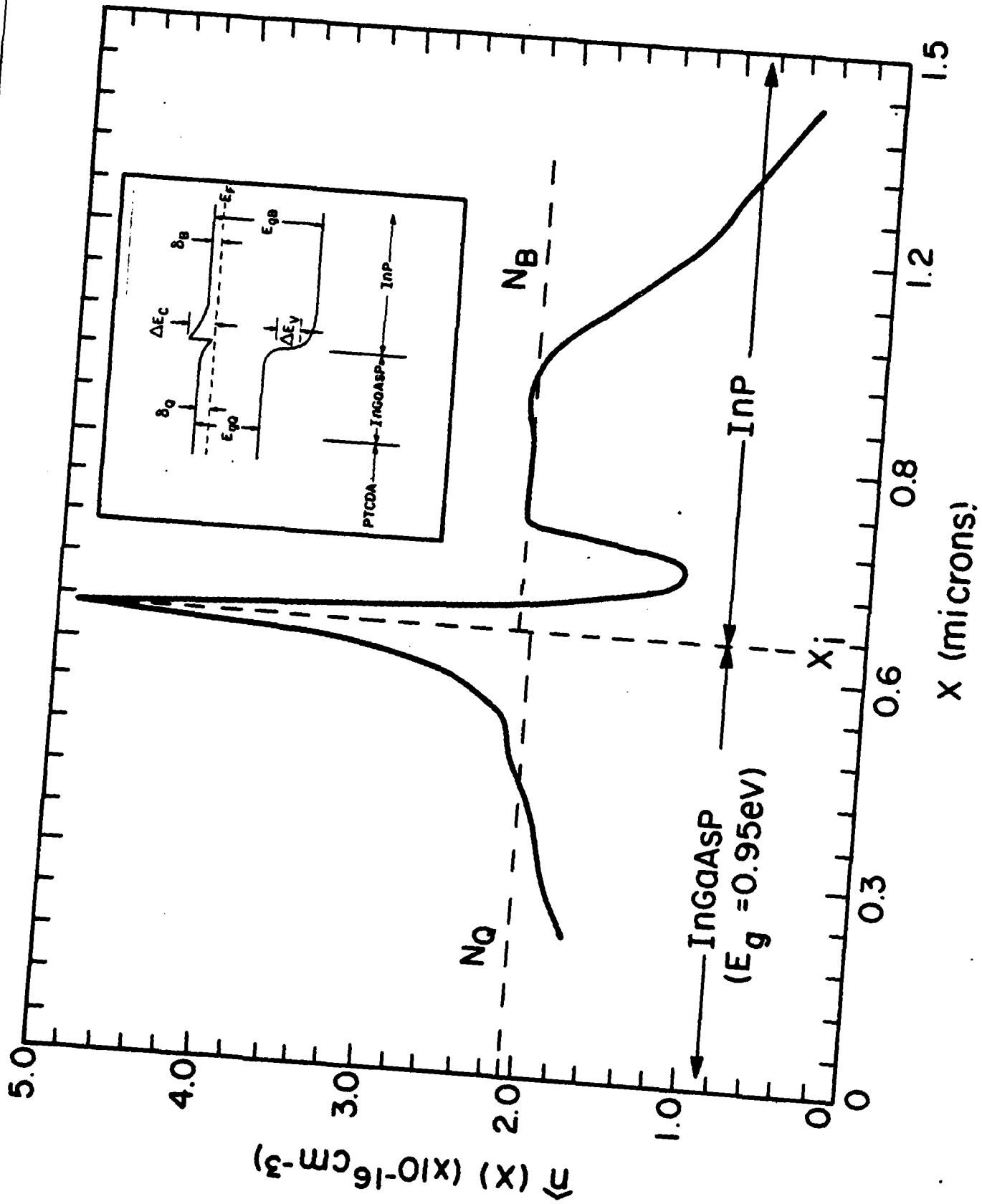5.0   4.0   3.0   2.0   1.0   0

0   0.3   0.6   0.8   1.2   1.5

33

accumulation, thus giving rise to a large peak in the n(x) data. Although the resolution limits inherent in C-V analysis preclude direct correlation of the apparent (measured) concentration profile with the actual carrier density in the region of rapidly varying potentials, it can be shown that the total potential difference can nevertheless be inferred from such concentration measurements[10]. Thus, the diffusion potential difference across a heterojunction is given by:

$$V_{DK} = q/\kappa_s \int_0^\infty (N - n^*(x^*))(x^*))(x^* - x_j^*)dx \qquad (10)$$

where x_j^* is the apparent position of the heterojunction inferred from the position of the peak in $n^*(x^* = x^*_I)$. Once the diffusion potential is known, the conduction band discontinuity energy (ΔE_c) is easily obtained by taking into account the positions of the Fermi energies in the bulk of the two contacting semiconductors.

The large energy barriers obtained using the OI technique have made it possible to measure the conduction band discontinuities of several different compositions of InGaAsP on InP using capacitance analysis techniques[11]. The C-V method requires that a large reverse bias be applied to the semiconductors such that the depletion region can be swept into regions far from the heterojunction both above and figure below x_I. Due to the relatively small Schottky barriers characteristic of InP-based compounds, this measurement has not been possible by means other than the OI technique (where the energy barrier is ~0.55 eV on InP-based compound semiconductors, independent of phosphorous concentration). We find that for InP-InGaAs(P)

heterojunctions the energy gap difference between the contacting materials, ΔE_g is related to ΔE_c via:

$$\Delta E_c = 0.39 \; \Delta E_g. \qquad\qquad (11)$$

ii) Deep level analysis

The OI technique can be applied to obtain any wafer information accessible via a measurement of the capacitance (and in some cases, the current) of the OI diode. An important application is therefore possible: deep level transient spectroscopy (DLTS) and other admittance spectroscopic means for determining the cross-sections, energies, and densities of deep levels present in the underlying semiconductor substrate. Such deep level analysis of some interesting semiconductors was not possible using alternate techniques due to the low barrier heights associated with conventional metal-semiconductor barriers generally used in these applications. Thus the nondestructive nature of the application of OI contacts, the high energy barriers, and the ability to apply large reverse biases make this technique advantageous for use in DLTS and other deep level analysis methods.

Figure 10 shows the DLTS spectrum obtained for both n- and p-type GaAs using the OI contact method. For comparison purposes, in Fig. 10a the data were obtained using both an OI diode and a conventional Au-GaAs Schottky contact, which works well for n-type GaAs. As can be seen, there are no significant differences in the peak positions observed using the two contact types, although the peak height of the EL 14 level is considerably higher for the OI diode than that obtained for the Au-contact diode. This variation is
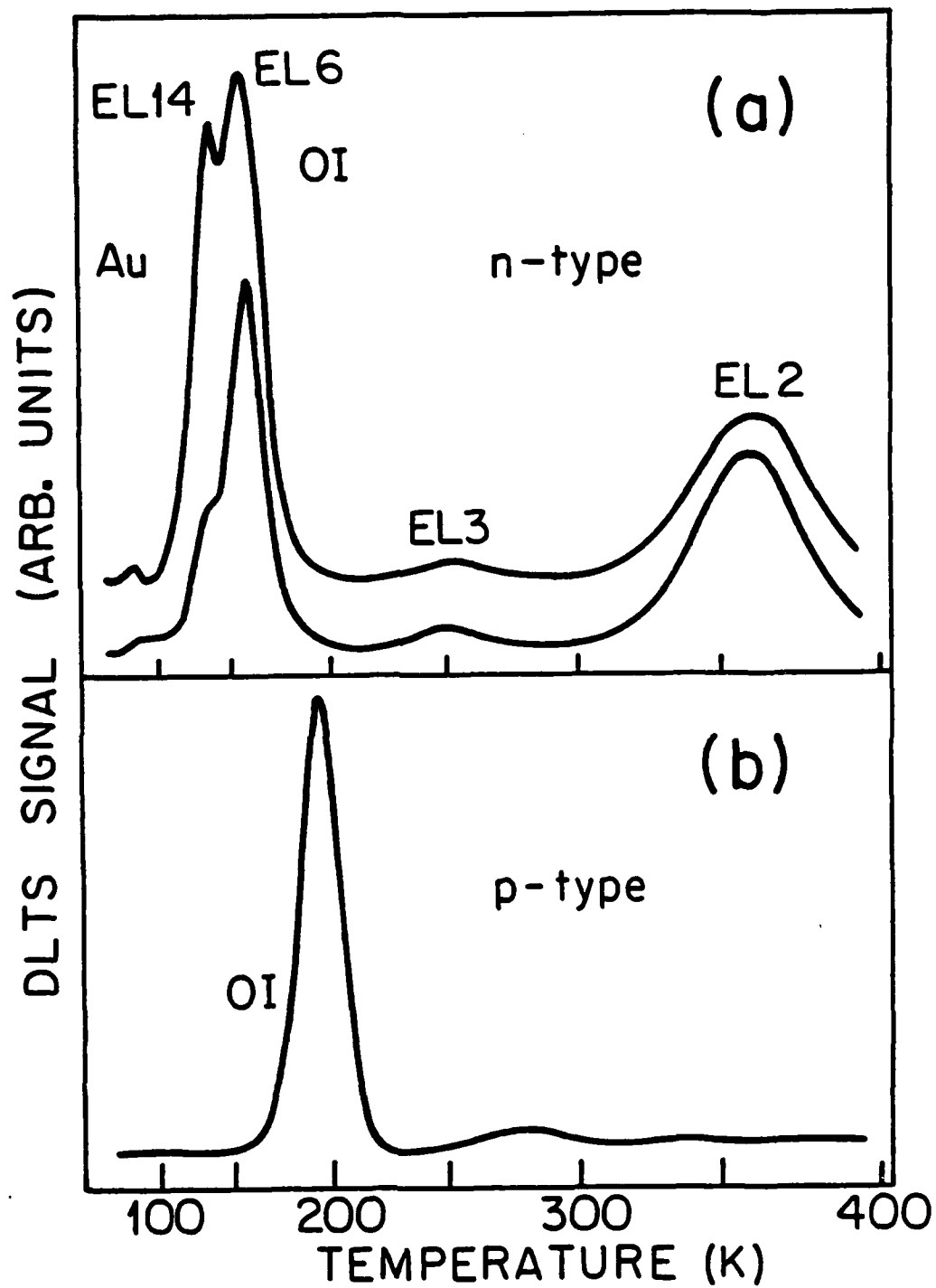
35

Fig. 10

36

. due to nonuniformities in the density of this level at different locations of the wafer under study.

The deep level spectrum for the p-type material (Fig. 10b) indicates two defect energy peaks. Typically, the barrier heights observed on p-GaAs are on the order of 0.5-0.6 eV, which makes DLTS profiling difficult at elevated temperatures. However, we have found barrier heights of 0.85 eV with both PTCDA and the related compound DIME-PTCDI when they are deposited onto the surface of p-GaAs. Thus, depletion and profiling of defect levels deep into the semiconductor bulk with a high degree of resolution of the positions and intensities for the transient spectral peaks become possible even at high temperatures.

III. Transport Theory

A primary objective of the theoretical work pursued in this program was to predict the value of the saturation current, J_0, in Eq. 1. By so doing, both the microscopic transport mechanisms and the dependence of the quasi-Fermi levels on applied voltage can be more clearly understood. These properties are required if we are to predict diode transient response, and they are also needed to interpret admittance data obtained using the surface analysis spectroscopic techniques described in earlier work.

The derivation of J_0 and other results obtained from this theoretical treatment are given in detail in Appendix A (S.R. Forrest and F. F. So, J. Appl. Phys., **64**, 402 (1988)). The most important aspects of this work are summarized in this section.

It can be shown that the saturation current density of p-P OI HJ's is given by:

$$J_0 = qN_{vs}<v_c>(1 + <v_c>/v_d)exp(-q\phi_{Bp}/kT) \qquad (12)$$

where N_{vs} is the effective density of states at the valence band maximum in the *inorganic* semiconductor, v_d is the diffusion velocity in the substrate, and $<v_c>$ is the mean carrier velocity in the organic thin film. Since the organic material is essentially a resistive medium (with conductivity, σ), the mean carrier velocity increases linearly with mobility and electric field. Due to the dependence of current on E-field ($J = \sigma E$) in resistive media, the drift component of the velocity vanishes under reverse bias or low forward bias in OI diodes. In this case, $<v_c>$ becomes limited by diffusion, and is given by:

$$<v_c>^2 = \mu_p kT/q\tau_p \qquad (13)$$

where μ_p is the hole mobility in PTCDA, and τ_p is its lifetime. We estimate that $<v_c>$ is 500 - 3000 cm/s from mobility and lifetime data obtained in independent experiments. Furthermore, using a direct measurement of the transient response time of PTCDA/p-Si diodes, mean carrier velocities within this same range of values have been observed.

Under larger forward bias, $<v_c>$ increases very rapidly with applied voltage, as seen from Fig. 11. This increase continues until polaron scattering becomes dominant, at which point the drift velocity saturates. The electric field at which velocity saturation occurs is as yet undetermined, although it appears to be at[12] $<v_c> >$ 10^4 cm/s.
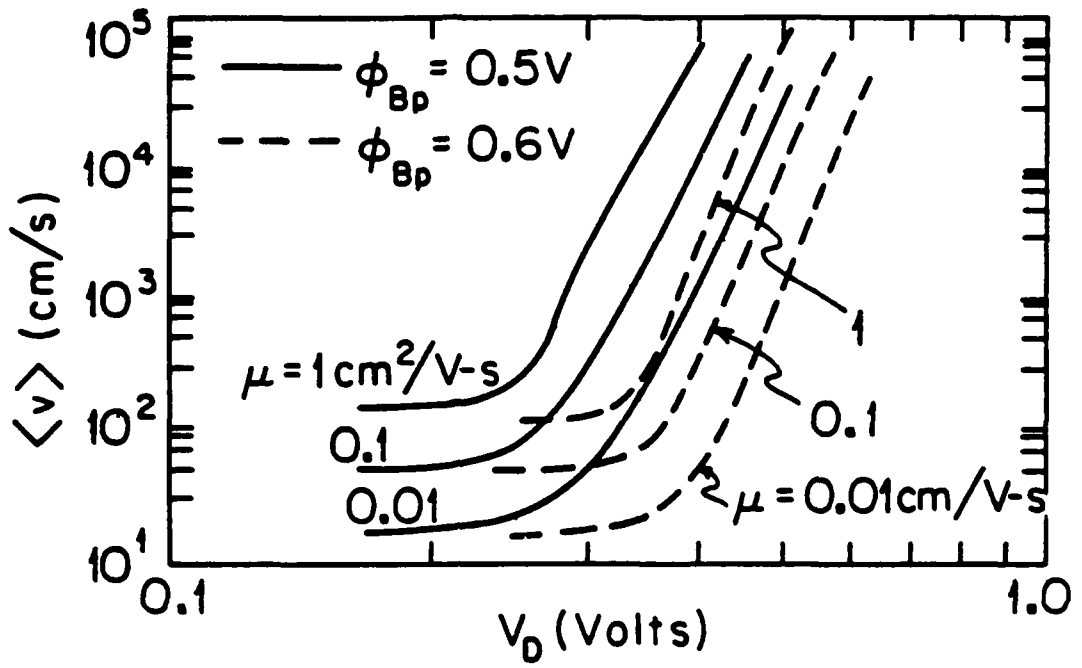
Fig. 11

A major conclusion of this theory which has been subsequently borne out in experimental tests is that the carrier velocities in OI HJ diodes are higher than initially expected, thus opening up many opportunities for the realization of high bandwidth optoelectronic devices using the OI structure.

A further conclusion of this theory is that the potential measured at the interface between the organic and inorganic semiconductors (or surface potential, ψ_s) is nearly linear with voltage applied across the substrate (V_D) over a wide range of both forward and reverse bias. This situation is considerably different than that obtained for Schottky diodes under reverse bias. In this case, the Fermi energy is "pinned" at the barrier energy, ϕ_B, and is thus independent of applied bias. Since the Fermi energy in OI diodes is not similarly pinned, it can be swept both above and below ϕ_B, which allows this structure to be used to obtain information regarding defect states in both the upper and lower halves of the semiconductor bandgap.

The dependence of ψ_s on V_D is shown in Fig. 12 for several different values of OI HJ diffusion potential. This linear relationship between surface potential and applied voltage arises since $\langle v_c \rangle \ll v_d$. Note that in the case of Schottky diodes, $\langle v_c \rangle \sim v_d$, resulting in a constant ψ_s with V_D under reverse bias, as shown in the figure. The linear relationship between these quantities in OI HJ diodes easily allows one to calculate the surface potential. By measuring the admittance of the diode as a function of voltage, one can then determine the semiconductor surface state density as a
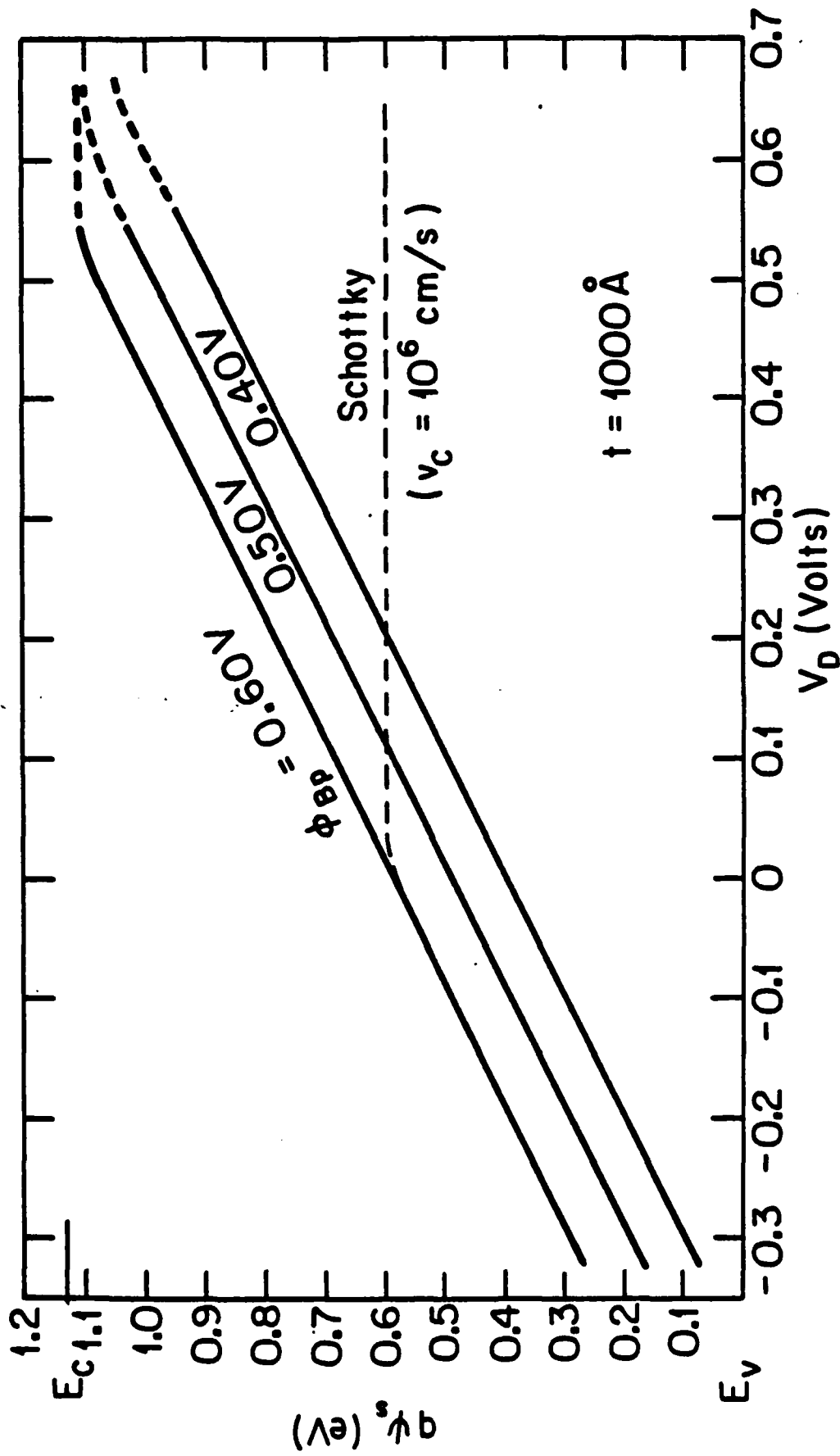
40

Fig. 12

function of position within the band gap, as required for the study of such defects.

The results of one such spectrum obtained for several different organic materials deposited onto the surface of p-type Si is shown in Fig. 13. A complete explanation of these surface spectra are described in Appendix A. However, we see that the surface state densities obtained for both PTCDA and NTCDA are uniformly distributed across the band gap of the substrate, and are approximately equal to 2×10^{12} $cm^{-2}eV^{-1}$ -- values expected for Si with a thin native oxide on the surface. On the other hand, results for Cu-phthalocyanine (CuPc), and to a lesser extent, metal-free Pc (H_2Pc) are considerably different. In the case of CuPc there is a large peak in the surface state spectrum at 0.5 eV above the valence band maximum in Si. This energy is approximately equal to the energy of bulk Cu acceptors in Si, as indicated by the arrow in the figure. From these results, we conclude that the Cu ligand atom in many of the CuPc molecules undergoes a reaction with the Si surface. The reaction process might proceed by the following two-step mechanism:

$$H_2O + CuPc <--> H_2Pc + CuO \qquad (14a)$$

$$2CuO + Si <--> SiO_2 + 2Cu \qquad (14b)$$

Due to the strength of the SiO_2 bond (as compared with the Cu-N bond in CuPc), these reactions are strongly favored from free-energy arguments. Also from the area under the CuPc peak in Fig. 13, we estimate that roughly 0.5% of the surface CuPc molecules are involved in such a reaction. The smaller peak observed in the H_2Pc spectrum probably has similar origins to that of the CuPc sample. However, in
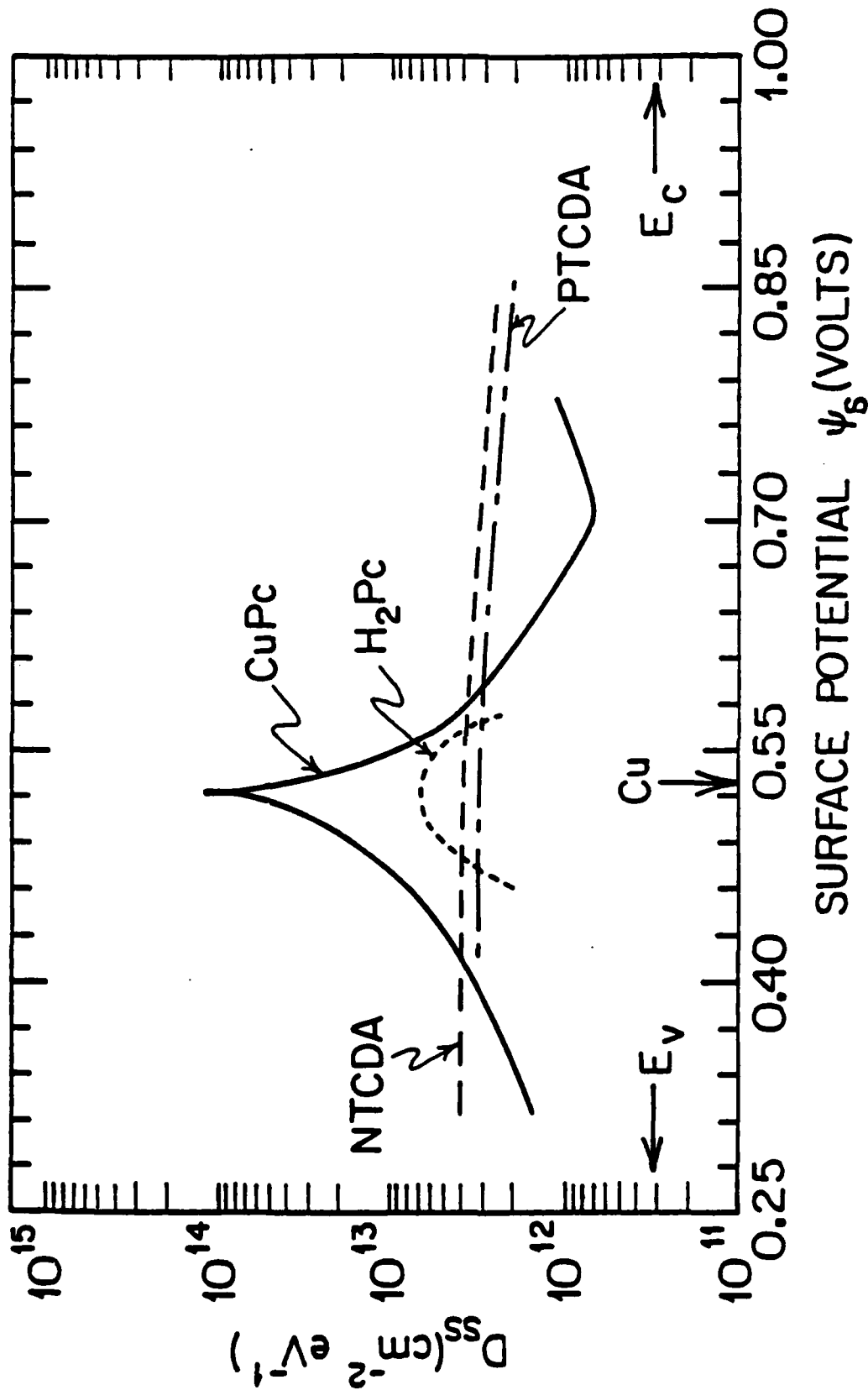
42

Fig. 13

43

the former experiment, the defects might be induced by metallic impurities deposited along with the organic film.

In summary, it is apparent that the theoretical treatment of the microscopic nature of charge transport across OI HJ's has lead to a substantial advance in our ability to interpret surface admittance data obtained from these structures, and indicates that they are indeed useful tools for studying the surface defects all across the bandgap of the underlying semiconductors. Furthermore, this theory has lead to the direct measurement, for the first time, of the valence band offsets at heterointerfaces made between crystalline organic molecular semiconductors and inorganic semiconductors (Sec. II). It was also used to predict high bandwidth operation of OI diodes which was later verified experimentally.

IV. Accurate Determination of Heterojunction Band Discontinuity Energies

The capacitance-voltage (C-V) technique proposed by Kroemer, et al.[10] and discussed briefly in Sec. II. has been widely used to measure the energy band discontinuities of many isotype heterojunctions (HJs). This method exhibits features which have advantages over many other techniques used in determining HJ band discontinuity energies. For example, the measurements are not sensitive to compositional gradients in the heterointerface region, and are relatively insensitive to materials parameters such as effective mass and permittivity· By comparison, photoluminescence spectroscopy of multiple quantum wells is strongly dependent on the

accurate knowledge of effective mass, quantum well width, and well profile. Likewise, x-ray photoelectron spectroscopy (XPS) is subject to errors due to the need of subtracting large valence bond energies (~10-15 eV) to obtain a small discontinuity energy (~0.1 - 0.5 eV). Further, current-voltage measurements are vulnerable to errors induced by parasitic current sources.

In addition to determining the band discontinuity energy, the C-V technique is also useful for measuring the density of shallow trapped charge near the heterojunction. With this information, the relative quality of a HJ can be assessed such that, *a priori*, the accuracy of the subsequent band discontinuity energy measurement can be ascertained.

The HJ properties are determined by first obtaining the apparent (or measured) free carrier concentration profile ($n^*(x^*)$) from C-V data using Eq. (7). These data result from depleting the HJ by applying reverse voltage to an adjacent rectifying contact. The density of shallow trapped interface charge, σ_{iK}, of an n-type, isotype HJ can then be obtained using:[10]

$$\sigma_{iK} = - \int_{-\infty}^{\infty} [N_D(x^*) - n^*(x^*)]dx^* \tag{15}$$

where $N_D(x^*)$ is the background donor concentration at the apparent position x^*, and x_j^* is the apparent position of the HJ as measured from the location of the charge accumulation peak in the carrier concentration profile. The conduction band discontinuity energy (ΔE_{cK}) is calculated using the diffusion potential calculated from Eq. 10 via: $\Delta E_{cK} = qV_{DK} + \delta_2 - \delta_1$, where δ_1 and δ_2 are the Fermi energies (with respect to the conduction band minima) in the bulk of

the contacting semiconductors. Here, subscripts 1 and 2 refer to the different materials comprising the HJ.

There are several inherent problems with the C-V technique which can lead to systematic errors in determining both ΔE_c and the actual fixed interface charge density, σ_i. For example, the use of Eqs. 10 and 15 is based on the assumptions that the apparent HJ position $(x_j{}^*)$ is equal to its actual position (x_j), and that the trap density σ_i is low enough such that it does not significantly perturb the often small intrinsic heterojunction dipole potential. However, due to the limited spatial resolution inherent in C-V data, $x_j{}^*$ is shifted away from x_j and toward the electron accumulation region at the HJ. In order to correct for this effect, Rao, et al.[13] calculated a series of pairs of σ_{iK} and ΔE_{cK} for (Ga,In)P/GaAs HJs by assuming different values of x_j, and then choosing the actual position of the HJ to minimize σ_{iK}. Since this approach assumes that the HJ has a very low density of interface states, it can only be applied reliably to samples where σ_i has been independently determined to be small.

On the other hand, we can expect that a high density of defects will influence the values obtained for V_{DK}, particularly if the diffusion potential is small.[14] This situation is made worse if the doping levels on both sides of the HJ are different. To illustrate this last point, in Fig. 14 we show the calculated apparent free carrier concentration profile of an InP/In$_{0.53}$Ga$_{0.47}$As HJ with background dopings of N_{D1} = 1.1 x 10^{16} cm^{-3} and N_{D2} = 3 x 10^{16} cm^{-3} for InP and In$_{0.53}$Ga$_{0.47}$As, respectively. The calculation is

Fig. 14

$\Delta E_C = 0.24\,eV$

$\sigma_i = -5 \times 10^{10}\,cm^{-2}$

$\sigma_{iK} = -5.8 \times 10^{9}\,cm^{-2}$

N_{D2}

X_j^*

X_j

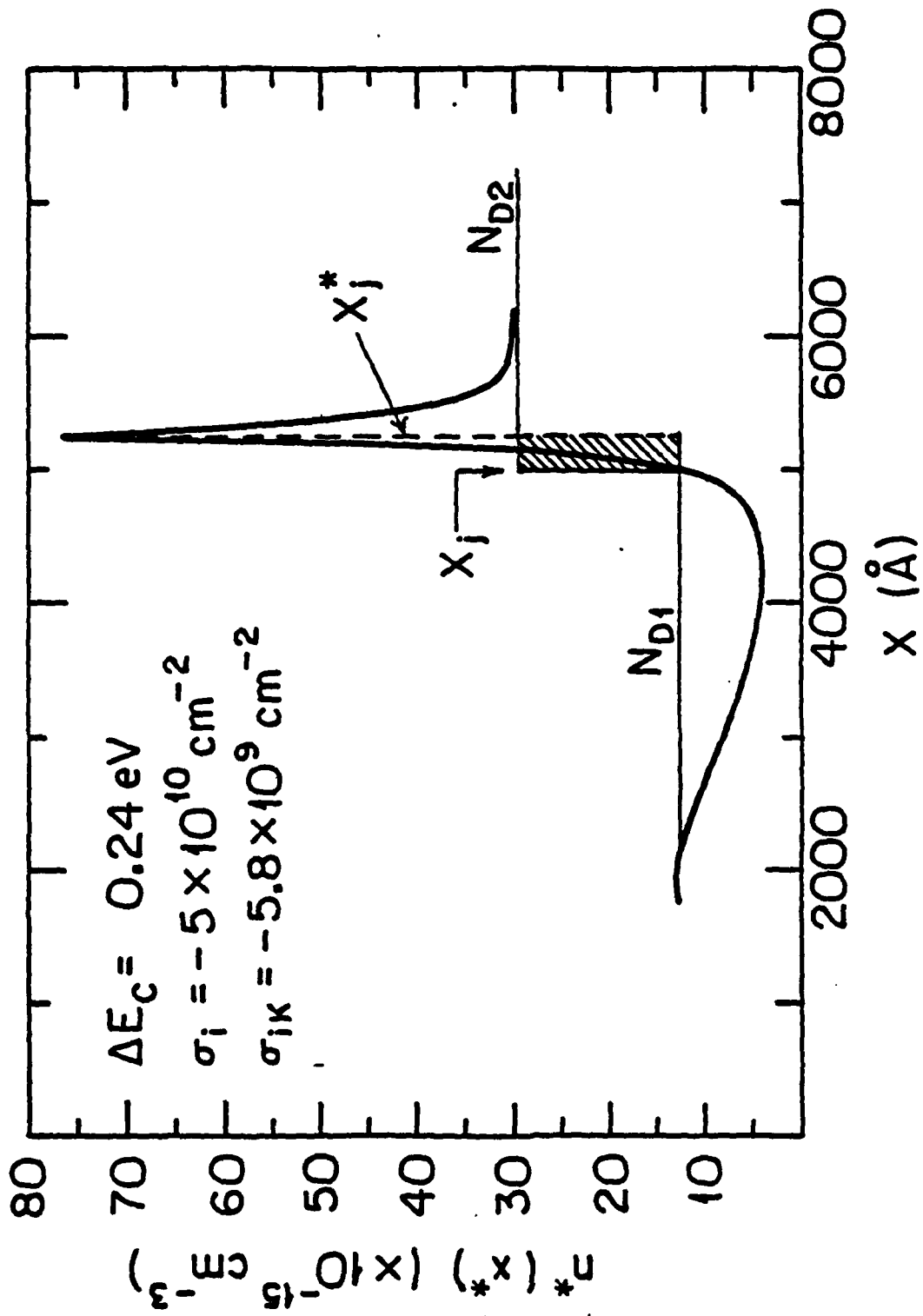N_{D1}

$X\,(\mathring{A})$

$n^*(x^*)\,(\times 10^{-15}\,cm^{-3})$

accomplished by numerically solving Poisson's Equation starting at the rectifying contact made to the InP layer, and assuming that ΔE_c = 0.24 eV, where the conduction band energy is greater on the InP side than on the InGaAs side of the HJ[15]. Furthermore, for this calculation we assume that the interface trap density is σ_i = -5 x 10^{10} cm^{-2}, and is confined to a region of width d = 200 A on the InP side of the heterointerface.

In using the C-V depletion technique, the background doping levels of both materials are obtained from the $n^*(x^*)$ profile at distances x^* far from either side of the HJ, and the integrals in Eq's. 10 and 15 are then evaluated by assuming that N_{D1} and N_{D2} are uniform in the HJ region. An abrupt step in doping between these values is assumed to occur at the HJ whose position is determined from x_j^*. As can be seen from the cross-hatched box in the figure, the integral in Eq. 10 will be incorrect due to the excess area arising from the difference between x_j^* and the actual position x_j. The error thus incurred is increased with an increasing difference between N_{D1} and N_{D2}. We can calculate the magnitude of the error by rewriting Eq. 15 as:

$$\sigma_{iK} = -\int_0^{x_j} [N_{D1} - n^*(x^*)]dx^* - \int_{x_j}^{x_j^*} [N_{D1} - n^*(x^*)]dx^*$$
$$- \int_{x_j^*}^{x_j} [N_{D2} - n^*(x^*)]dx^* - \int_{x_j}^{\infty} [N_{D2} - n^*(x^*)]dx^* \qquad (16)$$

The first and last integrals on the right hand side of Eq. (4) are just σ_i, whereas the middle integrals arise since $\Delta x_j = x_j - x_j^* \leq 0$. Evaluating these integrals for the profile in Fig. 14 indicates that σ_{iK} = -5.8 x 10^9 cm^{-2}, or about an order of magnitude less than the

48

actual value. Hence, these effects cannot be ignored without inducing large errors in the fixed interface charge density as obtained using previous methods.

These errors can be reduced or eliminated by solving the integrals in Eq. 16. Grouping terms we obtain:

$$\sigma_i = \sigma_{iK} - (N_{D1} - N_{D2})\Delta x_j. \tag{17}$$

By a similar analysis,[14] we obtain for the diffusion potential due only to the HJ dipole:

$$V_D(0) = V_{DK} + q/\kappa[\sigma_i(\Delta x_j - d/2) - (N_{D2} - N_{D1})\Delta x_j^2/2]. \tag{18}$$

In deriving Eq. 18, we assume the interface traps are uniformly distributed in a region of width, d. In other words, V_{DK} is the total potential drop due to the superposition of the intrinsic heterojunction electrostatic potential ($V_D(0)$), and the potential due to monopolar interface defects $[(q/2\kappa)\sigma_i d]$. Interface states which are dipolar in nature, however, are indistinguishable from the intrinsic HJ dipole and can potentially induce error in the determination of $V_D(0)$, provided such defects are present.

Note that $V_D(0)$ approaches V_{DK} as d or σ_i are decreased. Thus, measurements of ΔE_c using the depletion technique along with Eqs. 10 and 15 are only accurate in the absence of interface traps, or for very abrupt HJs. On the other hand, if d is large and V_{DK} is small, the second and third terms on the right in Eq. 18 may become larger than the measured value of V_{DK}. One example of HJs in which V_{DK} differs significantly from $V_D(0)$ are p-P $Hg_{0.7}Cd_{0.3}Te/Cd(4\%Zn)Te$ heterojunctions discussed in Sec. V. There, it will be shown that

d - 0.3 μm, and ΔE_v = 100 meV. In that case, $V_D(0)$ was found to be five times larger than V_{DK}.

Also note that monopolar defects (either donors or acceptors) are indistinguishable from shallow dopants. Thus, the net trap charge density calculated via Eq. 15 may arise from the wrong choice of N_{D1} or N_{D2}. Indeed, one problem with using Eqs. 10 and 15 is the assumption that N_{D1} and N_{D2} are known in the interface region, and that these values change abruptly at x_j^* (see Fig.14). However, if any doping nonuniformities occur over the heterointerface width, d, we can use both Eq's. 17 and 18 to eliminate this error source to obtain the exact value $V_D(0)$. In many cases the assumption that variations in doping occur over a distance, d, is justified since diffusion of dopants, semiconductor constituents and defects will probably be most pronounced over the same spatial region. Indeed in most experiments reported using Eqs. 10 and 15, a value of σ_{iK} - 1-3x10^{10} cm^{-2} is often observed. While this value may in fact be due to the presence of interfacial defects or even arise from limited experimental resolution, it can also be explained as due simply to deviations of N_{D1} and N_{D2} from their bulk values in the heterointerface region.

As inferred from Eqs. 17 and 18, Δx_j and d are the only two unknowns needed to obtain the exact trap density and diffusion potential using the measured values of σ_{iK}, V_{DK}, N_{D1} and N_{D2}. The width of the interface region (d) can be measured independently; for example, using secondary ion mass spectroscopy (SIMS), or other microscopically obtained data. Also Δx_j can be found using Fig. 15
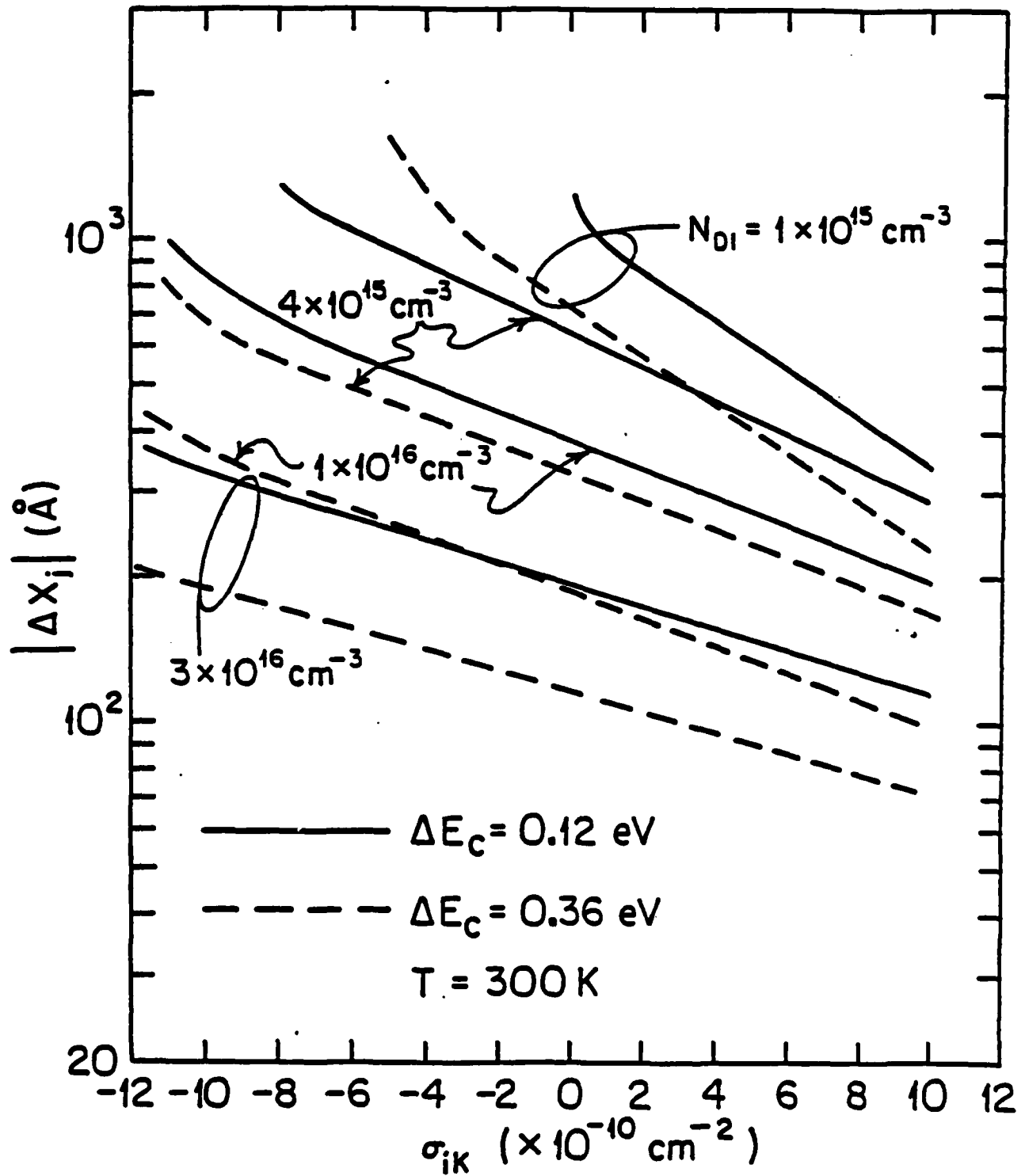
50

Fig. 15

51

where it is plotted versus both σ_{iK} and N_{D1}. These curves, which have been determined via a computer solution to Poisson's Equation assuming ΔE_c = 0.12, and 0.36 eV, are independent of N_{D2} in the range $1\times10^{15} < N_{D2} < 5\times10^{16}$ cm^{-3}. Here, each curve is obtained by specifying values of d and ΔE_c, although Δx_j is found to be relatively insensitive to d. For example, as d is varied from 50 A to 500 A, the variation of Δx_j is less than 2%. Furthermore, $|\Delta x_j|$ decreases linearly as ΔE_c increases from 0 eV to 0.5 eV, independent of doping level and interface charge density (σ_{iK}). Hence, for any value of ΔE_c within this range, the dependence of $|\Delta x_j|$ on σ_{iK} can be found by interpolation from the values shown in this figure. The error incurred by obtaining Δx_j for a particular σ_{iK} via interpolation is less than 5%. Finally, note that Δx_j is relatively insensitive to the effective conduction band density of states (N_c) of both HJ materials. For example, as N_c increases from 3×10^{17} cm^{-3} to 3×10^{18} cm^{-3}, the variation of Δx_j is only 4% (where $N_{D1} = N_{D2} = 6\times10^{15}$ cm^{-3} and $\sigma_i = 5\times10^{10}$ cm^{-2} are assumed).

Using Eq's. 17 and 18, in conjunction with Fig. 15, $V_D(0)$ and σ_i were obtained for a N-n InP/In$_{0.53}$Ga$_{0.47}$As isotype heterojunction grown by hydride vapor phase epitaxy (VPE) on (100) n$^+$-InP substrates S-doped to 5×10^{18} cm^{-3}. The first layer grown was an approximately 1 μm thick, InP buffer layer, followed by 4 μm of adventitiously doped n$^-$-In$_{0.53}$Ga$_{0.47}$As. Next, a 0.6 μm layer of S-doped N-InP was grown, and the final layer was a 1.2 μm thick, undoped N$^-$-InP cap. A rectifying organic-on-inorganic (OI) semiconductor contact was formed on the top N$^-$-InP surface using the organic compound, PTCDA. The

free carrier concentration profile for the sample which were obtained by reverse-biasing the 0I contact is shown by the solid line in Fig. 16.

SIMS data for this sample are shown in the inset of Fig. 16. From the indium and sulfur concentration profiles, the N^--InP, N-InP, and n^--$In_{0.53}Ga_{0.47}As$ layers can be identified. The heterointerface region width (cross hatched area) is inferred from the gradual drop of both the indium and sulfur concentrations at the N-InP/n^--$In_{0.53}Ga_{0.47}As$ interface. The heterointerface width is estimated from these data to be $d = (350 \pm 50)$ A.

From the free carrier concentration profile of Fig. 16, we obtain $N_{D1} = (1.00 \pm 0.02) \times 10^{16}$ cm^{-3}, $N_{D2} = (6.00 \pm 0.05) \times 10^{15}$ cm^{-3}, and $x_j^* = (1.83 \pm 0.01)$ μm. Using Eqs. 10 and 15, we calculate $\sigma_{iK} = (1.8 \pm 0.3) \times 10^{10}$ cm^{-2} and $V_{DK} = (0.21 \pm 0.01)$ V. Taking the electron effective masses of InP and $In_{0.53}Ga_{0.47}As$ as 0.07 m_0 and 0.04 m_0, where m_0 is the free electron mass, we obtain $\Delta E_{cK} = (0.22 \pm 0.01)$ eV.

Using σ_{iK} and ΔE_{cK}, we determine σ_i and ΔE_c as follows: From Fig.15, Δx_j is obtained by linear interpolation using the curve corresponding to $\Delta E_c = \Delta E_{cK}$ -- the latter value being our first best estimate for the band discontinuity energy. In this manner, we obtain $\Delta x_j = -(250 \pm 12)$A. Substituting d, Δx_j, σ_{iK} and ΔE_{cK} into Eqs. 17 and 18, we get $\Delta E_c = (0.24 \pm 0.01)$ eV and $\sigma_i = (2.7 \pm 0.4) \times 10^{10}$ cm^{-2}. More accuracy in these latter two parameters can be achieved by iteratively repeating the process, always replacing σ_i and ΔE_c in Eqs.17 and 18 with the new values of σ_i and ΔE_c thus

Fig. 16

$\Delta E_c = 0.24$ eV
$\sigma_i = 2.7 \times 10^{10}$ cm^{-2}
$d = 350$ Å

X (μm)

$n^*(x^*)$ (cm^{-3})

CONCENTRATION (at/cc)

In (arb. units)

Sulfur

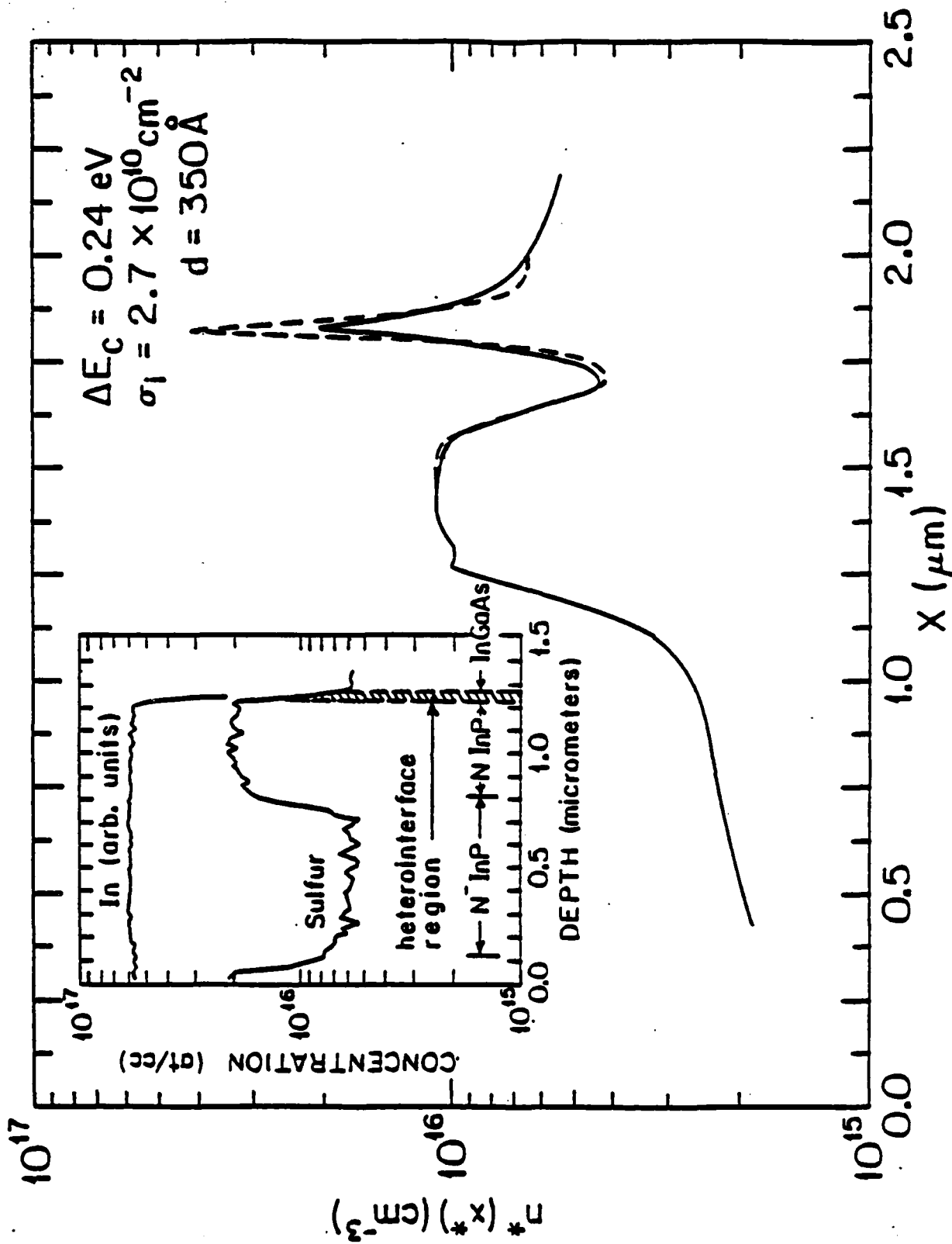heterointerface region

N$^-$ InP → N InP → InGoAs

DEPTH (micrometers)

54

obtained. The iterations are discontinued when the difference between both sides of Eq. 18 becomes small. In the present example, only a single iteration was required. Note that while ΔE_{cK} and ΔE_c differ by only 10% for this sample, σ_i is roughly twice σ_{iK}, consistent with our discussion of Fig. 14 vis-a-vis the sensitivity of this parameter to the choice of N_{D1} and N_{D2}.

The ability of Eqs. 17 and 18 to correct for the effects of fixed charge was tested further using a more extreme, albiet artificial example by assuming $N_{D1}' = 7 \times 10^{15}$ cm^{-3} for the sample in Fig.16 instead of its actual value of $N_{D1} = 1 \times 10^{16}$ cm^{-3}. In this case, we set $d = d'$ equal to the integration limit on the InP side of the HJ, thereby "assigning" the difference between N_{D1}' and N_{D1} to fixed interface charge. Following this procedure, we obtained $V_{DK} = 0.06$ V, and after two iterations using Eqs. 17, 18 and Fig. 15, we obtained, once more, the actual value of $V_D(0) = 0.23$ V and $\sigma_i' = (N_{D1} - N_{D1}')/d' + \sigma_i$. This example, although somewhat contrived, indicates the ability of the approach to achieve accurate values for ΔE_c even in the presence of a very high density of fixed charge.

In order to check the accuracy of σ_i and ΔE_c obtained for the InP/In$_{0.53}$Ga$_{0.47}$As HJ, the apparent free carrier concentration profile ($n^*(x^*)$) near the HJ was calculated assuming $\Delta E_c(0) = 0.24$ eV, $d = 350$ A and $\sigma_i = 2.7 \times 10^{10}$ cm^{-2}. This calculated $n^*(x^*)$ profile is shown by the dashed line in Fig. 16. The agreement between the experimental and calculated profiles is quite good, except that the peak value at x_j^* for the experimental data is lower. This also represents an improved fit over that which was obtained

using σ_{iK} and ΔE_{cK} inferred from Eqs. 10 and 15. We attribute the difference in peak values at x_j^* to the interfacial compositional gradient which tends to lower the measured peak due to a spatial broadening of the HJ dipole.

To our knowledge, these are the first measurements of the conduction band discontinuity energy of hydride VPE grown N-n InP/In$_{0.53}$Ga$_{0.47}$As HJ's. These data are consistent with data for MBE[20] grown samples for this same heterojunction, and furthermore, they are consistent with data for LPE grown n-N In$_{0.53}$Ga$_{0.47}$As/InP HJs[15]. This implies that the measured conduction band discontinuity energy is independent of growth sequence for (100) In$_{0.53}$Ga$_{0.47}$As/InP heterojunctions.

In summary, we have described a means for improving the measurement accuracy of the interface trap density and conduction band discontinuity energy obtained from capacitance-voltage analysis, and have used it to study hydride VPE grown InP/In$_{0.53}$Ga$_{0.47}$As HJs. This approach is especially useful for the measurement of band discontinuity energies of samples with high densities of shallow acceptor traps ($\sigma_i < 0$), or with large differences in free carrier concentrations between the contacting materials. The diffusion potential obtained from this improved C-V technique is insensitive to the variations in doping and trap density in the interface region. To our knowledge, this improved capacitance-voltage technique is the most accurate experimental means available for determining the interface trap density and band discontinuity energies of semiconductor heterojunctions.

V. The Application of the OI technique to the study of taper etched HgCdTe/CdTe heterojunctions.

CdTe and associated compounds are becoming increasingly important as a far IR detection material. Hence, in this study we investigated CdTe and HgCdTe/CdTe heterojunctions supplied by C. Jones at the Santa Barbara Research Center. During the course of these experiments, several difficulties had to be overcome, including finding a suitable organic contact for Hg-containing compounds once we discovered that PTCDA and associated compounds react with free Hg on the wafer surface, and also finding means to profile across p-n junctions and deep into very thick epitaxial layers. The details of this experiment are given below. Indeed, the experiments here were successful in that we have, for the first time, measured the energy band offsets in HgCdTe/CdTe heterojunctions by C-V techniques.

In addition, as a result of this work the OI method is now being used at Santa Barbara Research Center as a means for non-destructive wafer analysis.

In our work, the capacitance-voltage depletion method discussed in the previous section is utilized to measure the band offset of MCT HJ's. Since this technique is insensitive to compositional gradients at the heterojunction, it is particularly useful for studying liquid phase epitaxially (LPE) grown $Hg_{1-y}Cd_yTe/CdTe$ heterojunctions which can have a significant grading length due to the interdiffusion of Hg and Cd atoms at the heterointerface. Another unique property of this technique is that the band bending near the HJ can be directly and

57

unambiguosly inferred from the carrier concentration profile simply by observing the location of the carrier accumulation and depletion regions. This is different from other techniques such as XPS and photoluminescence, which can only measure the relative energy levels of the valence (or conduction) band edges of the two contacting materials.

For our experiment, a ~8 μm thick layer of p-type $Hg_{0.7}Cd_{0.3}Te$ was grown by LPE onto a (111), lightly p-type Cd(4%Zn)Te substrate, followed by a 1 μm thick n-type cap layer of $Hg_{1-y}Cd_yTe$ whose composition was y=0.4 at the p-n junction. Capacitance-voltage profiling is inherently limited in depth by the width of the depletion region at the diode breakdown voltage. For our samples this depth is approximately 3 μm from the surface, falling considerably short of the nearly 10 μm thick total layer thickness. In order to further extend the depth to which these samples were profiled, the wafer surface was taper-etched by slowly dipping it in a bromine-methanol solution[16]. Once the taper was formed, an array of OI diodes was deposited along the taper direction, and hence the profiles obtained from each diode could be assembled into a composite profile correlating a given C-V profile to the depth of that diode from the original, as-grown surface. To measure the depth of the taper as a function of position along the wafer, an array of dots was protected from the etchant using a photolithographically defined SiO_2 mask. After etching, mesas were left beneath the dots. Hence the taper depth from the original wafer surface was easily obtained using a surface profiler measurement of the mesa height.

To fabricate the OI diodes, the taper-etched sample was solvent cleaned, and then placed in a vacuum chamber with a pressure of $\sim 10^{-6}$ Torr where the pre-purified organic material was deposited at a rate of 2-3 A/s to a thickness of 500 A via vacuum-sublimation from a resistively heated source. Two organic materials, namely H_2Pc and CuPc were used to form rectifying contacts to the n and p-type MCT layers. Next, In was deposited through a shadow mask to form an array of contacts with areas of 5.5×10^{-4} cm^2. To form a contact to the MCT, an In strip was also deposited alongside the organic film directly onto the wafer surface.

Typical room-temperature bipolar current-voltage characteristics for $H_2Pc/p\text{-}Hg_{0.7}Cd_{0.3}Te$ and $CuPc/n\text{-}Hg_{0.7}Cd_{0.3}Te$ diodes are shown in the inset of Fig. 17. Since the breakdown voltage observed for the CuPc/MCT diodes is less than for the H_2Pc/MCT device are shown in Fig. 17. Soft breakdown is observed at -8V at T = 100K. Here, the breakdown voltage is defined as when the reverse dark current reaches 10 μA, and is considerably larger than the <1V breakdown observed for metal/MCT Schottky barrier diodes. Majority carrier types are deduced from the polarity of the I-V characteristics, and are consistent with the doping of the MCT layers during growth. As discussed in Sec. II, the forward characteristic is determined by thermionic emission over the OI energy barrier at low voltage, followed by space charge limited currents at high voltage. This is apparent from the I-V characteristic in Fig. 17 where the exponential increase of the current rolls off at high voltage due to space charge
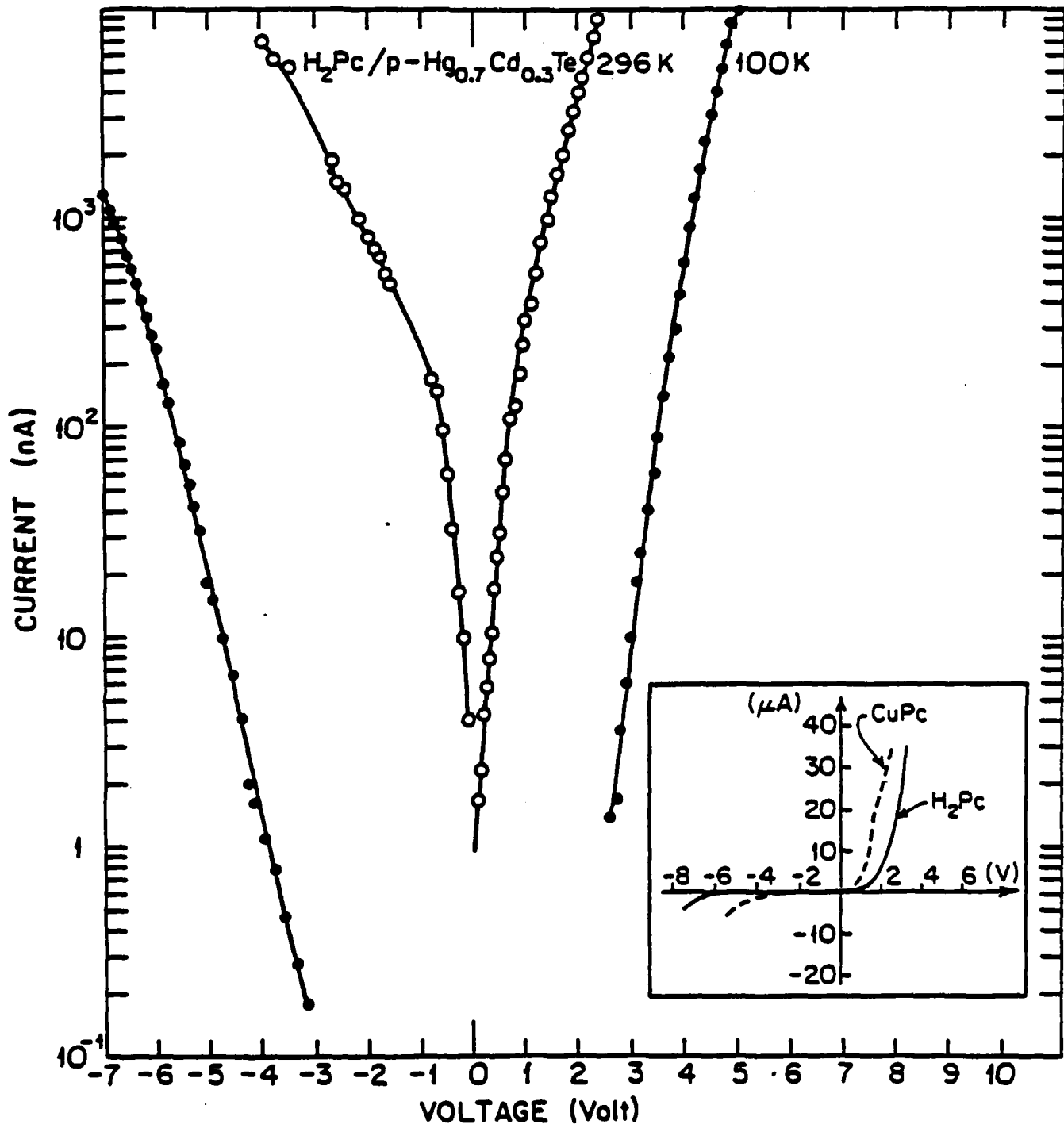
Fig. 17

60

effects. From these data we deduce a H_2Pc/p-$Hg_{0.7}Cd_{0.3}Te$ barrier energy of $\phi_B = 0.41 \pm 0.04$ V.

Carrier concentration profiles taken from diodes along the taper were obtained from C-V data measured at 1 MHz at different temperatures (down to 91 K). No appreciable temperature dependence of the carrier concentration is observed. From the room temperature profiles and the location of the dots, the composite carrier concentration profile from the top n-layer through the p-layer to the $Cd(4\%Zn)Te$ substrate is obtained as shown in Fig. 18. From the location of the peak in the concentration profile indicating the $Hg_{0.7}Cd_{0.3}Te/Cd(4\%Zn)Te$ HJ (at x_j^*), we deduce that the heterojunction between the p-$Hg_{0.7}Cd_{0.3}Te$ layer and p-$Cd(4\%Zn)Te$ substrate was located at about 8.5 μm relative to the top surface of the wafer; consistent with microscopic measurement. Further, we obtain a free carrier concentration with microscopic measurement. Further, we obtain a free carrier concentration of 1-$2x10^{16}$ cm^{-3}, $4x10^{15}$ cm^{-3} for the n-$Hg_{1-y}Cd_yTe$, p-$Hg_{0.7}Cd_{0.3}Te$ and p-$Cd(4\%Zn)Te$ layers, respectively.

The apparent free carrier concentration profile shown in Fig. 19 was measured at 91 K using a device located 6.6 μm from the original surface. From these data, we observe that holes are accumulated at the $Cd(4\%Zn)Te$ side, giving rise to a peak in $p^*(x^*)$, and depleted from the $Hg_{0.7}Cd_{0.3}Te$ side of the HJ. This implies that the band bending of both materials near the HJ is as shown in the inset of Fig. 19--i.e., the valence band of $Cd(4\%Zn)Te$ lies above that of $Hg_{0.7}Cd_{0.3}Te$ at the HJ. This is contrary to previous work indicating
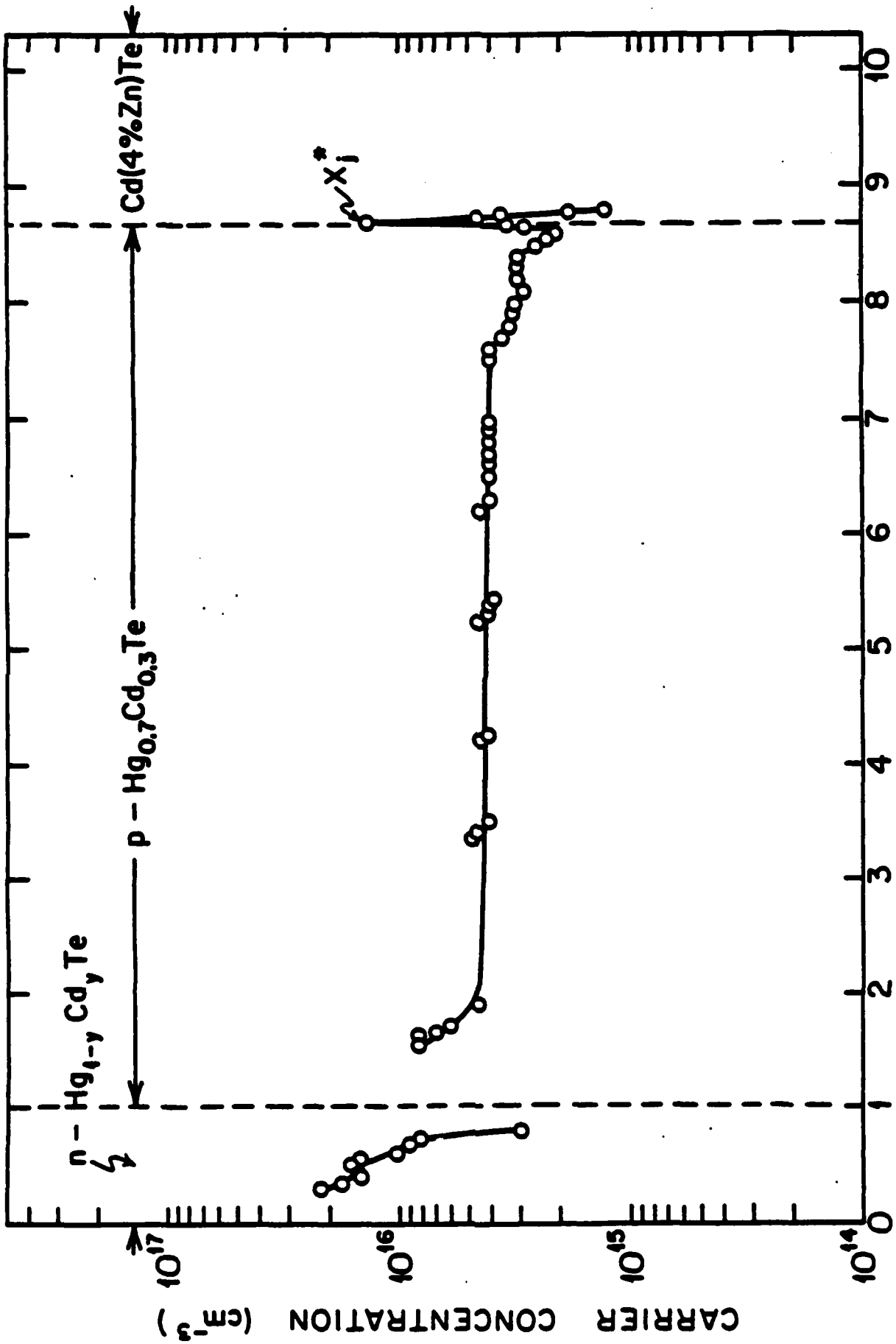
Fig. 18

62

that the valence band of CdTe is lower in energy than that of HgTe. Whereas the direction of the dipole can only be inferred in most of these measurement techniques and subject to error due to problems inherent in the data analysis, the C-V technique gives an unambiguous profile which can be simply correlated with the relative positions of the accumulation and depletion regions at the dipole. Hence, Fig. 19 gives an indication that holes are indeed accumulated at the Cd(4%Zn)Te substrate, contrary to previous expectations.

From the profile shown in Fig. 19, a valence-band discontinuity energy of (25 ± 4) meV is obtained via Eq 10 and 15. The density of fixed charge is calculated via Eq. 17, giving $\sigma = -(6.2 \pm 0.3) \times 10^{10}$ cm^{-2}. The negative sign of the fixed charge density indicates that the interface traps are acceptor-like, which might be due to the presence of Hg vacancies or impurities such as Cu, Ag and Au.

As noted above, Eqs. 10 and 15 are based on the assumptions that the apparent heterojunction depth, x_j^* (as determined from the peak position of the apparent carrier concentration profile), is equal to the actual HJ position, x_j; and that the shallow trap density σ is low enough such that it does not significantly perturb the intrinsic heterojunction dipole potential. With these assumptions lifted by using Eq. 18, the more accurate values obtained for the valence band offset ΔE_v and the fixed interface charge density are (110 ± 20) meV and $-(5.9 \pm 0.3) \times 10^{10}$ cm^{-2}, respectively.

To check the accuracy of the measured ΔE_v, the carrier concentration profile was "reconstructed" by solving Poisson's Equation using the valence-band energy ΔE_v and interface charge
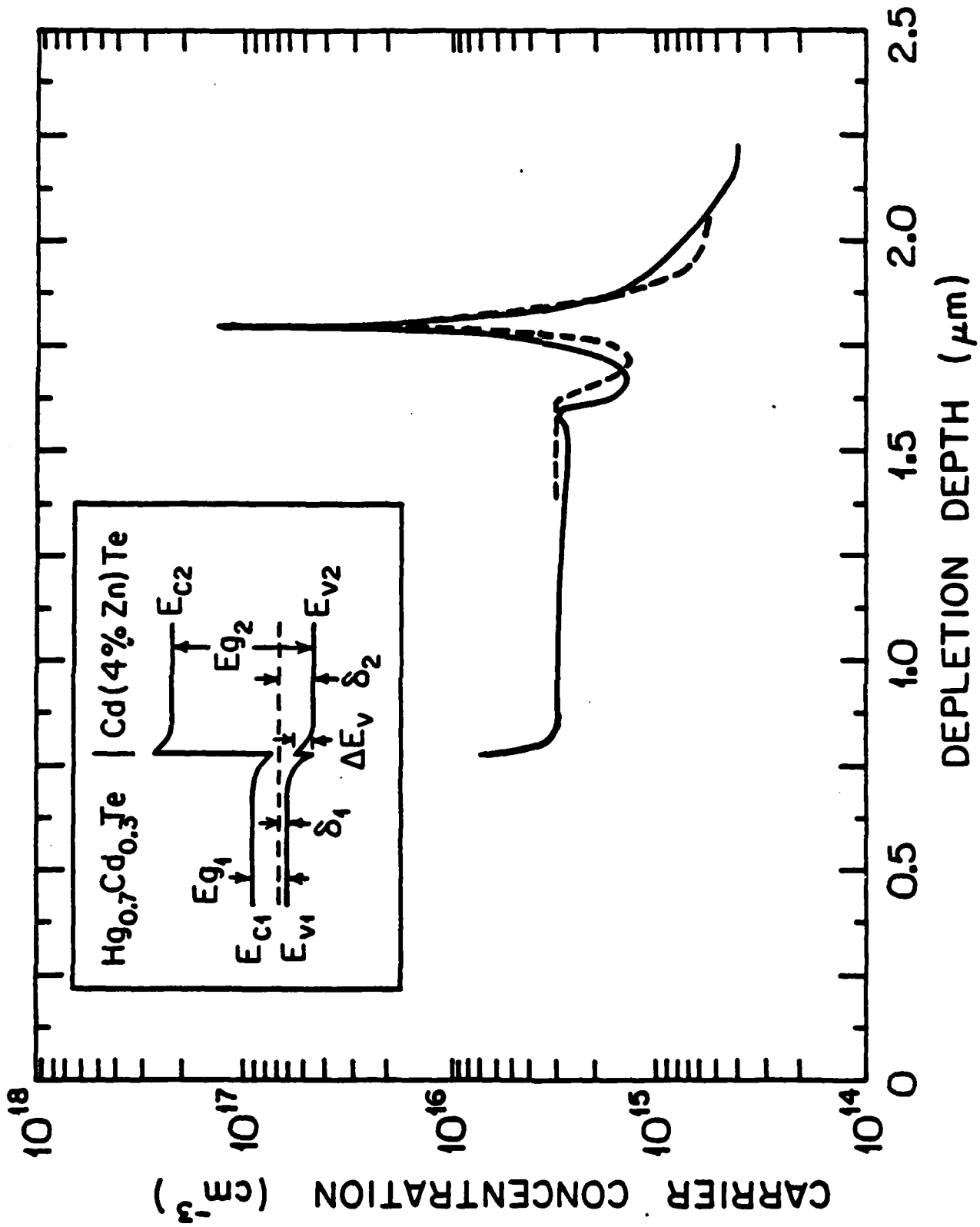
63

Fig. 19

64

density given above. Other parameters used in this simulation are given in Table III. To accomplish this fit, we assume a width for the interface region of d $\simeq$ 3000 A. We note, however, that the quality of the fit is not strongly dependent on the value of d chosen. As shown in Fig. 19, the agreement between the measured hole concentration profile and the simulation result is quite good, providing an independent check of our values for ΔE_v and σ.

VI. Conclusions

We have shown that the OI HJ structure is an extremely useful tool in the non-destructive analysis of semiconductor properties. That is, the OI device can be used to obtain detailed information regarding such materials properties as: epitaxial layer thickness and doping, bulk deep level energy and density, heterojunction band offset energies and the nature of defect states at the HJ band discontinuity, and the details of semiconductor surface states which exist on both as-grown and processed wafers. Furthermore, the OI technique can be used in combination with a wide range of semiconductors including Si, Ge, GaAs, AlGaAs, InGaAs(P), InP, HgCdTe, CdTe, GaSb and polycrystalline $CuInSe_2$. Since the organic material forms a HJ on the underlying substrate, it can be used on both n and p type materials.

In this work, we greatly increased the utility of the OI analysis technique, and applied it to the in-depth characterization of the analysis of surface reactions which occur on Si substrates. This work was made possible by developing a theory of transport

Table III

Parameters[a] Used for $Hg_{0.7}Cd_{0.3}Te/Cd(4\%Zn)Te$ Heterojunction Simulations

Quantity	Unit	Value
Energy gap (E_{g1})	eV	0.24
Energy gap (E_{g2})	eV	1.60
Effective density of states ($N_{v1}=N_{v2}$)	cm^{-3}	1.8×10^{18}
Trap region width (d)	A	3000
Doping concentration (N_{A1})	cm^{-3}	2.5×10^{15}
Doping concentration (N_{A2})	cm^{-3}	5×10^{14}

a. Subscripts 1 and 2 refer to $Hg_{0.7}Cd_{0.3}Te$ and $Cd(4\%Zn)Te$, respectively.

66

across the OI HJ which indicated that the structure could be used in obtaining surface state information across nearly the entire band gap of the underlying semiconductor being investigated. This theory also allowed, for the first time, for the measurement of the valence band offset energies between a crystalline molecular semiconductor (PTCDA) and an inorganic semiconductor (Si).

A further outcome of this theory was the prediction of a surprisingly high carrier velocity across the thin films in OI diodes. This prediction was subsequently verified in a OI photodiode which exhibited fast response to optical pulses.[17] These observations point to the possible usefulness of the OI diode in numerous, high bandwidth applications. This aspect of the OI HJ opens up an exciting and original avenue of research which we are pursuing under a current program supported by RADC.

In other work, we report the development of a method for the very accurate determination of inorganic semiconductor heterojunction band offsets using capacitance-voltage techniques which are facilitated by the OI contact. This technique provides what is possibly the most accurate method for measuring band offset energies since it can separate the potential contributions due to defect charge from that contribution due to the intrinsic HJ dipole. This technique was applied to the study of InGaAs/InP and HgCdTe/CdTe heterojunctions which were contacted by various organic films. In the case of the HgCdTe/CdTe HJ, it was found that, contrary to conventional wisdom, the band-offset symmetry suggests that this is a Type II HJ system with a staggered offset of the valence band edges.

In summary, this program has led to significant advances in the understanding and application of the OI HJ structure. We are continuing to pursue this structure as a potential solution to many long-standing optoelectronic device problems. Future research must result in a broadening of the utility of the OI structure from a purely electronic device, to a structure which makes full use of all of the interesting electronic *and optical* properties of the family of organic semiconductors exemplified by PTCDA.

VII. References

1. Most chemicals listed are available from Aldrich Chemical Co., Milwaukee, WI.

2. S. R. Forrest, M. L. Kaplan and P. H. Schmidt, J. Appl. Phys., 55, 1492 (1984) and J. Appl. Phys., 56, 543 (1984).

3. F. F. So and S. R. Forrest, J. Appl. Phys., 63, 442 (1988).

4. S. R. Forrest, M. L. Kaplan, and P. H. Schmidt, Ann Rev. Mater. Sci 17, 189 (1987).

5. A. J. Lovinger, S. R. Forrest, M. L. Kaplan, P. H. Schmidt and T. Venkatesan, J. Appl. Phys., 55, 476 (1984).

6. S. R. Forrest and F. F. So, J. Appl. Phys., 64, 399 (1988).

7. F. F. So and S. R. Forrest, Appl. Phys. Lett., 52, 1341 (1988).

8. S. M. Sze, Physics of Semiconductor Devices, 2nd Ed., Wiley, NY (1982).

9. S. R. Forrest and P. H. Schmidt, J. Appl. Phys., 59, 513 (1986).

10. H. Kroemer, Wu-Yi Chien, J. S. Harris, Jr. and D. D. Edwall, Appl. Phys. Lett. 36, 295 (1980).

11. S. R. Forrest, P. H. Schmidt, R. B. Wilson, and M. L. Kaplan, J. Vac. Sci. Technol., B4, 37 (1986).

12. W. Warta, R. Stehle, and N. Karl, Appl. Phys. A, 36, 163 (1985).

13. M. A. Rao, E. J. Caine, H. Kroemer, S. I. Long and D. I. Babic, J. Appl. Phys. 61, 643 (1987).

14. L. Y. Leu and S. R. Forrest, J. Appl. Phys., 64, 5030 (1988).

15. S. R. Forrest, P. H. Schmidt, R. B. Wilson and M. L. Kaplan, J. Vac. Sci. Technol., B4, 37 (1986).

16. J. P. Rosbeck and M. E. Harper, J. Appl. Phys. 62, 1717 (1987).

17. F. F. So and S. R. Forrest, IEEE Trans. Electron. Dev., 36, 66 (1989).

APPENDIX A

Reprints of Papers Published

Under Program Sponsorship

Dependence of the electrical characteristics of organic-on-inorganic semiconductor contact barrier diodes on organic thin-film composition

F. F. So and S. R. Forrest

Departments of Materials Science and Electrical Engineering/Electrophysics, University of Southern California, Los Angeles, California 90089-0241

Several aromatic compounds (such as 3,4,9,10 perylenetetracarboxylic dianhydride) have previously been reported to form rectifying heterojunction energy barriers when vacuum deposited onto inorganic semiconductor substrates such as Si, GaAs, and InP. In this paper we report the formation of rectifying heterojunction barriers using phthalocyanine-based compounds layered onto p-Si substrates. In many respects, the characteristics of phthalocyanine/Si heterojunctions are similar to those formed using the aromatic anhydrides insofar as the electrical properties can be explained using the thermionic emission space-charge-limited transport model introduced in previous work. However, in contrast to the earlier results, we find that a high density of surface states exist at the phthalocyanine/Si interface. Quantitative study of the interface state density provides insight into the mechanisms of formation of the organic-on-inorganic energy barrier.

I. INTRODUCTION

Recently, it has been shown that when certain organic semiconductors, such as 3, 4, 9, 10 perylenetetracarboxylic dianhydride (PTCDA), are deposited onto inorganic semiconductor substrates such as Si[1,2] or InP,[3] a rectifying energy barrier is formed at the organic-inorganic (OI) interface. Transport of charge[2] across the energy barrier is limited at low-current density ($J < 100$ mA/cm^2) by thermionic emission, while at higher current density, the current-voltage (I-V) characteristics are determined by space-charge injection from the metallic ohmic contacts into the crystalline organic thin film. The energy barrier limiting charge transport has been found to range from approximately 0.55 eV in InP-based compounds,[3] to 0.85 eV on GaAs,[4] and is often observed to exceed values obtained for conventional metal/semiconductor contacts.[5] The resulting rectifying characteristics of OI diodes, which are similar to those typical of ideal p-n junctions, have been attributed to the low reactivity of the deposited organic species, along with the low energy associated with the deposition of the thin films.[3] These factors allow for the formation of an OI heterojunction barrier with relatively little perturbation of the initial surface of the underlying semiconductor as compared with surface damage induced during the formation of conventional metal/semiconductor contacts.[6]

To test this hypothesis, and to gain a deeper understanding of the transport mechanisms governing the OI heterojunction characteristics, it is important to examine the role that the organic thin film plays in determining the electrical properties of the OI diode. In previous work,[2] it has been pointed out that the criteria for identifying organic materials which will form contacts with inorganic semiconductors such that current transport across the interface is limited by thermionic emission and space-charge injection (the TE-SCL model) are as follows: (1) The organic molecules must form stacks such that the individual molecules in the stack are closely spaced. In this way, the hybrid pi orbitals will overlap to the extent that carriers moving along the stack axis are highly delocalized as predicted by tight-binding theory. In other words, high mobility organic materials are required such that thermionic emission over the organic-inorganic heterojunction energy barrier will dominate at low-current densities. At high currents, the film resistance is dominant, thereby giving rise to SCL behavior. (2) Appropriate metal contacts must be available such that ohmic contact to the organic film allows for the injection of carriers from the external circuit. In past work, we have found that the highly stable perylene-based and naphthalene-based dianhydrides such as PTCDA and 3,4,7,8 naphthalenetetra-carboxylic dianhydride (NTCDA) follow at least these few criteria and hence form rectifying contacts when deposited onto many inorganic semiconductor substrates. With the exception of polymeric OI heterojunctions,[7] there have been no reports of OI heterojunctions having been formed using non-polymeric organic materials outside of this narrow class of aromatic dianhydride dye compounds. This has limited both the usefulness of the OI barrier, as well as the progress made in understanding the mechanisms involved in its formation.

In this work we report the fabrication of similar OI contact barrier diodes using phthalocyanine-based compounds (Pc's) deposited onto Si substrates. The Pc's are a technologically interesting class of dye compounds in that they are considered potential candidates for photovoltaic cell applications.[8-10] Hence, their broad range of structural, optical, and electronic properties have been intensively studied over the past several years.[11,12] These crystalline materials form infinite stacks when deposited in vacuum.[13] Furthermore, using appropriate metals, it has been possible to form ohmic contacts to the Pc surface. Thus, these materials fulfill the minimum criteria necessary for observing TE-SCL transport across OI heterojunctions. In this work we report on the formation of OI barriers using two members of this broad class of compounds—specifically metal-free Pc (H$_2$Pc) and copper Pc (CuPc). Our results suggest that the presence of

the relatively weakly bound central ligand atoms in the Pc molecular core might be responsible for a significantly higher density of surface states induced at the OI interface than are apparent for perylene and naphthalene-based OI heterojunctions. Indeed, the deposition of CuPc induces the highest density of surface states yet observed in OI diodes, suggesting that chemical bonding of Cu to the Si surface atoms occurs at the OI interface. These observations clarify our understanding of the mechanisms involved in determining the OI heterointerface energy barrier height.
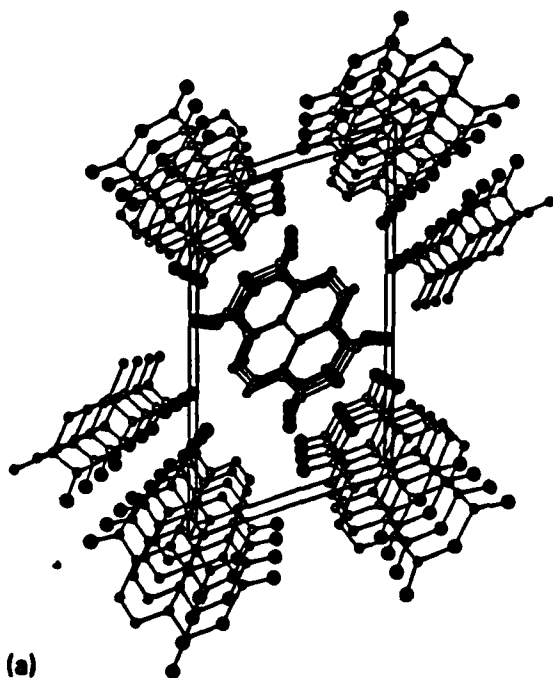
II. THEORY

The crystal and molecular structures of two (NTCDA and CuPc) of the four compounds studied in this work are shown in Fig. 1. We note that the structure of PTCDA has been published elsewhere,[14] whereas the structure of H_2Pc is similar to that of CuPc except that the Cu atom is replaced by two hydrogen atoms.[12] From the figures, it is apparent that the molecules form stacks which maximize the overlap of the pi systems between adjacent molecules in the stack. This accounts for the relatively high free-carrier mobilities of these compounds, ranging between 10^{-2} cm^2/V s for NTCDA to > 1 cm ^{2}/V s for PTCDA. An exception to this is H_2Pc, where a relatively low mobility[13] of 10^{-3} cm^2/V s is attributed to the reduced pi-orbital overlap resulting from the alignment of the H atoms in one molecule over the N rings in the adjacent molecule. Furthermore, charge transport between adjacent stacks in all the molecules studied is inhibited by the lack of overlap in the direction transverse to the stacking axis. These several structural characteristics result in improved confinement of charge transport to the region directly under the contact electrode.

Details regarding the molecular structure and the stacking habits of the deposited films are given in Table I. In this table, θ is the angle between the plane of the molecules and the substrate surface, and d is the minimum intermolecular stacking distance. Due to the molecular stacking, charge is readily transported from the ohmic contact metal, through the organic layer, across the OI barrier and into the inorganic semiconductor substrate. This results in a current density limited by thermionic emission (J_{TE}) over the OI barrier at the low-current densities achieved at small forward bias and under reverse bias. At higher current densities attained at moderate forward bias voltages and under reverse breakdown conditions, the current is space-charge injection limited (J_{SCL}). As has been discussed elsewhere, the current density-voltage (J-V) characteristics[2] are described by the following set of simultaneous equations:
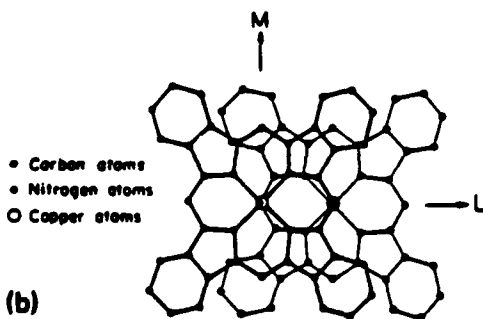
$$J_{TE} = J_0[\exp(qV_b'/nkT) - 1],\qquad (1)$$

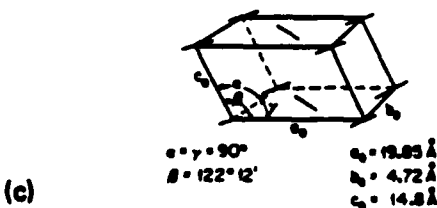$$J_{SCL} = -\tfrac{9}{8}\kappa_0\mu V_0^2/t^3,\qquad (2)$$

with $J_{TE} = J_{SCL}$ and $V_a = V_0 + V_b'$. Here, kT is the Boltzmann energy at temperature T, J_0 is the saturation current

(a)

(b)

• Carbon atoms
• Nitrogen atoms
O Copper atoms

M ↑

←L

(c)

$\alpha = \gamma = 90°$ $a_0 = 19.85$ Å
$\beta = 122°12'$ $b_0 = 4.72$ Å
                      $c_0 = 14.8$ Å

FIG. 1. (a) The crystal and molecular structure of 3,4,7,8 naphthalenetetracarboxylic dianhydride (NTCDA). Open circles are carbon atoms and filled circles are oxygen atoms. (b) Normal projection of two CuPc molecules. Heavy lines outline the upper molecule; light lines outline the underlying molecule. L and M are the molecular axes of the upper molecule. (c) Positions of phthalocyanine molecules in the base-centered monoclinic crystal. The short line segments indicate the orientation of the molecular axes (Ref. 10).

TABLE I. Materials properties of organic compounds.

	PTCDA[a]	NTCDA	CuPc[b]	H_2Pc[b]
Interplanar spacing, d(Å)	3.21	3.506	3.38	3.4
Stacking habit				
Stacking angle (θ)	11°	0°	0°,20°	0°,20°

[a] Data taken from Ref. 2.
[b] Data taken from Refs. 11 and 12.

443   J. Appl. Phys., Vol. 63, No. 2, 15 January 1988

F. F. So and S. R. Forrest   443

72

density which is proportional to $\exp(-q\phi_s/kT)$, where q is the electronic charge, and ϕ_s is the OI heterojunction band discontinuity energy, μ is the carrier mobility, κ_0 is the permittivity, and t is the thickness of the organic film. Finally, V_a is the total externally applied voltage, V_0 is the voltage dropped across the organic layer, V_D' is the voltage dropped across the inorganic layer depletion region and any interfacial layer which might exist, and n is a number greater than unity. Substrate series resistance has been neglected.

III. EXPERIMENT

The devices studied in this work were fabricated as follows: First, it was necessary to identify appropriate metals useful in forming ohmic contacts to the organic thin-film. For this purpose, a symmetrical metal/organic/metal thin film device was fabricated by depositing an approximately 2000-Å-thick metallic layer onto a precleaned glass substrate. This was immediately followed by the deposition via vacuum sublimation of approximately 1000 Å of the prepurified[14] organic film across the entire metal/substrate surface. The vacuum prior to thin-film deposition was $<2\times10^{-6}$ Torr. Finally, contact dots using the same metal as that used for the full area back contacts were deposited through a shadow mask placed onto the organic thin film. To test whether the metal formed a blocking (Schottky) or ohmic contact, the J-V characteristics were tested by applying a potential between the top and back metal electrodes. Only those metals which exhibited linear J-V characteristics over a range of at least $0 < V < 0.2$ V, and whose specific resistance was nominally less than 5×10^{-3} Ω cm^2 were considered acceptable for further investigation.

Once the ohmic contact metal and deposition parameters were established, the OI diode was fabricated using (100) p/p^+ epitaxial Si wafers. The resistivity of the p layer was roughly 5 Ω cm. Details of the fabrication of the OI diodes have been described elsewhere.[14] After back contact deposition, the top wafer surface was degreased and then dipped for 1 min in a 1:1 deionized (DI) water:30% HF solution to remove surface oxides. The wafer was then thoroughly rinsed in DI water, blown dry in filtered nitrogen, and quickly inserted into the vacuum system for a full surface organic thin film deposition. Typically, between 100- and 1000-Å-thick films were used. The final step was to de-
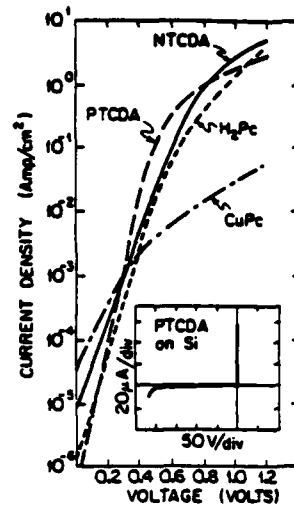
TABLE II. Characteristics of several organic/p-Si diodes.

	PTCDA	NTCDA	CuPc	H$_2$Pc
Thickness[a] (Å)	1000	150	300	200
Ohmic contact metal	In	In	Au	Au
ϕ_s (V)	0.78 ± 0.01	0.71 ± 0.02	0.67 ± 0.02	0.77 ± 0.01
n	1.45 ± 0.1	2.4 ± 0.1	3.2 ± 0.2	2.0 ± 0.1
$(D_{ss})_{max}$ (cm^{-2} eV^{-1})	2×10^{12}	2×10^{12}	2×10^{14}	8×10^{12}

[a] Refers to organic layer thicknesses employed for OI diodes discussed in Figs. 2 and 3, and in text.

FIG. 2. Forward-biased current density vs voltage (J-V) characteristics of organic/p-Si devices taken at room temperature. For comparison, J-V data for PTCDA, NTCDA, H$_2$Pc, and CuPc-based devices are shown. Inset: Bipolar I-V characteristics of an In/PTCDA/p-Si diode.

posit the 0.027-cm-diam ohmic metal dot contact using a procedure similar to that used in fabricating the metal/organic/ metal test structures. Specific layer thicknesses and contact metals used in the study are listed in Table II.

Typical bipolar current-voltage (I-V) characteristics of an In/PTCDA/p-Si diode are shown in the inset of Fig. 2. As in previous work,[2] the OI diode characteristics exhibit exponentially increasing forward current characteristics, as well as low reverse-bias leakage currents until avalanche breakdown in the Si substrate occurs at $V_a = 200$ V. The characteristics of the OI diodes using the three other organic materials investigated are qualitatively similar as shown in Fig. 2. Here, the TE-limited regime is clearly apparent from the region where the current increases exponentially with applied voltage. At higher voltage, the rate of increase in current decreases due to space-charge injection into the thin film. Using Eq. (1), we can obtain the n value and OI barrier height. These values for the four materials under investigation are listed in Table II. It is apparent that the lowest n value and highest barrier are 1.45 and 0.78 V, respectively, for PTCDA. On the other hand, n values as high as 3.2 for CuPc are obtained indicating a high density of OI heterointerface states. However, due to the low forward bias at which the current through CuPc becomes space-charge-limited, the n value thus obtained is subject to significant error. Furthermore, we point out that the barrier heights measured from the J-V characteristics of devices with n values significantly greater than 1, as in the case of CuPc and NTCDA, should not be considered to be accurate. That is, the apparent ϕ_s value obtained from I-V data is reasonably accurate only if the density of interface states and thin-film resistivity is small. As pointed out earlier,[15] a high interface state density will result in $n \gg 1$. We therefore suspect that the CuPc/p-Si interface has a considerably higher number of defects than that observed for the more ideal PTCDA/Si interface.

The details of the interface state density can be more quantitatively understood via analysis of the 1-MHz capacitance-voltage (C-V) characteristics shown in Fig. 3(a). These characteristics are measured over the range $0.2 > V_a$

73

$$D_{ss} = \frac{\kappa_i}{q\delta_{ss}}\left(1 + \frac{tg_0}{\sigma_p} - \frac{\partial V_a}{\partial V_D} + \frac{\kappa_s}{\kappa_i}\frac{\delta_{ss}}{W(V_D)}\right). \qquad (3)$$

Here, δ_{ss} is the thickness of the interfacial layer existing between the two semiconductors and consists of semiconductor oxides and possibly a region where chemical bonds have formed between the organic and inorganic materials. Further, κ_i is the permittivity of the interfacial layer, g_0 is the conductance of the OI barrier; σ_p is the organic layer conductivity; and $W(V_D)$ is the depletion region width at voltage $V_D = V'_D/n$, and $\partial V_a/\partial V_D$ is obtained from C-V and conductance data as discussed elsewhere.[15] Using these data, the interface state density can be obtained as a function of voltage; and hence the dependence of D_{ss} on energy within the semiconductor band gap can be inferred. In Fig. 3(b) we show the results of such analysis for the four OI diodes studied. The relative differences between PTCDA and NTCDA and the Pc's are readily apparent. For example, the surface-state densities of the former compounds are at a relatively low value of approximately $10^{12}/(\text{cm}^2\,\text{eV})$, whereas the CuPc sample has a very pronounced peak in surface state density at 0.7 eV above the valence-band maximum. This peak is nearly two orders of magnitude higher than the background values of $10^{12}/(\text{cm}^2\,\text{eV})$. Although a similar peak exists for the H_2 Pc sample, its magnitude is considerably less than that observed for CuPc.

IV. DISCUSSION AND CONCLUSIONS

One potential mechanism which explains the existence of the high surface state density observed at the CuPc/p-Si interface involves reactions between water and CuPc. Adsorption of water onto the semiconductor surface can readily occur via diffusion through the ~ 30 Å (Ref. 2) gaps between adjacent Pc stacks. The water diffusion into the thin film can occur when the OI diodes are exposed to the laboratory environment. Note that it has already been found that exposure of CuPc/metal Schottky barrier devices to oxygen[15] and hydrogen[16] has a significant influence on their electrical characteristics. Once at the OI interface, the water molecule can react with CuPc to form H_2 Pc and CuO. Such a reaction might occur via

$$H_2O + CuPc \rightleftharpoons H_2Pc + CuO. \qquad (4)$$

Given the Gibb's free energies (ΔG°s) of CuO and H_2 O and assuming the difference in ΔG°s between H_2 Pc and CuPc is approximately equal to the free-energy difference between H–N and Cu–N bonds, then $\Delta G^\circ = -66.2$ kcal/mole for the above reaction. Since $\Delta G^\circ < 0$, the possibility for the reaction above to occur is favorable. The CuO molecules thus formed can diffuse through the thin surface SiO_2 and participate in the following reaction:

$$2CuO + Si \rightleftharpoons SiO_2 + 2Cu. \qquad (5)$$

Here $\Delta G^\circ = -143$ kcal/mole, indicating that this reaction, too, is probable. It should be noted that a similar mechanism was proposed by Fan and Faulkner[17] to account for the change of the electrical characteristics of the Al/H_2 Pc Schottky barrier diode exposed to atmosphere. They suggested that the change in short-circuit photocurrent in the diodes was due to the oxidation of the Al electrode. In the
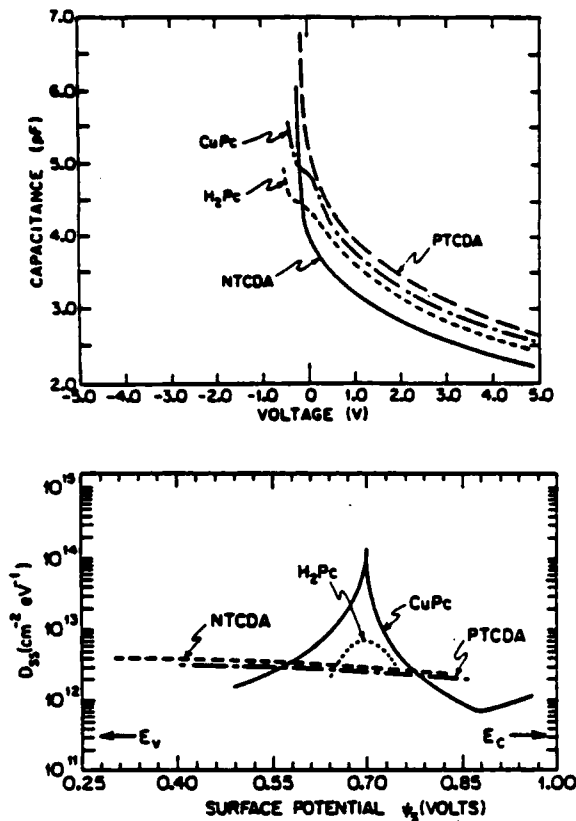
FIG. 3. (a) Capacitance-voltage (C-V) characteristics near $V_a = 0$ of four OI diodes employing the same organic materials as those discussed in Fig. 2. (b) Density of interface states (D_{ss}) as a function of surface energy (ψ_s) in the p-Si band gap for the four diodes in (a). Here, D_{ss} is obtained from analysis of capacitance and conductance data. The energy is with respect to the conduction (E_c) and valence (E_v) band edges of the Si substrate.

> -5 V, where $V_a > 0$ indicates forward bias. Over this voltage range, the conductance of the OI diode is smaller than the susceptance which is nearly purely capacitive.[15] While the detailed nature of the C-V characteristics near $V_a = 0$ V varies somewhat from device to device around a wafer, it is, nevertheless, immediately apparent that the C-V characteristics of the dianhydride-containing compounds (PTCDA and NTCDA) are qualitatively different than those obtained for the phthalocyanines. For example, the data for PTCDA and NTCDA indicate a smooth, monotonic decrease in capacitance with increasing reverse voltage. This is characteristic of OI diodes with a low density of interface states. In contrast, the curves for both H_2Pc and CuPc show a small but pronounced step near $V_a = 0$ V. Features of this nature have been shown (cf., Fig. 11, Ref. 15) to be due to the existence of a high density of charged defect states at the OI interface, which tend to screen the externally applied potential from the semiconductor bulk. Indeed, it has been shown[15] that these data can be used to quantitatively determine the distribution of charged interface states (D_{ss}) within the inorganic semiconductor band gap by applying an analysis technique analogous to that used for metal-insulator-semiconductor structures. Thus, the interface state density is approximately given by

445   J. Appl. Phys., Vol. 63, No. 2, 15 January 1988

F. F. So and S. R. Forrest   445

74

case of Au/CuPc/Si, however, it is unlikely that Au is oxidized and, therefore, the top metal contact should be stable in the laboratory environment. On the other hand, the silicon surface readily forms a native oxide. Hence, free copper atoms and Cu-O-Si complexes can be formed at the CuPc/Si interface, giving rise to the high surface state density near the midgap energy. These states have the effect of pinning the surface Fermi level at the peak in charge density near ϕ_B = 0.7 V. To our knowledge this is the first case in which a crystalline organic semiconductor has been found to perturb the OI interface to the extent that the energy barrier is pinned at the extrinsically induced defect levels.

An analogous sequence of reactions can also occur in the case of H_2 Pc, whereby the molecule is oxidized, liberating hydrogen which then forms Si-OH complexes at the SiO_2/Si interface. Such complexes can exist in a charged state which, in turn, pins the Fermi level. Although the details of such reactions are as yet not established, we emphasize here that, in general, the surface state densities at the midgap energy observed for the Pc's significantly exceeds that observed for the dianhydrides [Fig. 3(b)] suggesting that surface reactions are taking place in the former class of compounds. The mechanisms proposed in Eqs. (4) and (5) indicate that these reactions are energetically favorable.

Integrating the area under the peak in Fig. 3(b), we estimate that the total number of surface states, at the CuPc/Si interface is $\sim 5 \times 10^{11}$/cm^2. Since a CuPc molecule has an area of ~ 100 Å^2, the number of CuPc molecules that are contributing to the reactions postulated by Eqs. (4) and (5) is about 0.5%. This model suggests that the surface-state density of the Pc/Si interface is sensitive to the environment. On the other hand, in the case of PTCDA and NTCDA, the C = O bond in the anhydride groups, as well as the core C = C bonds are extremely stable (with bond energies of — 532 kcal/mole for the C = O bond, for example). Hence, it is unlikely that reactions will occur between these compounds and the underlying Si or SiO_2 surface. For this reason, we have been unable to detect a large density of surface states after the deposition of these latter thin-film materials. In fact, the "background" surface-state density that is observed for the dianhydrides may be due to the presence of a thin native oxide film rather than having been induced by the deposition of the organic compound. For example, typical values of D_{ss} observed at the native oxide/Si interfaces have been found[18] to be on the order of 10^{12}/(cm^2 eV). It should be noted that this value is about the same for grown thin oxides (> 40 Å) whose D_{ss} value is generally higher than for thicker oxides.[19,20] In contrast, earlier work has shown that the background surface state densities measured for InP and related compounds[3] can be as low as 8×10^{11}/(cm^2 eV), indicating a highly nondestructive contact using PTCDA on many semiconductor substrates.

In conclusion, we have shown that an entirely new class of stable, crystalline aromatic dye compounds—the phthalocyanines—form rectifying barriers when vacuum-deposited onto inorganic semiconductor substrates such as Si. This result extends the range of optical and electronic properties of the organic materials which can be utilized in novel organic-on-inorganic semiconductor heterojunction devices. We find that the electrical characteristics of the Pc-based devices are consistent with previous theories used to describe the performance of dianhydride-based structures. Thus, the devices exhibit exponentially increasing I-V characteristics under forward bias, whereas the reverse-bias attainable is limited only by avalanche breakdown in the underlying inorganic semiconductor material.

Unlike the anhydrides, however, the Pc's (and, in particular, CuPc) appear to interact strongly with the inorganic semiconductor surface. This interaction results in a high density of interface states which pin the surface Fermi energy in the inorganic semiconductor band gap, thereby determining the magnitude of the OI barrier energy. While this extrinsic phenomenon may also be responsible for determining the OI barrier height for the anhydrides, it has not yet been possible to observe a surface-state spectrum which might support the existence of strong organic-inorganic chemical interactions and bond exchange, as has been proposed for the phthalocyanines.

ACKNOWLEDGMENTS

[1]S. R. Forrest, M. L. Kaplan, P. H. Schmidt, W. L. Feldman, and E. Yanowski, Appl. Phys. Lett. 41, 90 (1982).

[2]S. R. Forrest, M. L. Kaplan, and P. H. Schmidt, J. Appl. Phys. 56, 543 (1984).

[3]S. R. Forrest, M. L. Kaplan, and P. H. Schmidt, J. Appl. Phys. 60, 2406 (1986).

[4]S. R. Forrest, M. L. Kaplan, P. H. Schmidt, and J. M. Parsey, Jr., J. Appl. Phys. 58, 867 (1985).

[5]P. H. Schmidt, S. R. Forrest, and M. L. Kaplan, J. Electrochem. Soc. 133, 769 (1986).

[6]W. E. Spicer, P. W. Chye, P. R. Skeath, C. Y. Su, and I. Lindau, J. Vac. Sci. Technol. 16, 1422 (1979).

[7]M. Ozaki, D. Peebles, B. R. Weinberger, A. J. Heeger, and A. G. MacDiarmid, J. Appl. Phys. 51, 4252 (1980).

[8]C. W. Tang, Appl. Phys. Lett. 48, 183 (1986).

[9]N. Yamamoto, S. Tonomura, and H. Tsubomura, J. Appl. Phys. 52, 5705 (1981).

[10]R. O. Loutfy, J. H. Sharp, C. K. Hsiao, and R. Ho, J. Appl. Phys. 52, 548 (1981).

[11]K. J. Hall, J. S. Binham, and L. E. Lyons, Aust. J. Chem. 31, 1661 (1978).

[12]S. R. Harrison and J. M. Assour, J. Chem. Phys. 40, 365 (1964).

[13]R. S. Kirk, Mol. Cryst. 5, 211 (1968).

[14]S. R. Forrest, M. L. Kaplan, and P. H. Schmidt, J. Appl. Phys. 55, 1492 (1984).

[15]S. R. Forrest and P. H. Schmidt, J. Appl. Phys. 59, 513 (1986).

[16]N. Yamamoto, S. Tonomura, and H. Tsubomura, J. Appl. Phys. 52, 5705 (1981).

[17]F.-R. Fan and L. R. Faulkner, J. Chem. Phys. 69, 3334 (1978); 69, 3341 (1978).

[18]M. C. Card and E. H. Rhoderick, J. Phys. D 4, 1589 (1971).

[19]J. Maserjian and N. Zamani, J. Appl. Phys. 53, 559 (1982).

[20]S. K. Lai, Electrochem. Soc. Proc. 81-5, 416 (1981).

446   J. Appl. Phys., Vol. 63, No. 2, 15 January 1988

F. F. So and S. R. Forrest   446

75

Organic-on-inorganic semiconductor heterojunctions: Energy-band discontinuities, quasi-Fermi levels, and carrier velocities

S. R. Forrest and F. F. So

Departments of Electrical Engineering and Materials Science, University of Southern California, Los Angeles, California 90089-0241

Organic-on-inorganic semiconductor heterojunctions (OI-HJs) exhibit rectification whereby the current-voltage characteristics are limited by the properties of the inorganic semiconductor substrate and the magnitude of the energy barrier at the heterointerface. In this paper we calculate the potential distribution and the quasi-Fermi level energy (or imref) across the OI diode bulk. Both ohmic as well as space-charge-limited conduction regimes of the organic thin film are considered. Previous work considered the OI-HJ to be similar to a Schottky, metal-semiconductor contact. While this can give a good approximation to OI-HJ transport processes under some bias regimes, it results in a misleading picture of the position of the imrefs under reverse bias, as well as errors in measurements of the band discontinuity energy at the OI-HJ. Unlike Schottky contacts, the imref in the OI diode is flat throughout the substrate under both low forward *and* reverse biases. These results are used to calculate carrier velocities within the organic film. The hole velocity is in the range of 100–2000 cm/s under reverse bias and is as high as 10^5 cm/s under forward bias. Experimental measurements of the energy-band discontinuities are presented that are in agreement with the predictions of the current-voltage model.

I. INTRODUCTION

The study of semiconductor heterojunctions has been a topic of great interest due to their ubiquitous use in numerous optical and electronic devices.[1] Indeed, the advent of optoelectronic devices employing multiple quantum-well heterojunction structures has led to entirely new classes of physical phenomena. This has resulted in the development of devices which perform highly complex and novel functions impossible to achieve with homogeneous semiconductor materials. Central to our utilization of these semiconductor-semiconductor contacts is the ability to accurately measure the magnitude of the energy-band discontinuities at the heterointerface.

Recently, investigations of a new class of heterojunctions, i.e., organic-on-inorganic semiconductor heterojunctions (OI-HJ), have attracted some interest[2,3] due to both the unusual nature of these contacts as well as to the potential new devices to which these heterojunction contacts can be applied. In particular, crystalline molecular semiconductors exhibit rectification when vacuum deposited onto inorganic semiconductor substrates,[2] and hence both the forward and reverse current-voltage characteristics exhibit properties limited by the magnitude of the OI-HJ band discontinuity and the properties of the bulk inorganic semiconductor material. As with fully inorganic semiconductor heterojunctions, it is essential that the energy-band discontinuities at the heterointerface be accurately determined in order that the mechanisms of charge transport across the energy barriers be fully understood. In the case of molecular semiconductor/inorganic-semiconductor heterojunctions, this has been done by analysis of room-temperature current-voltage characteristics, whereby an "apparent" barrier energy is measured which is generally larger than half the band gap of the underlying inorganic substrate.

In addition to determining the barrier height, it is important to understand the nature of the charge transport across the OI-HJ barriers. To do this, two essential quantities must be studied; the position of the nonequilibrium, or quasi-Fermi levels, and the carrier velocities throughout the heterojunction region. These quantities are of particular interest since a technique has been proposed whereby the surfaces of inorganic semiconductors such as InP, GaAs, and Si, can be electrically studied for the existence of surface states via the analysis of the quasistatic admittance properties of organic-on-inorganic heterojunction structures. The so-called semiconducting organic-on-inorganic surface analysis spectroscopic (or SOISAS) technique[4] is based on the assumptions that:

(1) The majority-carrier quasi-Fermi level at the OI-HJ is flat for small forward and reverse voltages. Quantitatively, this criterion should be loosely adhered to at applied voltages $|V_a| < E_g/2q$, where E_g is the band-gap energy of the inorganic semiconductor substrate and q is the electronic charge.

(2) The magnitude of the OI-HJ energy barrier is known to reasonable accuracy.

This technique was first applied[5] to InP and $In_{0.53}Ga_{0.47}As$ to evaluate the effects that various surface treatments have on the density of surface states. More recently, it has also been applied to Si as a means of determining whether various crystalline organic materials, such as 3,4,9,10 perylenetetracarboxylic dianhydride (PTCDA) and copper phthalocyanine (CuPc) react strongly with semiconductor surfaces.[6]

It is the purpose of this paper to calculate the potential distribution across all regions of the OI-HJ (Sec. II). This treatment departs from previous work in that (i) both ohmic and space-charge-limited (SCL) current regimes are consid-

76

ered in the organic thin film, and (ii) the effects of diffusion and drift in the thin film and substrate are discussed. These results are then used to determine the OI-HJ valence-band discontinuity energy between PTCDA and various inorganic semiconductors which heretofore has not been possible using previously reported "apparent" barrier energies. Data from several experimental tests of this theory are presented. In Sec. III we calculate the carrier velocities across the OI-HJ barrier. This is useful in understanding both the temporal response of the HJ, as well as in determining the majority-carrier quasi-Fermi level across the diode bulk, as is done in Sec. IV. In Sec. V we present conclusions concerning the implications of these results.

II. OI-HJ POTENTIAL DISTRIBUTION AND THE ENERGY-BAND DISCONTINUITIES

An OI-HJ device consists of a polycrystalline organic thin film vacuum deposited onto the polished surface of an inorganic substrate.[7] Typically, the organic film is between 100 and 5000 Å thick and can be layered onto either p- or n-type substrates with similar results. Metallic ohmic contacts are then made to both the organic and inorganic materials to complete the two-terminal device. It is observed that a rectifying heterojunction barrier is formed between certain crystalline organic dianhydrides (such as lightly p-type PTCDA) and many inorganic semiconductors. These heterojunction energy barriers determine the current-voltage characteristics of the complete device structure.

In analyzing charge transport across the OI-HJ barrier, we assume that the current in OI diodes is limited at low current levels by thermionic emission (TE) over the OI heterojunction band discontinuity, and at low bias by a combination of ohmic and trap-free space-charge-limited transport through the organic layer.[7] A band diagram of an isotype OI-HJ diode (assuming a ~-type substrate) with a valence-band discontinuity energy of ΔE_v is shown in Fig. 1.

The potential distribution and the electric field (E) within the organic film are determined as a function of position (x) using Gauss' law. Thus, assuming single carrier (hole) injection:

$$\frac{dE}{dx} = \frac{q[p(x) - p_0]}{\kappa_0},$$ (1)

where κ_0 is the permittivity of the organic thin film, p_0 is the free-hole concentration, and $p(x)$ is the total hole concentration consisting of the sum of p_0 and holes injected (p_{inj}) from the contact at $x = 0$. Assuming a constant mobility (μ_p) at small E, the current density within the film is

$$J = qp(x)\mu_p E(x),$$ (2)

which, via charge conservation, is independent of position (assuming no charge trapping). These equations have the following solution[8] for the voltage dropped (V_0) across an organic film of thickness t:

$$(q^3 p_0^3 \mu_p^2 V_0)/(\kappa_0 J^2) = u_t^2 - u_t - \ln(1 - u_t),$$ (3)

where

$$J = q^2 p_0^2 \mu_p t /\{[- u_t - \ln(1 - u_t)]\kappa_0\}$$ (4)
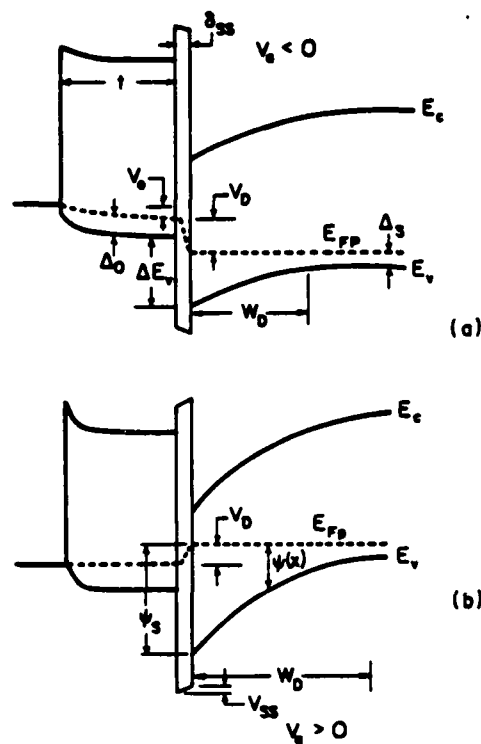
and

FIG. 1. Proposed energy-band diagram for an organic-on-inorganic semiconductor heterojunction device under (a) forward and (b) reverse bias.

$$u_t = p_0/p(t)$$ (5)

are related to the hole density at $x = t$. To solve Eqs. (3) and (4), we first choose a value of J from which the parameter, u_t, is determined via Eq. (4). This is substituted into Eq. (3), from which the voltage across the thin film, V_0, is calculated. The results of this calculation are shown in Fig. 2, where J is plotted as a function of V_0 for organic thin films with hole mobilities of $\mu_p = 0.01$ cm^2/V s and 0.1 cm^2/V s, a free-hole concentration of 5×10^{14} cm^{-3}, and a film thickness of 1000 Å. These values are typical of an OI diode using polycrystalline PTCDA as the organic layer.[7] In the figure, the ohmic transport regime at $V_0 < V_x \approx 0.02$ V (for $\mu_p = 0.01$ cm^2/V s) is distinguishable from the SCL regime at higher voltages. That is, at $V_0 < V_x$, $J \propto V_0$, whereas at $V_0 > V_x$, then $J \propto V_0^2$. This plot is in good agreement with observations of the J-V characteristics of metal/PTCDA/metal devices published earlier.[7] The important aspect of this plot is the low-current density ($J < 2$ mA/cm^2 for $\mu_p = 0.01$ cm^2/V s) at which ohmic gives way to SCL transport. Thus, at small forward voltages, and even at modest reverse biases for "leaky" OI diodes with small barrier diffusion potentials ϕ_{B_p}, the position of the hole quasi-Fermi level in the organic thin film is determined extrinsically by the amount of charge injected from the contacts (p_{inj}) rather than from the equilibrium concentration of carriers (p_0).

To calculate the potential distribution [$\psi(x)$] throughout the thin film, we replace V_0 by $\psi(x) < V_0 = \psi(t)$ in Eq. (3), and solve for $u(x) < u_t$. Then x is found using [cf. Eq. (4)]:
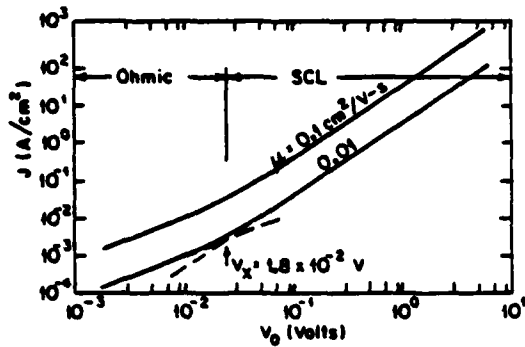
77

FIG. 2. Current (J) vs voltage (V_0) characteristics of a 1000-Å-thick organic film. The two curves correspond to films with mobilities of 0.1 and 0.01 cm²/V s. Regions corresponding to ohmic and space-charge-limited (SCL) transport regimes are shown.
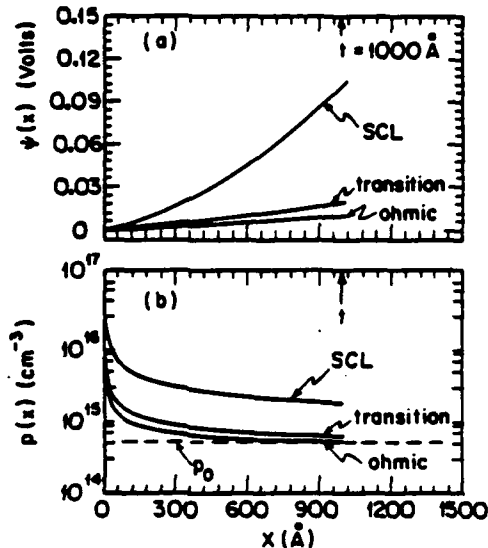

FIG. 3. (a) Potential distribution vs position within the organic thin film under three applied voltage regimes. The mobility of the 1000-Å-thick film is 0.01 cm²/V s. (b) The free-hole distribution calculated for the film in 3(a). Here, p_0 corresponds to the equilibrium hole concentration.

$$q^2 p_0^2 \mu_p x / \kappa_0 J = -u(x) - \ln[1 - u(x)] . \quad (6)$$

A plot of $\psi(x)$ is shown in Fig. 3(a) for the same film parameters as those used in Fig. 2, with $\mu_p = 0.01$ cm²/V s. Note that $\psi(x)$ scales inversely with μ_p. Here, $\psi(x)$ is shown for three different voltages, V_0, corresponding to the ohmic, transition, and SCL regimes. In the transition regime, $V_0 \approx V_x$. As expected, in the ohmic regime the potential increases nearly linearly with distance from the metal contact at $x = 0$ to the OI heterointerface at $x = t$. However, even in the ohmic regime, there is some nonlinearity in $\psi(x)$ near $x = 0$ due to charge injection effects. In the SCL regime, the potential increase is nearly quadratic with distance, indicating a substantial amount of injected charge.

To determine the charge distribution as a function of x, the value of $u(x)$ for a given $\psi(x)$ and J is substituted into Eq. (5), which is then solved for $p(x)$. The results are shown in Fig. 3(b) for the same three regimes considered in Fig. 3(a). As expected, the charge piles up near the metallic cathode and decreases with distance toward the OI heterointerface where it reaches a minimum value of $p(t)$. In the ohmic regime, $p(t) \approx p_0$. For SCL transport, $p(t)$, which is the sum of the injected (p_{inj}) and background (p_0) carrier concentrations, can be considerably larger than p_0.

The current at the organic side of the heterojunction (at $x = t$) is given by

$$J(t) = J = q[p_s(V_D) - p_s(0)]\langle v_c \rangle , \quad (7)$$

where $p_s(V_D)$ is the hole density at the OI interface corresponding to the lowest point in the valence-band maximum at the inorganic-semiconductor surface (Fig. 1). Also, V_D is the voltage drop across the inorganic substrate. Equation (7) suggests that current injected from the substrate into the organic thin film is limited by the rate at which carriers are transported toward the contacts. This limit is determined by the mean carrier velocity, $\langle v_c \rangle$, within the organic film, and at low V_0 is approximately given by

$$\langle v_c \rangle = v_{c0} = V_0 \mu_p / t . \quad (8)$$

Equation (8) is the drift velocity in the ohmic regime where diffusion is neglected (see below), and once again assumes μ_p is independent of E. At higher voltages it is more

appropriate to use the full expression for the mean carrier velocity, viz:

$$\langle v_c \rangle = \frac{1}{t} \int_0^t v_c(x)dx = \frac{1}{t} \int_0^t \mu_p(x)E(x)dx . \quad (9)$$

We note that the above treatment considers only drift. However, diffusion becomes important at $V_0 \lesssim kT/q$. Since V_x is approximately equal to the thermal, or diffusion potential, this suggests that diffusion is important under some (low voltage) diode operating conditions. When diffusion of holes in the organic layer is significant, the drift velocity is replaced by

$$\langle v_c \rangle = (D_{p0}/\tau_{p0})^{1/2} = (\mu_p kT/q\tau_{p0})^{1/2} , \quad (10)$$

where D_{p0} and τ_{p0} are the diffusion constant and lifetime of holes within the organic thin film, respectively. It has recently been found[9] that $\tau_{p0} < 10^{-7}$ s in PTCDA, suggesting a minimum carrier velocity due to diffusion through the thin film of 500 cm/s for $\mu_p = 1$ cm²/V s.

The current on the inorganic side of the heterojunction is given by

$$J = qD_{pn}\left(\frac{qpE}{kT} - \frac{dp}{dx}\right), \quad (11)$$

where D_{pn} is the diffusion constant for holes in the inorganic-semiconductor substrate and E is the electric field. This equation is solved using Eq. (7) along with:

$$p(x) = N_{\omega} \exp[-q\psi(x)/kT] , \quad (12)$$

where $\psi(x)$ is the energy difference between the valence-band maximum and the substrate quasi-Fermi level (Fig. 1), and N_{ω} is the effective valence-band density of states for the inorganic material.

Using Eqs. (7), (11), and (12) gives

401   J. Appl. Phys., Vol. 64, No. 1, 1 July 1988

78

$$J = [qN_{vs}\langle v_c \rangle/(1 + \langle v_c \rangle/v_d)]$$

$$\times \exp(-q\phi_{Bp}/kT)[\exp(-qV_D/kT) - 1] \,. \quad (13)$$

Here, ϕ_{Bp} is the diffusion potential due to the OI-HJ barrier and v_d is the inorganic material diffusion velocity given by

$$v_d = D_{pm}\left[\int_l^{W_D+l} \exp\left(\frac{q[\phi_{Bp} - \psi(x)]}{kT}\right) dx\right]^{-1}, \quad (14)$$

where W_D is the depletion region width.

We now express the barrier diffusion potential, ϕ_{Bp} in terms of the valence-band discontinuity energy ΔE_v. For isotype heterojunctions[1]:

$$\Delta E_v = q\phi_{Bp} + \Delta_s - \Delta_0, \quad (15)$$

where Δ_s and Δ_0 are the energy differences between the equilibrium Fermi levels in the bulk of the semiconductor substrate and organic thin film, respectively. That is, for the inorganic material:

$$\Delta_s = -kT\ln(p_s/N_{vs}), \quad (16)$$

where p_s is the equilibrium hole concentration. An expression similar to Eq. (16) is also used to determine Δ_0.

Equation (15) implies that, under certain conditions, ϕ_{Bp} is bias dependent. Since the equilibrium carrier concentration, p_0, in the organic layer is relatively small in many crystalline organic compounds, then under conditions of large injected currents where $p_{inj} > p_0$, the value of Δ_0 can change significantly from its equilibrium value. As ΔE_v is an intrinsic property of the HJ which is unaffected by the presence of injected charge, we therefore conclude that ϕ_{Bp} must also be bias dependent. This dependence is in addition to relatively small[10] image force lowering of ϕ_{Bp}. In effect, when $p_{inj} > p_0$, Δ_0 must decrease, thereby inducing a corresponding decrease in ϕ_{Bp}. This effect is very pronounced in OI diodes, whereas in Schottky devices it is negligible due to the large free-carrier concentration in the metal contact. Thus, Eq. (13) is similar to that which is obtained in the case of Schottky barriers,[11] with the exception that for OI devices ϕ_{Bp} can be voltage dependent under strong, forward biased current injection. Also, $\langle v_c \rangle$ is used in place of v_c, i.e., the "collection" velocity of the metal contact. Nevertheless, if ϕ_{Bp} is measured under low injection conditions, the valence-band discontinuity energy (or conduction-band discontinuity, ΔE_c, in the case of n-type substrates) can be inferred using p_0.

Equation (13) is also similar to the results obtained for thermionic emission over the OI barrier,[7] except that the exponential prefactor for TE limited currents used in previous work is simply A^*T^2, where A^* is the Richardson constant. If J_{SB} is the current due to thermionic emission over a Schottky-like OI barrier, and recognizing that in most cases $\langle v_c \rangle/v_d \ll 1$ (Sec. III), then

$$J/J_{SB} = \langle v_c \rangle(2\pi m^*/kT)^{1/2}, \quad (17)$$

where m^* is the effective mass of holes in the inorganic substrate. Taking $\langle v_c \rangle = 10^3$ cm/s (see Sec. III), $m^* = m_0$ (where m_0 is the electron rest mass), and $T = 300$ K, we obtain $J/J_{SB} \approx 3.7 \times 10^{-4}$. As the forward bias is increased, $\langle v_c \rangle$ is also increased [Eq. (9)]. In this case, J/J_{TE} approaches 1, implying that the conduction mechanism under strong forward injection approaches that of an ideal

Schottky diode. Here, the organic material becomes degenerate due to the presence of a high density of injected charge, and hence its behavior approximates that of a metal contact. Indeed, the ratio J/J_{SB} is a qualitative measure of the validity of the use of the Schottky approximation in analyzing OI diode transport. Clearly, this approximation fails at low current injection, where $\langle v_c \rangle$ becomes small.

Using these current-voltage relationships, we can calculate the potential distribution across the entire OI diode, assuming that there is no significant charge trapping in the device volume. In this case, Eqs. (4) and (13) are equal. Furthermore, the applied voltage is given by[4]

$$V_a = V_D + V_{ss} + V_0 \approx nV_D + V_0, \quad (18)$$

where V_{ss} is the voltage drop across any interfacial (oxide or trap) layer existing between the organic and inorganic layers, respectively, and $n > 1$ is the n value in the exponential voltage dependence of the dark current under forward bias.

In Fig. 4 we plot the various forward biased component voltages as a function of V_a, assuming two values of OI barrier height. Other parameters used in this calculation are similar to those in Fig. 3. Also, we take $n = 1.5$, $T = 300$ K, $N_{vs} = 2 \times 10^{19}$ cm^{-3} for p-Si, and $\langle v_c \rangle$ is given by the greater of Eq. (9) or (10), which is a function of the voltage drop across the organic thin film. As expected, at low forward bias the voltage is predominantly dropped across the inorganic substrate (i.e., $V_D > V_{ss}$, V_0). At higher voltages, SCL transport through the organic layer dominates, leading to a larger voltage drop across the organic thin film. The shift between ohmic and SCL transport in the film is evidenced by the change in slope in the curves at the value of V_a where all the voltage components are approximately equal. Below this transition point, we expect the J-V characteristic to depend exponentially on $V_a \approx V_D$ as indicated by Eq. (13). At higher voltages, $V_a \approx V_0$, and in this case $J \propto \sim V_a^2$, typical of SCL transport. Note that the transition from TE to SCL dominated currents occurs at lower values of V_a as the OI barrier height is decreased. This results since the current is higher at a given voltage as the barrier height is lowered [cf. Eq. (13)].

Under the reverse bias, V_0 and V_{ss} are considerably smaller than V_D due to the small leakage currents character-
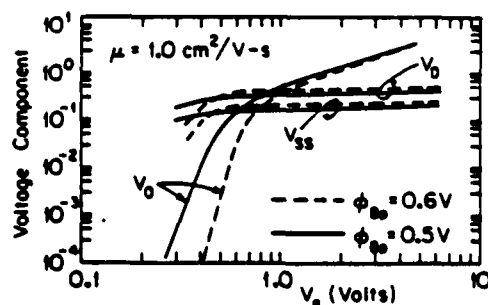

FIG. 4. Component voltages vs applied voltage for a forward biased OI-HJ diode, assuming two different barrier potentials of 0.6 and 0.5 V. Here, V_D, V_{ss}, and V_0 correspond to the voltage across the substrate depletion region, interfacial region, and thin film, respectively. A film thickness of 1000 Å is assumed.
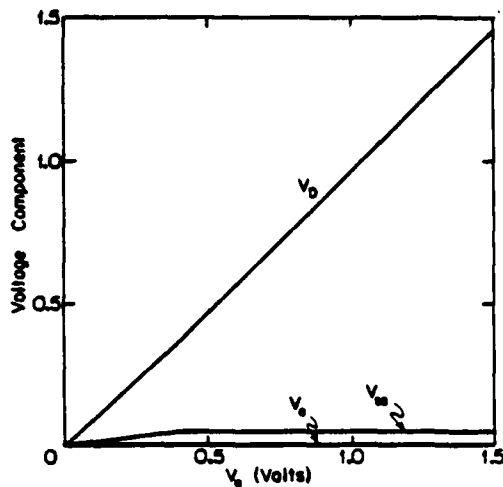
79

FIG. 5. Component voltages vs reverse applied voltage for the device in Fig. 4.

FIG. 6. (a) Forward current-voltage characteristics of an In/PTCDA/p-Si diode measured at several different temperatures (cf. Ref. 12). The PTCDA thickness is 2000 Å. (b) Saturation current density vs $1/T$ for the diode in (a). The solid line represents a best fit to the data, and gives a barrier diffusion potential of $\phi_{B_p} = 0.56$ V, and an intercept with the J_s axis of $J_0 = 1700$ A/cm^2.

istic of OI-HJ structures. The division of voltages in reverse biased devices has been treated in detail elsewhere,[4] ar l hence is shown for only a single set of conditions in Fig. 5 for reference.

The validity of the assumptions leading to the expression for current density [Eq. (13)] needs to be tested. This is particularly important since the magnitude of J/J_{SB} in Eq. (17) is significantly less than one, such that large errors in determining the barrier energy from the forward current-voltage characteristics can be incurred. To distinguish between the diffusion and thermionic models, we note that the total saturation current density, J_s, is given by

$$J_s = J_0 \exp(-q\phi_{B_p}/kT),\qquad(19)$$

where J_0 is equal to either the prefactor in Eq. (13), or in the case of pure thermionic emission, $J_0 = A^*T^2$. Thus, a plot of $\log(J_s)$ vs $1/T$ should be nearly exponential, with small deviations due to the weak temperature dependence of J_0. The slope of this plot gives the barrier energy and the intercept with the $\log(J_s)$ axis yields $\log(J_0)$.

In Fig. 6(a) is shown the temperature dependence of the forward biased J-V characteristics of an In/PTCDA/p-Si device (cf. Fig. 4, Ref. 12). From the intercept of these curves with the $V_d = 0 = V_D$ axis, we obtain the saturation current as a function of T, which is replotted in Fig. 6(b). The saturation current density is thermally activated, and a least-squares fit to the data—as indicated by the solid line— gives $\phi_{B_p} = 0.56 \pm 0.02$ V and $J_0 = 1700$ A/cm^2. This value for the barrier height is significantly smaller than the "apparent" values obtained using thermionic emission, where $\phi_{B_p} = 0.75$ V is typical for these diodes. Furthermore, $J_0 = A^*T^2 = 9 \times 10^6$ A/cm^2 for p-Si Schottky diodes, which is several orders of magnitude larger than the value of J_0 actually obtained. Returning to Eq. (13), we see that for $\langle v_c \rangle / v_d \ll 1$, then $J_0 = qN_w \langle v_c \rangle$. Using $J_0 = 1700$ A/cm^2, and $N_w = 2 \times 10^{19}$ cm^{-3} for p-Si, then $\langle v_c \rangle = 450$ cm/s. This is in satisfactory agreement with the lower limit value of 500 cm/s previously estimated using carrier lifetime data.
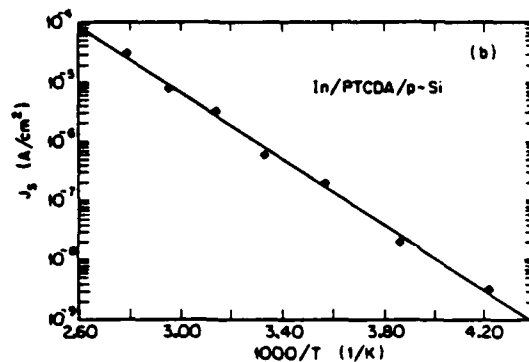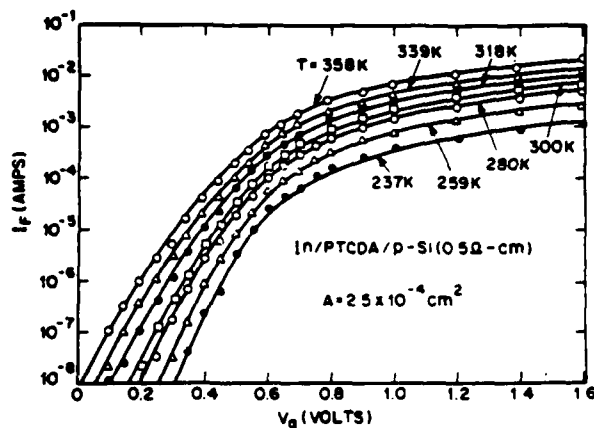
This result is therefore in strong support of the model of current transport across the OI-HJ barrier limited by both diffusion and drift [Eq. (13)]. Using $\phi_{B_p} = 0.56 \pm 0.02$ V along with Eq. (15), a valence-band discontinuity energy for PTCDA/p-Si devices of $\Delta E_v = (0.48 \pm 0.02)$ eV is obtained. To our knowledge, this represents the first such measurement of an energy-band discontinuity in crystalline organic/inorganic semiconductor heterojunctions.

The values for ϕ_{B_p} obtained through the use of Eq. (13) are still subject to errors induced by approximations used in developing the transport model. In particular, although there is no direct evidence of a high density of surface charge,[6] one would expect that such interfacial defects could affect the measurement of ΔE_v using J-V analysis. Therefore, ΔE_v was also measured via internal photoemission.

In Schottky[13] or isotype heterojunction[1,14] barriers, free majority carriers can be photoexcited over the barrier by sub-band-gap energy photons. The photocurrent (I_{ph}) induced per photon absorbed is given by[15]

$$I_{ph} \propto (h\nu - \Delta E_v)^2,\qquad(20)$$

where h is Planck's constant and ν is the frequency of the

incident light. To directly measure ΔE_v in OI-HJ devices, the photoemission current spectrum for a PTCDA/p-Si diode was investigated. For this experiment, the diode was fabricated in the same manner as that used in obtaining the data in Fig. 6. This diode was placed perpendicular to a chopped (1 kHz) monochromatic light source incident via the substrate such that light with $h\nu$ greater than the band gap of Si was filtered out before reaching the diode active area at the OI interface. To further suppress the signal due to the fundamental absorption in Si, a second Si wafer was placed between the light source and the OI diode. The band gap[7] of PTCDA is 2.2 eV, such that no direct absorption in the organic material is expected in this experiment.

The resultant photoresponse as a function of light energy and wavelength is shown in Fig. 7(a). In obtaining these data, the OI diode was operated at $V_a = 0$. A maximum response is clearly observed in the photoemission spectrum at 0.57 eV. No signal is observed between the energy of this peak and the band edge of Si. The peak height did not change with temperature (varied from 20 to 100 °C) or light chopping frequency (varied from 100 Hz to 2 kHz). Furthermore, the peak was unaffected by strong white light illumination (or bleaching) incident on the thin-film surface. Finally, an In/PTCDA/indium-tin-oxide device was also fabricated and illuminated in the same wavelength region as the In/PTCDA/p-Si sample. However, the former device had no photoresponse peak as that shown in Fig. 7(a), indicating that the peak is not due to a photoemission process in the PTCDA itself. These observations, coupled with the relatively high intensity of the signal, rule out the possibility that the peak is due to a high density of traps in the semiconductor bulks or at the OI-HJ interface.

We attribute this response to the photoemission of carriers from the highest occupied molecular orbital (or HOMO) in PTCDA to the valence-band maximum in p-Si over the interface barrier energy. However, note that the signal shown in Fig. 7(a) is considerably different than that predicted for photoemission, where we expect a monotonic increase in I_{ph} with energy. The dip in the OI-HJ photoemission data at high energy can be understood in terms of the band diagram in the inset of Fig. 7(a) where the widths of the organic energy bands are indicated by the crosshatched regions.[16] Unlike Schottky diodes or inorganic semiconductors, molecular semiconductors are characterized by relatively narrow bands, with a high density of states within those bands. Optical absorption experiments[7] have shown that the total HOMO plus LUMO (lowest unoccupied molecular orbital) bandwidth is 0.9 eV for PTCDA. If we now assume that the valence bandwidth is on the order of ΔE_v, then the peak absorption occurs at photon energies comparable to this barrier height [processes "a" and "c" in the inset of Fig. 7(a)]. However, as the photon energy increases the transitions are forbidden in the organic material as a result of the narrow bandwidth (process "b"), and hence a decrease in I_{ph} with increasing $h\nu$ is observed. Finally, for $h\nu < \Delta E_v$, the photon has insufficient energy for photoemission to occur.

From these arguments, the photocurrent on the long wavelength side of the peak should follow Eq. (20). Thus, in
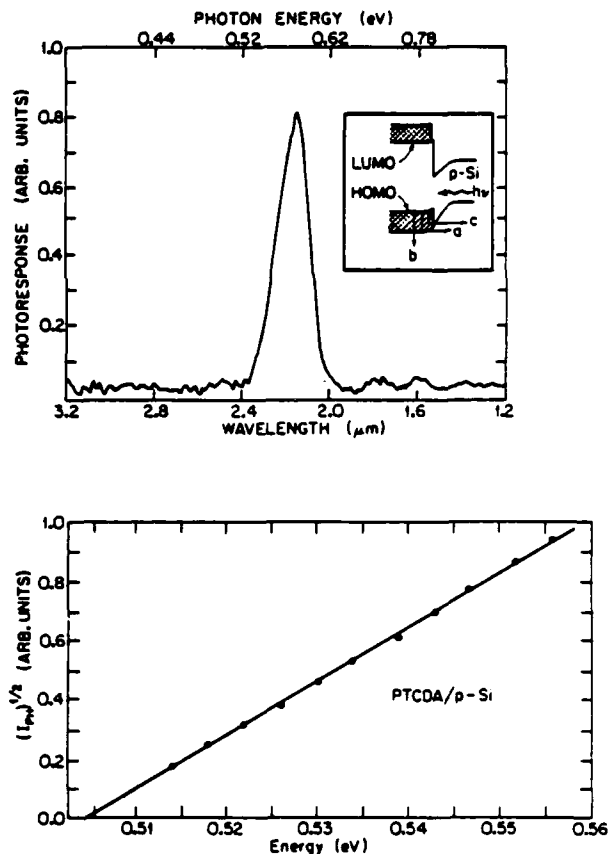

FIG. 7. (a) Photoemission spectrum of an In/PTCDA/p-Si heterojunction diode. Inset: Band diagram of the OI-HJ showing the allowed emission processes ("a" and "c") and the forbidden, high-energy process "b." The crosshatched regions refer to width of the organic bands. (b) The square root of the photocurrent on the long wavelength branch of the response peak in (a) plotted vs photon energy. The intercept of the straight line fit to the data with the $(I_{ph})^{1/2} = 0$ axis gives $\Delta E_v = (0.50 \pm 0.01)$ eV.

Fig. 7(b) we plot $(I_{ph})^{1/2}$ vs photon energy ($h\nu$), and find that the dependence is linear along nearly the entire long wavelength edge. The intercept of these data with the energy axis gives $\Delta E_v = (0.50 \pm 0.01)$ eV, a value consistent with that obtained from the J-V analysis.

Accurate determination of the barrier height as provided above has important implications as to the interpretation of the mechanisms affecting the formation of OI-HJ contact barriers. For example, as discussed in Sec. I, measurements of the density of interface states using the SOISAS technique are affected by the value of the OI-HJ barrier energy. In Fig. 8 is shown the density of states in equilibrium with a p-Si substrate (D_{ss}) as a function of energy in the Si band gap for a Cu-phthalocyanine/p-Si OI-HJ. The solid line corresponds to the data assuming an apparent barrier height of 0.70 V as determined from thermionic emission theory,[6] and the dashed line is this same data replotted assuming a barrier height of 0.50 V, which would be obtained from Eq. (13), assuming the hole velocity in Cu-phthalocyanine (CuPc) is approximately the same as that in PTCDA. This latter as-
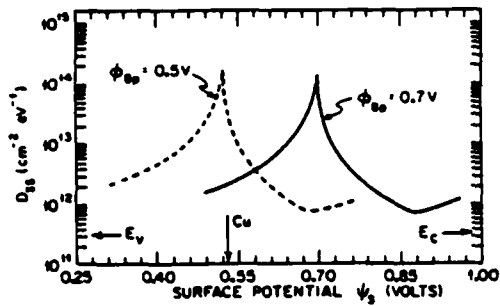
FIG. 8. Density of surface states (D_{ss}) vs potential at the Si surface for a CuPc/p-Si heterojunction. The solid line refers to data from Ref. 6 using a barrier height of 0.7 V. The dashed line is for this same data except that $\phi_{Bp} = 0.5$ V estimated using the OI-HJ current model. The arrow labeled "Cu" corresponds to the position of the Cu acceptor defect level in bulk Si. Also, E_c and E_v refer to the conduction and valence-band extrema in Si, respectively.

sumption is justified by the nearly equal hole mobilities of these two organic compounds. Thus, the position of the trap density curve is linearly related to the barrier energy.

We note that the large peak value for D_{ss} for CuPc/p-Si OI-HJs has been attributed[6] to reactions between these two materials at the heterointerface, resulting in free Cu at the Si surface. The corrected data appear to support this model, since the peak in D_{ss} nearly coincides with the Cu acceptor defect energy of 0.52 eV above the valence-band maximum in Si.[17] The position of this Cu defect is indicated by the vertical line in Fig. 8. Hence, knowledge of the actual, rather than the apparent values for ϕ_B is central to our understanding of the OI-HJ barrier.

For purposes of comparison, OI-HJ energy barrier heights measured assuming both thermionic emission and diffusion-limited transport models are given in Table I. These data are for PTCDA-based OI-HJ diodes only, and are taken from Ref. 2. Also included in the table are values of ΔE_v for selected OI-HJs as inferred from the diffusion model values of ϕ_{Bp} using Eq. (15).

III. CARRIER VELOCITIES

The carrier velocity $\langle v_c \rangle$ in the thin film is determined using Eqs. (9) and (10). The results for forward biased de-

vices are given in Fig. 9. Here, the velocity is plotted for several values of thin-film hole mobility ranging from 0.01 to 1 cm^2/V s, and for two values of ϕ_{Bp} (cf. Fig. 2 for other parameters used). It is apparent that the carrier velocity strongly depends on voltage, V_D, with $\langle v_c \rangle$ increasing exponentially when $V_D > 0.3$ V. Velocities as high as 10^5 cm/s are expected for thin films with high mobilities, and for diodes with barrier heights of 0.50 V. The dependence of these curves on V_D is a result of the increase of $\langle v_c \rangle$ with voltage V_0, when $V_0 > kT/q$. At low voltage, the electric field in the thin film is small, such that diffusion dominates. In this case, $\langle v_c \rangle$ is given by Eq. (10), where $\tau_p = 1.0 \mu s$ was assumed in these calculations. As V_D increases beyond 0.3 V, the voltage drop across the thin organic film increases due to the transition into the SCL current regime. The velocity at a given voltage decreases as the barrier height increases due to the reduced forward current, hence resulting in a lower voltage drop across the thin film.

The above treatment assumes a constant hole mobility in the organic crystal, independent of the magnitude of the applied electric field. The relatively high mobility of holes arises from the large overlap of electronic wave functions in the s-p orbitals of adjacent molecules in a crystalline stack. At the highest electric fields, it is expected[18,19] that the mobility will decrease somewhat due to the increased generation of phonons. Such processes depend on temperature, crystallinity, and film purity, and need to be taken into consideration; especially under large forward bias.

Under reverse bias, the electric field in the thin film is small, such that the drift velocity is much smaller than the diffusion velocity [Eq. (10)] for all but the smallest values of ϕ_{Bp}. Hence, under reverse bias, $\langle v_c \rangle$ varies from 100 cm/s to approximately 2000 cm/s, depending on the mobility and lifetime of holes in the organic layer. For these conditions the film will respond to even low-frequency signals as if it were a leaky dielectric in a metal-insulator-semiconductor (MIS) capacitor. However, due to the high conductivity of the thin film compared with that of glassy insulators such as SiO$_2$, it is not possible to strongly invert the surface of the OI diode. As greater reverse voltages are applied such that the Fermi level at the OI interface is brought to well above the center of the inorganic semiconductor band gap, the minority carriers (electrons) arriving from the semiconductor bulk are either

TABLE I. Barrier energies for selected PTCDA-on-inorganic semiconductor diodes using thermionic emission and diffusion models.

Inorganic substrate	Majority-carrier type	J_t/J_{TE}[a]	$q\phi_{Bp}$ (eV)		ΔE_v[b] (eV)
			TE	diffusion	
Si	n	2.0×10^{-4}	0.61 ± 0.01	0.39 ± 0.01	$\cdots$
	p	1.4×10^{-4}	0.73 ± 0.02	0.56 ± 0.02	0.50 ± 0.02
Ge	p	6.6×10^{-5}	0.53 ± 0.03	0.30 ± 0.03	0.25 ± 0.04
GaSb	p	1.2×10^{-4}	0.60	0.37	0.29 ± 0.04
	n	3.9×10^{-5}	ohmic	ohmic	$\cdots$
GaAs	n	5.2×10^{-5}	0.64	0.39	$\cdots$
	p	1.4×10^{-4}	0.73	0.52	0.43 ± 0.05
InP	n	5.5×10^{-5}	0.55	0.30	$\cdots$

[a] Values at $T = 300$ K, with $\langle v_c \rangle = 500$ cm/s.
[b] ΔE_v for p-type substrates only. For these calculations $m^* = m_0$ for PTCDA. The value for p-Si is measured; whereas for other materials, ΔE_v is calculated using ϕ_{Bp} obtained from Ref. 2 and reproduced here. Doping of p-Si and p-GaSb: 5×10^{15} cm^{-3}; p-Ge: 5×10^{14} cm^{-3}; and p-GaAs: 2×10^{16} cm^{-3}.
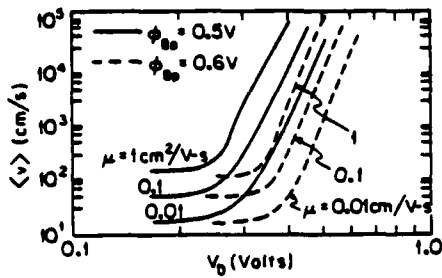
FIG. 9. Mean carrier velocity ($\langle v_c \rangle$) vs voltage across the substrate for OI-HJ diodes using organic thin films with different mobilities, and assuming barrier heights of 0.5 and 0.6 V. For these curves, a film thickness of 1000 Å and a hole lifetime of 1 μs are assumed.

TABLE II. Operating regimes for organic-on-inorganic semiconductor heterojunctions.

Regime	Voltage range[a]	Current density	$\langle v_c \rangle$ (cm/s)	p_s	Organic conductivity
Schottky	$-V_a > \phi_a$	$J > J_s$	10^4–10^6	$> p_0$	SCL
MIS	$\lvert V_a \rvert \lesssim E_g/q$	$J < J_s$	~ 100–10^4	$\lesssim p_0$	leaky insulator
HJ	$V_a < V_a < \phi_a$	$J \sim J_s$	100–10^3	$\ll p_0$	ohmic

[a] Positive voltage refers to reverse bias for p-type substrates.

swept across the organic film and collected at the metal contact, or else they recombine with injected holes arriving at the OI interface from the metal contact. In either case, this leakage current density is determined by the rate at which minority carriers are generated within the inorganic semiconductor.

Turning now to the carrier velocity in the inorganic substrate, Eq. (14) must be solved to obtain the diffusion velocity, v_d. Assuming that the doping density in the substrate (N_A) is uniform, the potential $\psi(x)$ (see Fig. 1) is parabolic. Thus:

$$\psi(x) = qN_A(W_D - x + t)^2/2\kappa_s + \Delta_s/q, \tag{21}$$

where κ_s is the semiconductor permittivity. Substituting this into Eq. (14) gives[11]

$$v_d \approx D_{pn}/2L_D = \mu_{pn}kT/2qL_D, \tag{22}$$

where $\mu_{pn} \approx 600$ cm^2/V s is the hole mobility in the (Si) inorganic material, and $L_D \sim 1000$ Å is the Debye screening length.[10] From this expression, we obtain $v_d \sim 10^6$ cm/s at room temperature.

One additional characteristic velocity of the OI diode is the hole drift velocity in inorganic semiconductor, which limits the rate at which holes can transit the depletion region under reverse bias. For most cases, this approaches the saturation velocity of holes in p-type semiconductors, which is typically between 5 and 10×10^6 cm/s.

Thus, we find that under nearly all bias regimes, the OI diode satisfies the condition that $\langle v_c \rangle / v_d \ll 1$. Furthermore, due to the large range over which $\langle v_c \rangle$ can vary for a small change in bias near $V_D = 0$, we have the circumstance that the OI diode changes its behavior from "Schottky-like" under large forward bias, to a "MIS-like" regime under small forward and reverse voltages. Under large reverse voltage, the device enters a "heterojunctionlike" regime whereby minority-carrier generation in the semiconductor substrate is balanced by recombination at the OI interface, thereby preventing charge inversion. The "heterojunction" regime also allows for Zener, or avalanche breakdown to occur at the largest applied reverse voltages.[7]

The characteristics of these various modes of OI-HJ op-

eration are summarized in Table II. In the table, p_s refers to the density of holes at the OI interface, which is calculated in Sec. IV. The last column labeled "organic conductivity" gives a qualitative description of the current transporting nature of the thin film in each of the various bias regimes. More discussion of this unusual character of the OI-HJ is presented in Sec. V.

IV. QUASI-FERMI LEVELS

To calculate the position of the quasi-Fermi level (or imref) within the organic thin film, we employ:

$$E_{Fp}(x) - E_{v0} = kT \log[N_{v0}/p(x)], \tag{23}$$

where N_{v0} is the valence-band effective density of states [cf., Eq. (16)], and E_{v0} is the energy of the valence-band maximum (or HOMO) in the organic film. In Fig. 10, $E_{Fp}(x) - E_{v0}$ is plotted as a function of x, where $p(x)$ is obtained with the aid of Eqs. (3)–(5). This function dips toward the valence-band maximum at the metal anode [i.e., $E_{Fp}(0) - E_{v0}$], increasing to a nearly constant value as the OI interface is approached. By examining the position of the imref at $x = t$, we see that while V_0 increases from 5 mV in the ohmic regime to 100 mV in the SCL regime (Fig. 3), $E_{Fp}(t) - E_{v0}$ changes by only 30 meV. That is, the relationship between the imref position at the OI interface, and the voltage applied to the thin film (V_0), is sublinear. Furthermore, under reverse bias, the conduction mechanism within the thin film is nearly always ohmic in nature, suggesting that V_0 is generally less than 10 mV for all bias levels of interest. Therefore, it can be concluded that under reverse, or even moderately large ($\lesssim 0.7$ V) forward biases, the imref position at the organic side of the OI-HJ is only a weak function of voltage dropped across the layer. This is consistent with assertions[4] that the occupancy of traps in equilibrium with the thin film does not change significantly with bias, and hence their contribution to total diode admittance is generally small.

To calculate the imref in the inorganic substrate, we assume that the doping is uniform, in which case the potential distribution, $\psi(x)$, is given by Eq. (21). Substituting Eq. (21) into Eq. (11), and using Eq. (23) (with N_{vs} substituted for N_{v0}) one then obtains:

$$E_{Fp}(x) - qV_D = kT \ln\left(1 - \frac{\exp(-\beta)D(\theta/\beta)\exp(\theta^2\beta)[1 - \exp(qV_D/kT)]}{v_d/\langle v_c \rangle + D(\sqrt{\beta})}\right), \tag{24}$$
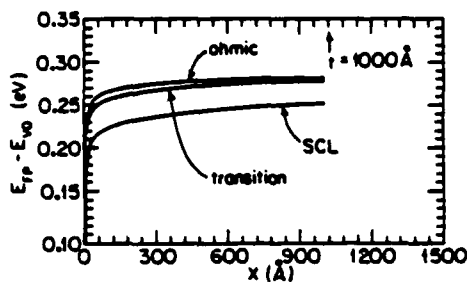
FIG. 10. Quasi-Fermi energy (E_{Fp}) vs position within the organic film for several different bias regimes. Parameters used in this calculation are the same as those in Fig. 3.

where the normalized position is $\theta = (W_D + t - x)/W_D$, and[20]

$$D(\sqrt{\beta}) = \exp(-\beta)\int_0^{\sqrt{\beta}} \exp(t^2)dt$$

$$= \sqrt{\beta}\cdot\exp(-\beta)\sum_{n=0}^{\infty}\frac{\beta^n}{(2n+1)n!}. \quad (25)$$

Here β is the band bending parameter, given by

$$\beta = -q[\psi(W_D) - \psi(t)]/kT. \quad (26)$$

To determine E_{Fp} at the semiconductor surface, Eq. (24) is solved at $\theta = 1$, giving:

$$E_{Fp}(t) - qV_D$$

$$= kT\ln\left(\frac{v_d/\langle v_c\rangle + D(\sqrt{\beta})\exp(qV_D/kT)}{v_d/\langle v_c\rangle + D(\sqrt{\beta})}\right). \quad (27)$$

This is similar to the result obtained for Schottky barrier diodes,[11] except that $\langle v_c\rangle$ is the mean carrier velocity in the organic layer rather than the collection velocity in the metal, and V_D is used in place of V_a.

It is apparent that the magnitude of $v_d/\langle v_c\rangle$ determines the functional dependence of E_{Fp} on voltage. For example, under forward bias where $V_D < 0$, and where $v_d/\langle v_c\rangle$ is large (as is the case for most OI diodes, see Sec. III), Eq. (27) reduces to $E_{Fp}(t) - qV_D \approx 0$. That is, the imref is flat throughout the substrate, independent of voltage, thereby allowing the majority-carrier imref in p-type diodes to sweep through the lower half of the band gap with V_a. Under reverse bias, $V_D > 0$, implying that $E_{Fp}(t) - qV_D = 0$ as long as the second term in the numerator of Eq. (27) is smaller than $v_d/\langle v_c\rangle$. For small reverse biases, this is indeed the case in OI diodes. On the other hand, for Schottky diodes where $v_d/\langle v_c\rangle \approx 1$, the second term dominates at almost all applied voltages. In this latter case,

$$E_{Fp}(t) - qV_D = -qV_D, \quad (28)$$

which results in the surface imref being "pinned" to its value at $V_D = 0$.

Returning to Eq. (27), we can calculate the potential at the inorganic side of the OI-HJ as a function of V_D using the values determined for $\langle v_c\rangle$ in Sec. III. The surface potential (Fig. 1) is just

$$q\psi(t) = q\psi_s = E_{Fp}(t) + q\phi_{Bp}. \quad (29)$$

84

In Fig. 11, ψ_s is plotted versus V_D for both forward ($V_D < 0$) and reverse ($V_D > 0$) bias. This function is determined for several barrier heights. For comparison, it is also plotted for a Schottky barrier device, where $v_c \sim 10^6$ cm/s. It can be seen that the surface potential for a Schottky barrier diode is essentially constant under reverse bias, as expected from diffusion and thermionic emission theory.[11] On the other hand, ψ_s decreases linearly with V_D under forward bias. For this reason, the Schottky diode is useful for exploring traps which are located between the equilibrium Fermi level and the majority-carrier band edge, as has been suggested by Barret and co-workers.[21,22] This is due to the ability to "scan" the imref through the trap energies by changing the applied voltage, and hence altering the net trap occupancy.

In the case of the OI diode, the carrier velocity, $\langle v_c\rangle$, is several orders of magnitude less than v_d. Thus, the surface potential varies linearly with V_D in both forward and reverse bias over nearly the entire band gap of the inorganic semiconductor, as shown in Fig. 11. This result is largely independent of hole mobility within the organic film, as long as the mobility is in the range typical of organic crystalline solids[23] (i.e., $\mu_p < 10$ cm^2/V s). However, if the barrier height is sufficiently small, the surface potential cannot be brought near to the minority-carrier band edge due to the increased leakage currents. Under forward bias, the behavior of the surface potential is identical to that of the Schottky barrier device, i.e., it decreases linearly with applied voltage.

Finally, Fig. 12 is a plot of the free-hole concentration in the inorganic material at the OI interface [see Eq. (12)]. The same parameters employed in Fig. 11 are also used in this figure. The surface charge concentration is seen to vary over fourteen decades as the potential changes from a forward bias of -0.5 V (where $p_s \approx 10^{15}$ cm^{-1}), to a reverse bias of 0.5 V (with $p_s = 1$ cm^{-1}). The surface charge density can be understood directly in terms of the carrier velocity. For example, under strong forward bias $\langle v_c\rangle$ is large, resulting in a hole transit time which is small compared with τ_{p0}. In this case, p_s must be very large. However, as $\langle v_c\rangle$ is reduced, τ_{p0} becomes small with respect to the transit time, thereby depleting the thin film of injected charge near the OI interface.
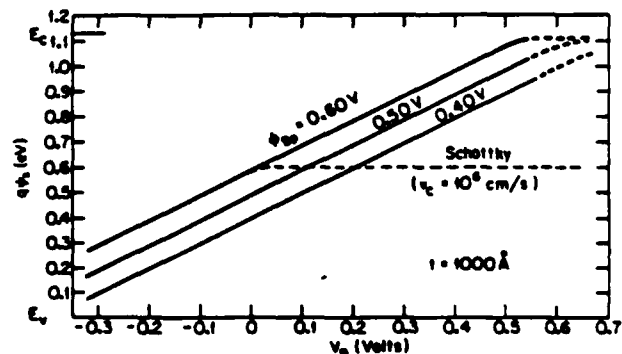

FIG. 11. Potential at the inorganic semiconductor surface as a function of voltage across the depletion region for OI-HJ diodes with several different values of barrier energy. The surface potential for a Schottky barrier diode (with barrier energy of 0.6 eV) is shown for comparison.
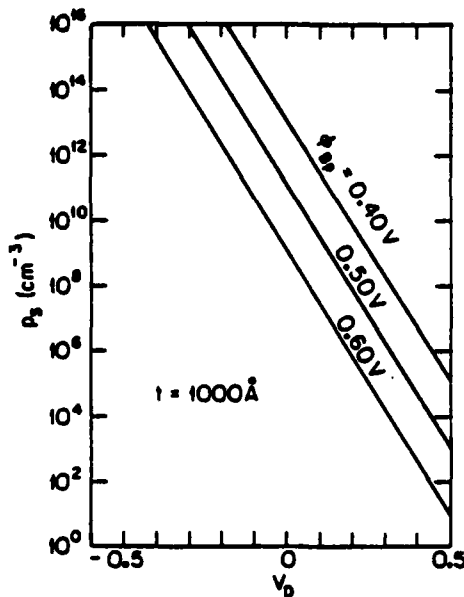
FIG. 12. Hole concentration (p_s) at the OI-HJ interface as a function of voltage for the same parameters used in Fig. 11.
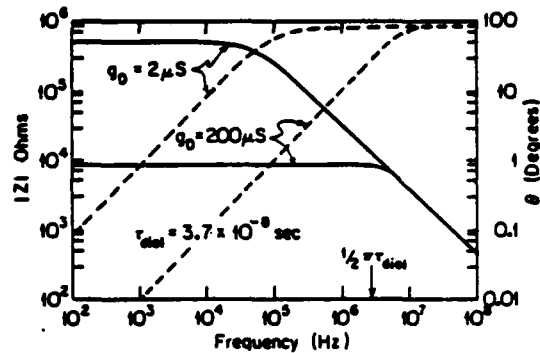

FIG. 13. OI-HJ impedance ($|Z|$, solid lines) and phase angle (θ, dashed lines) vs frequency. A dielectric relaxation time of 37 ns is assumed for the organic thin film. These functions are calculated for two values of barrier conductance: $g_D = 2$ and $200\ \mu S$, the latter value corresponding to a "leaky" diode. Also, a depletion region capacitance of $C_D = 5$ pF is assumed.

V. DISCUSSION AND CONCLUSIONS

A significant result of this work is that the transport theory presented in Sec. II results in an expression for diffusion-limited current in OI-HJ diodes from which an accurate barrier energy, and hence ΔE_v, for these novel heterojunctions can be determined. Several experimental results have also been presented which corroborate the theoretical treatment. In addition, we have shown that the majority-carrier quasi-Fermi level in OI-HJ diodes is flat throughout the bulk of the inorganic semiconductor substrate for small forward and reverse bias voltages. Thus, applying a bias to the OI-HJ causes the majority-carrier imref to sweep through nearly the entire semiconductor bandgap. Provided that the density of surface states at the OI-HJ is small ($\lesssim 10^{12}\ cm^{-2}\ eV^{-1}$), these states will be thermalized as E_{Fp} is lowered below the trap energy, and thus will contribute to diode admittance.[4,5] A higher surface state density can result in Fermi level pinning at the OI-HJ, thereby leading to nonlinear, and hence difficult to determine relationships between the applied voltage V_a, the voltage dropped across the substrate V_D, and E_{Fp}.

The dependence of the quasi-Fermi level on voltage results from the relatively low carrier velocities and carrier concentrations in the organic thin film. By calculating both E_{Fp} and $\langle v_c \rangle$ as a function of V_D, we find that the OI-HJ has unique electrical properties as compared with conventional inorganic semiconductor devices. For example, near $V_D \approx 0$, there is only a small voltage drop across the organic film, and the film can be considered similar to a leaky insulator. Thus, the device at low voltages behaves like a MIS capacitor whose impulse response is limited by the thin-film dielectric relaxation time, $\tau_{diel} = \kappa_0/\sigma$. Here σ is the conductivity of the film, and is typically[7] $\sigma \sim 10^{-5}$ S/cm. Using[7] $\kappa_0 = 0.37 \times 10^{-12}$ F/cm, we obtain $\tau \approx 37$ ns. Hence, under

reverse or low forward voltages, the OI-HJ diode varies from a resistive response at $f < 1/2\pi\tau_{diel} \approx 5$ MHz (depending on the inorganic semiconductor depletion capacitance C_D) to a reactive response at higher frequencies. The impedance and phase versus frequency characteristics of a typical OI diode operated in the MIS regime is illustrated in Fig. 13, assuming a conductance for the OI-HJ barrier (g_D) of 2 or 200 μS. The latter value corresponds to a "leaky" OI-HJ with a low barrier potential, ϕ_{Bp}. In this case the organic film can be approximated by a resistor-capacitor network in series with a resistor due to the HJ, whose characteristic time is τ_{diel}. As the network becomes reactive ($\theta > 45^\circ$), then $|Z| \propto 2\pi fC$, which decreases inversely with frequency. For less leaky barriers (e.g., $g_D = 2\ \mu S$), the network is in series with capacitance C_D, and hence becomes reactive at frequencies lower than $2\pi\tau_{diel}$.

Under large forward bias, the diode performs analogous to a Schottky diode. In this case, a large charge density (p_{inj} or n_{inj}) is injected from the substrate and metal contacts into the thin film such that n_{inj} or $p_{inj} \gg p_0$. Here, conduction in the organic material becomes extrinsically space-charge limited. This effectively "pulls" the Fermi energy to the organic band edge, hence making the organic material degenerate. With the exception that the resistance of the thin film in this regime is a nonlinear function of voltage, in most other respects the film behaves as if it were an ohmic metal contact forming a Schottky barrier with the substrate. In the Schottky regime, the carrier velocity $\langle v_c \rangle$ can be as high as 10^4–10^5 cm/s. With a film thickness of 100 Å, a response time of between 10 and 100 ps would result.

Finally, a third "heterojunction" regime is obtained under moderate to large reverse bias voltages. The poor insulating properties of the organic material prevent the OI-HJ interface from being strongly inverted. Hence, under reverse bias this charge must either recombine at the interface within the bulk of the film, or diffuse to the ohmic metal contact made to the film surface. As the bias is further increased, large electric fields are developed in the semiconductor substrate, leading to eventual bulk breakdown in the inorganic

material.[8] Note that when large breakdown currents are developed, charge transport is once more limited by space-charge effects in the organic material, similar to conditions of large forward bias.

ACKNOWLEDGMENTS

[1] F. Capasso and G. Margaritondo, Eds., *Heterojunction Band Discontinuities: Physics and Device Applications* (North-Holland, Amsterdam, 1987).

[2] P. H. Schmidt, S. R. Forrest, and M. L. Kaplan, J. Electrochem. Soc. 133, 769 (1986).

[3] M. Ozaki, D. Peebles, B. R. Weinberger, A. J. Heeger, and A. G. MacDiarmid, J. Appl. Phys. 51, 4252 (1980).

[4] S. R. Forrest and P. H. Schmidt, J. Appl. Phys. 59, 513 (1986).

[5] S. R. Forrest, M. L. Kaplan, and P. H. Schmidt, J. Appl. Phys. 60, 2406 (1986).

[6] F. F. So and S. R. Forrest, J. Appl. Phys. 63, 442 (1988).

[7] S. R. Forrest, M. L. Kaplan, and P. H. Schmidt, J. Appl. Phys. 55, 1492 (1984).

[8] M. Lampert and P. Mark, *Current Injection in Solids* (Academic, New York, 1970).

[9] F. F. So, S. R. Forrest, H. L. Garvin, and D. J. Jackson, Technical Digest of Integrated and Guided Wave Optics Conference, Santa Fe, March 28–30, 1988.

[10] S. M. Sze, *Physics of Semiconductor Devices*, 2nd ed. (Wiley, New York, 1981).

[11] C. R. Crowell and M. Beguwala, Solid-State Electron. 14, 1149 (1971).

[12] S. R. Forrest, M. L. Kaplan, and P. H. Schmidt, J. Appl. Phys. 56, 543 (1984).

[13] C. R. Crowell, W. G. Spitzer, L. E. Howarth, and E. E. LaBate, Phys. Rev. 127, 2006 (1962).

[14] M. A. Haase, M. A. Emanuel, S. C. Smith, J. J. Coleman, and G. E. Stillman, Appl. Phys. Lett. 50, 404 (1987).

[15] R. H. Fowler, Phys. Rev. 38, 45 (1931).

[16] S. R. Forrest, M. L. Kaplan, and P. H. Schmidt, Annu. Rev. Mater. Sci. 17, 189 (1987).

[17] A. G. Milnes, *Deep Impurities in Semiconductors* (Wiley, New York, 1973).

[18] W. Warta, R. Stehle, and N. Karl, Appl. Phys. A 36, 163 (1985).

[19] W. Warta and N. Karl, Phys. Rev. B 32, 1172 (1985).

[20] This is known as Dawson's integral; see M. Abramowitz and I. Stegun, *Handbook of Mathematical Functions* (Dover, New York, 1965), p. 298.

[21] C. Barret and A. Vapaille, J. Appl. Phys. 50, 4217 (1979).

[22] C. Barret, F. Chekir, and A. Vapaille, J. Phys. C 16, 2421 (1983).

[23] F. Gutman and L. E. Lyons, *Organic Semiconductors* (Wiley, New York, 1967).

Measurement of the valence-band discontinuities for molecular organic semiconductor/inorganic semiconductor heterojunctions

F. F. So and S. R. Forrest

Departments of Electrical Engineering/Electrophysics and Materials Science & Engineering, University of Southern California, Los Angeles, California 90089-0241

Using the temperature dependence of the forward-biased current-voltage characteristics as well as internal photoemission, we directly measure the barrier potential and valence-band discontinuity energy (ΔE_v) of isotype heterojunctions formed between thin films of the crystalline organic semiconductor: 3,4,9,10-perylenetetracarboxylic dianhydride (PTCDA) and p-Si. We find $\Delta E_v = (0.50 \pm 0.02)$ eV. This, to our knowledge, is the first report of a measurement of a band discontinuity energy between a crystalline organic semiconductor and an inorganic semiconductor. These results are consistent with predictions of a current model involving diffusion and drift in the organic-on-inorganic (OI) semiconductor device. This model is employed to calculate ΔE_v using previously obtained barrier energies for several different PTCDA/inorganic semiconductor devices. In all cases, values of the barrier diffusion potential and ΔE_v are considerably smaller than apparent barrier energies obtained previously using pure thermionic emission theory to explain transport of charge over the OI barrier.

During the last several years, considerable interest has been focused worldwide on the study of semiconductor heterojunctions. The source of this interest lies in the ability of heterojunctions to control optical fields and charge transport in numerous devices such as semiconductor lasers and photodetectors used in optoelectronic applications. Furthermore, the ability to grow epitaxial materials with atomic scale precision has led to the realization of multiple quantum well structures which exhibit a wealth of exciting new physical phenomena, some of which are already finding novel device applications.

In addition to the more traditional heterojunctions being investigated, there have been a few reports of an entirely new class of heterojunctions[1-3] which are also finding interesting new applications,[4,5] and are leading to a greater understanding of semiconductors in general. These heterojunctions consist of organic (either crystalline molecular or disordered polymeric) semiconductors in contact with inorganic semiconductors. In this work, we present for the first time, measurement of the valence-band discontinuity energy between crystalline organic semiconductors and both elemental and compound inorganic semiconductor substrates. This differs from past work[1] in that the previous quantity measured was the "apparent barrier height," i.e., the heterojunction barrier energy inferred from the room-temperature, forward-biased current-voltage (I-V) characteristics using thermionic emission theory. While the apparent barrier height can be used to give a very accurate phenomenological model of transport across organic-on-inorganic semiconductor heterojunction (or OI-HJ) barriers, it is not successful in providing an accurate value for the energy-band discontinuities. Knowledge of these latter quantities, however, is central to our understanding of the physics underlying the formation of the OI-HJ barrier.

In the inset of Fig. 1 is shown a schematic cross section of an archetypal OI-HJ rectifier. The OI-HJ's consist of a thin (1000–2000 Å) layer of the purified crystalline organic dye: 3,4,9,10-perylenetetracarboxylic dianhydride (PTCDA) vacuum deposited onto inorganic semiconductor substrates using techniques described elsewhere.[4] The conductivity type of PTCDA is lightly p type. The inorganic semiconductor is Si, which is the material used in most of the studies to be discussed. The OI-HJ device is completed by making ohmic In contact to the substrate surface as well as to the organic thin film.

It has been shown[6] that the current density (J) is related to the voltage drop across the inorganic semiconductor (V_D) via

$$J = J_0 \exp(-q\phi_{Bp}/kT)[\exp(-qV_D/kT) - 1]$$
$$= J_s[\exp(-qV_D/kT) - 1]. \tag{1}$$

Here, k is Boltzman's constant, T is the temperature, q is the electronic charge, J_s is the saturation current, and ϕ_{Bp} is the OI-HJ barrier potential which may be voltage dependent. Also, we assume that the substrate is p type, in which case $V_D > 0$ for reverse bias. The value taken for J_0 strongly de-

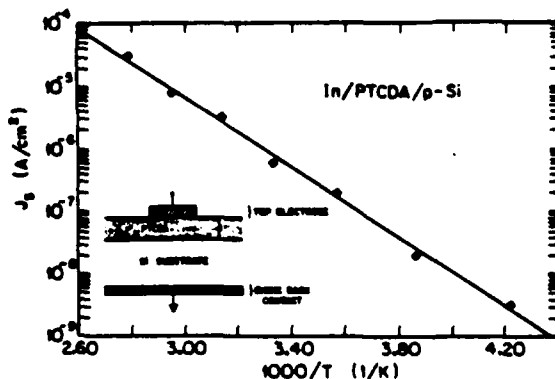FIG. 1. Saturation current density (J_s) vs inverse temperature for an In/PTCDA/p-Si heterojunction. The solid line is a linear least squares fit to the data points. Inset: Schematic cross-sectional view of an organic/inorganic semiconductor heterojunction device.

pends on the mechanisms governing transport across the OI-HJ barrier. For example, it has often been assumed[1,2] that transport across the OI-HJ barrier is similar to that in a Schottky barrier diode and hence $J_0 = J_{SB} = A^*T^2$, where A^* is the Richardson constant. While this assumption is true for large forward bias, where a high density of charge is injected from the ohmic contacts into the organic thin film, it is not true under low forward or reverse voltage. In this bias regime, the very small hole concentration ($\sim 5 \times 10^{14}$ cm^{-3}) in the organic thin film, coupled with its limited total density of states, suggests that diffusion and drift within the thin film will modify the value of J_0 from J_{SB}. Indeed, it can be shown[7] that for an OI-HJ diode

$$J_0 \approx J_{OI} = qN_v \langle v_c \rangle, \qquad (2)$$

where N_v is the effective density of states at the inorganic semiconductor valence-band edge and $\langle v_c \rangle$ is the mean hole velocity in the organic thin film. Depending on the bias regime, $\langle v_c \rangle$ is determined either by hole drift (at moderate to high forward bias) or diffusion (at low forward or reverse bias). This latter case is typical for the conditions explored in this experiment. Assuming $\langle v_c \rangle$ is limited by diffusion, then $\langle v_c \rangle = (D_p / \tau_p)^{1/2} = (\mu_p kT/q\tau_p)^{1/2}$, where D_p is the diffusion constant, $\mu_p = 1$ cm^2/V s is the hole mobility of PTCDA,[6] and $\tau_p < 100$ ns is the hole lifetime obtained from current transient measurements.[8] For these conditions, $\langle v_c \rangle > 500$ cm/s, which is consistent with time-resolved measurements of the response of OI-HJ diodes to fast optical pulses.[9]

Note that typically $J_{SB} = 10^7$ A/cm^2. On the other hand, using $N_v = 2 \times 10^{19}$ cm^{-3}, we obtain $J_{OI} \approx 2000$ A/cm^2, leading to $J_{OI}/J_{SB} = 2 \times 10^{-4}$. In using the forward I-V characteristics to determine the apparent barrier height ϕ_{Bp}, one often measures the saturation current at $V_D = 0$ and equates that value to the prefactor to the term in square brackets in Eq. (1). Then, assuming a value (and hence a model) for J_0, one can extract the apparent barrier height. However, from the above discussion there would appear to be a large uncertainty in the value to use for J_0 in which case the actual barrier height cannot be determined with any reasonable accuracy. Indeed, without a direct measurement of the barrier height, one is also not capable of determining the valence-band discontinuity energy (ΔE_v). Thus, in our measurements we directly determine the barrier energy. Using this actual value for ϕ_{Bp}, J_0 is calculated giving a basis from which the appropriate model can be developed.

From Eq. (1) it is apparent that a measurement of the saturation current density (J_s) as a function of temperature can directly yield its activation energy ϕ_{Bp}.

Thus, a plot of $\log(J_s)$ as a function of   is shown in Fig. 1. The device used had a contact area of 2.5×10^{-4} cm^2, and consisted of 2000 Å of PTCDA deposited on a 0.5 Ω cm (100) p-Si substrate.[6] A linear least squares fit to the data, as indicated by the straight line, gives $\phi_{Bp} = 0.56 \pm 0.02$ V and $J_0 = 1700$ A/cm^2. Note that both these values are considerably different from those obtained using thermionic emission theory,[1,6] where it was found that $\phi_{Bp} = 0.75$ V and $J_{SB} = 10^7$ A/cm^2. However, as indicated above, $J_0 \approx J_{OI}$

≈ 2000 A/cm^2, in agreement with the model based on diffusion in the organic thin film.

The valence-band discontinuity energy for this isotype (p-P) heterojunction, ΔE_v, can be obtained from the actual (not apparent) value of ϕ_{Bp} using[10]

$$\Delta E_v = q\phi_{Bp} + \Delta_i - \Delta_o, \qquad (3)$$

where Δ_i and Δ_o are the differences between the equilibrium Fermi energies and the valence-band maxima in the inorganic and organic semiconductor bulks, respectively. Using a hole concentration of $p_s = 5 \times 10^{15}$ cm^{-3} and[8] $p_0 = 5 \times 10^{14}$ cm^{-3} (where the subscripts "s" and "o" have the same meanings as used previously), with the effective hole mass (m^*) in the organic taken to be equal to the free-electron mass,[11] we obtain $\Delta E_v = (0.48 \pm 0.02)$ eV for PTCDA/p-Si heterojunctions. Note that PTCDA has a band-gap energy[4] of 2.2 eV, suggesting that $\Delta E_c = \Delta E_g - \Delta E_v \approx 0.6$ eV, where ΔE_g is the difference in band gaps between PTCDA and Si.

Although this analysis suggests that the actual barrier potential ϕ_{Bp} differs significantly from previously reported "apparent" values, the barrier height obtained from such transport measurements can lead to error in the presence of a high density of defect states at the heterojunction. While evidence from capacitance-voltage measurements[3,4] indicates a relatively low interface defect density for PTCDA/Si OI-HJ's, it is nevertheless worthwhile to utilize a more direct measurement of ΔE_v via internal photoemission.[11] In this experiment, a PTCDA/p-Si diode similar to that used in Fig. 1 was illuminated via the Si substrate using a 1-kHz chopped light source. In this manner, all light of energy ($h\nu$) greater than the Si band edge at 1.1 eV was eliminated from the OI-HJ region. To further attenuate the short wavelength radiation, a second Si wafer was interposed between the light source and the OI diode. The short-circuit photocurrent was then measured as a function of photon energy, resulting in the peak shown in Fig. 2(a) at $h\nu = 0.57$ eV.

The peak height was found to be insensitive to changes in both temperature and chopping frequency. In addition, to test whether the peak was due to excitation of traps in the bulk PTCDA, an In/PTCDA/indium tin oxide (ITO) photoconductor was fabricated. We found that no photoresponse was observed between $\lambda = 1$ and 3μm for this device. Based on these observations, we can rule out the possibility that the peak is due to traps in the bulk semiconductors or at the OI-HJ interface.

We interpret this peak as follows. At $h\nu < 0.57$ eV, holes in the p-type organic thin film are excited above the OI-HJ, and are subsequently emitted over the barrier and collected in the external circuit [processes "a" and "c" in the inset of Fig. 2(a)]. Since this is the process of internal photoemission, the photocurrent at $h\nu < 0.57$ eV is expected to follow[12] $I_{PH} \propto (h\nu - \Delta E_v)^2$. Hence, Fig. 2(b) is a plot of $I_{PH}^{1/2}$ vs $h\nu$ for data taken on the long-wavelength side of the emission peak. A linear least squares fit to these data gives $\Delta E_v = (0.50 \pm 0.01)$ eV—a value in excellent agreement with that obtained using the forward-biased I-V characteristics in Fig. 1. Note, however, at $h\nu > 0.57$ eV, the data strongly deviate from that predicted for simple photoemission. At these
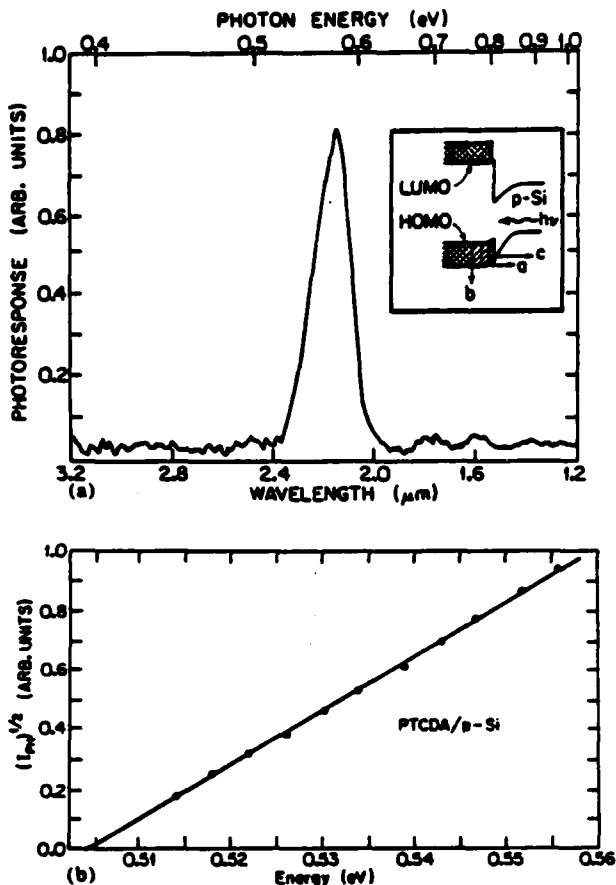
PHOTON ENERGY (eV)

FIG. 2. (a) Photocurrent spectrum for an In/PTCDA/p-Si heterojunction illuminated via the p-Si substrate. The film thickness is 1000 Å. Inset: Band diagram of a PTCDA/p-Si heterojunction showing allowed ("a" and "c") and forbidden ("b") photoemission transitions resulting in the spectrum shown. (b) Square root of the photocurrent vs photon energy for the data on the long-wavelength side of the peak shown in (a). The solid line is a linear least squares fit to the data points.

TABLE I. Valence-band discontinuities for p-P PTCDA/inorganic semiconductor heterojunctions.

Inorganic substrate	J_{OI}/J_{SB}[a]	$q\phi_{Bp}$ (eV)		ΔE_v[d] (eV)
		TE[b]	Diffusion[c]	
Si	1.4×10^{-4}	0.75 ± 0.02	0.56 ± 0.02	0.50 ± 0.02
Ge	6.6×10^{-5}	0.55 ± 0.03	0.30 ± 0.03	0.25 ± 0.04
GaAs	1.4×10^{-4}	0.75	0.52	0.43 ± 0.05
GaSb	1.2×10^{-4}	0.60	0.37	0.29 ± 0.04

[a] Assumes $(v_c) = 500$ cm/s and $T = 300$ K.
[b] Values obtained for the apparent barrier height using thermionic emission (TE) theory from Ref. 1.
[c] Obtained using Eq. (1) and (2) in text.
[d] Doping of Si and GaSb: 5×10^{15} cm^{-3}, Ge: 5×10^{16} cm^{-3}, and GaAs: 2×10^{16} cm^{-3}.

high energies, I_{PH} drops with increasing $h\nu$. This effect can also be understood in terms of the band diagram in the inset of Fig. 2(a). Molecular semiconductors are characterized by narrow bandwidths,[13] as indicated by the cross-hatched region in the figure. For PTCDA, the total bandwidth bounded by the highest occupied molecular orbital (or HOMO) and lowest unoccupied MO (or LUMO) is only[4] 0.9 eV. Thus, transitions "b" beyond the bandwidth of the organic are forbidden, and hence a drop is expected in I_{PH} for this high-energy light.

Both of the experiments described above give support to a value of $\Delta E_v = (0.50 \pm 0.02)$ eV for PTCDA/p-Si heterojunctions, and for $J_0 = J_{OI}$ given by Eq. (2). With this confidence in determining J_0, we can calculate ΔE_v using Eqs. (1)–(3) for several PTCDA-based OI-HJ's where different inorganic substrates have been employed. Hence, in Table I, ΔE_v is listed for heterojunctions containing PTCDA along

with Ge, GaAs, and GaSb using the apparent barrier height data of Ref. 1. In all cases, these values of ΔE_v are significantly smaller than their previously reported apparent values of ϕ_{Bp}.

In conclusion, we have measured the barrier potential ϕ_{Bp}, and the valence-band discontinuity energy ΔE_v, for PTCDA/p-Si heterojunctions. These data are consistent with predictions of a model of hole transport in the devices which includes the effects of diffusion and drift in the OI diode. To our knowledge, this is the first report of the measurement of a band discontinuity energy for molecular organic/inorganic semiconductor heterojunctions, and the results further our understanding of these interesting structures.

The authors thank the Joint Services Electronics Program, the Air Force Office of Scientific Research, and Rome Air Development Center for support of this work.

[1] P. H. Schmidt, S. R. Forrest, and M. L. Kaplan, J. Electrochem. Soc. 133, 769 (1986).
[2] M. Ozaki, D. Peebles, B. R. Weinberger, A. J. Heeger, and A. G. MacDiarmid, J. Appl. Phys. 51, 4252 (1980).
[3] F. F. So and S. R. Forrest, J. Appl. Phys. 63, 442 (1988).
[4] S. R. Forrest, M. L. Kaplan, and P. H. Schmidt, Ann. Rev. Mater. Sci. 17, 189 (1987).
[5] C.-L. Cheng, S. R. Forrest, M. L. Kaplan, and P. H. Schmidt, Appl. Phys. Lett. 47, 1217 (1986).
[6] S. R. Forrest, M. L. Kaplan, and P. H. Schmidt, J. Appl. Phys. 56, 543 (1984).
[7] S. R. Forrest and F. F. So, J. Appl. Phys. 63, June (1988).
[8] S. R. Forrest, M. L. Kaplan, and P. H. Schmidt, J. Appl. Phys. 55, 1492 (1984).
[9] F. F. So, S. R. Forrest, H. J. Garvin, and D. L. Jackson, Integrated and Guided Wave Optics Technical Digest, Santa Fe, 1988 (Optical Society of America, Washington, DC, 1988).
[10] A. G. Milnes and D. L. Feucht, Heterojunction and Metal-Semiconductor Junctions (Academic, New York, 1972).
[11] Although setting m^* equal to the free electron mass (m_0) is a rough approximation, we note that $\Delta_0 \sim \ln(m^*/m_0)$. Hence, small deviations of m^* from m_0 are not expected to lead to significant inaccuracies in ΔE_v obtained from Eq. (3).
[12] M. A. Haase, M. A. Emanuel, S. C. Smith, J. J. Coleman, and G. E. Stillman, Appl. Phys. Lett. 50, 404 (1987).
[13] M. Pope and C. E. Swenberg, Electronic Processes in Organic Crystals (Clarendon, Oxford, 1982).

89

A Reprint from the

PROCEEDINGS

Of SPIE-The International Society for Optical Engineering

Volume 944

Growth of Compound Semiconductor Structures

15–16 March 1988
Newport Beach, California

**Growth and characteristics of organic-on-inorganic
semiconductor heterostructures**

F. F. So, S. R. Forrest
Departments of Electrical Engineering and Materials Science
University of Southern California, Los Angeles, CA 90089-0241

Growth and Characteristics of Organic-on-Inorganic Semiconductor Heterostructures

F. F. So and S. R. Forrest
Departments of Electrical Engineering and Materials Science
University of Southern California
Los Angeles, CA 90089-0241

ABSTRACT

Recently, several crystalline organic semiconductors have been found to form rectifying heterojunctions when deposited onto inorganic semiconductor substrates. In this paper, we discuss the growth and characterization of these organic-on-inorganic (OI) heterostructures. Both the purification of organic materials, and the fabrication procedures for OI heterostructures are described in detail. The electrical properties, as well as the microstructure of the organic material are found to be very sensitive to the deposition conditions. The valence band discontinuity at the OI heterojunction is measured for the first time, using both forward current-voltage characteristics and internal photo-emission. The interface state densities have been studied for several different organic semiconductors deposited on p-Si substrates. A model is proposed to account for the observed results.

I. Introduction

In the past ten years, considerable effort has been focused on the study of semiconductor heterojunctions[1]. Understanding of the nature of these heterojunctions (HJ's) is essential if we are to use them to advantage in many semiconductor devices such as lasers and photodetectors. More recently, there have been a few reports on an entirely new class of semiconductor heterostructures[2-5] which are also potentially useful for optoelectronic device applications[6-7]. These HJ's consist of an organic (crystalline molecular or polymeric) semiconductor in contact with an inorganic semiconductor, which form rectifying energy barriers at the organic-on-inorganic (OI) semiconductor interface. The resulting rectifying characteristics of the OI-HJ's have been attributed to the low reactivity between the deposited organic materials and the inorganic substrate, and to the low energy associated with the deposition of the thin films. These factors enable one to use OI heterostructures in non-destructive surface analysis of inorganic semiconductors.[8-9]

In this paper, we discuss the different aspects of the growth of OI heterostructures, including the purification of organic materials and the techniques for device fabrication. The nature of the OI heterointerface and band discontinuities also be discussed in detail.

II. Growth of OI-HJ Heterostructures

Purification Organic Material

The organic materials that have been used most extensively in OI-HJ's are aromatic compounds, such as 3,4,9,10 perylenetetracarboxylic dianhydride (PTCDA)[2-4]. These materials are crystalline molecular solids which are both thermally and hydrolytically stable.[11] We present here the purification procedures for PTCDA; and it is noted that the procedures for purifying other organic materials are similar. It is critical that all organic materials be purified prior to deposition onto inorganic substrates. This ensures highly stable and reproducible electrical and optical characteristics of the resulting devices.

PTCDA is available commercially[12] in powder form. Among the different methods to purify PTCDA, gradient sublimation[11,13] gives the highest purity source material. To purify PTCDA, a few grams of powder are put into the sealed end of a quartz tube. The tube is evacuated to about 10^{-5} torr, and the closed end of the tube is inserted into a preheated furnace. The sample is kept at 425–450°C (i.e. just below the sublimation temperature of PTCDA) during the process of purification, which proceeds for between 24 and 48 hours. After this period, the tube is cooled while the sample is maintained under vacuum. The wall of the tube shows bands of different colors. Only the dark red, unsublimed source material is used for fabrication of OI heterostructures.

Crystal and Molecular Structure of the Organic Thin Films

In order to understand the electrical properties of the OI heterojunction, it is necessary to study the crystal structure of these organic materials. For example, PTCDA is a monoclinic crystal[14], that forms infinite stacks of planar, uniformly spaced molecules in which the atoms of one molecule are located directly above adjacent molecules, as shown in Fig. 1. The interplanar spacings for several crystalline organic solids used in OI diodes are shown in Table I. The most important aspect of the crystal structure of PTCDA is its extremely small interplanar spacing of 3.21 Å, which is even smaller than that of graphite (3.37 Å). Thus, the -orbitals overlap to the extent that car-

91

riers moving along the stacking axis are highly delocalized, giving rise to a significant anisotropy of electrical conductivity when measured with respect to the crystalline axes. Typical anisotropies range from 10-1000.

Anistropy can also be caused by the presence of grain boundaries in the organic films. The deposited organic films are polycrystalline, with a grain size on the order of several thousand angstroms. Carriers moving in the vertical direction are not likely to cross the grain boundaries if the organic film is thin enough (<2000Å). On the other hand carriers moving along any in-plane directions will be trapped at the grain boundaries and therefore the mobility is drastically reduced, resulting in additional anisotropy in conductivity.
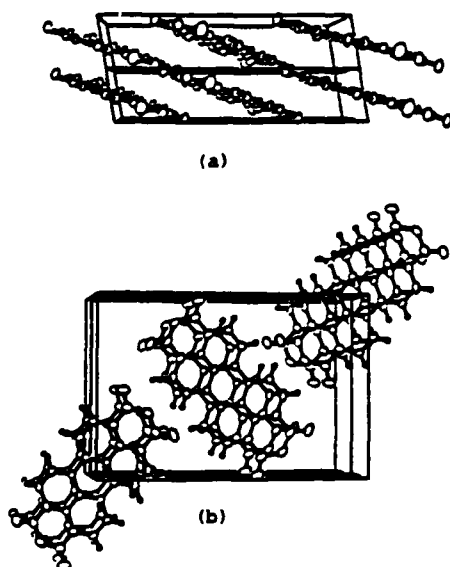

(a)

(b)

Fig. 1: Perspective view of the unit cell of PTCDA looking from (a) a-axis and (b) b-axis.

Table I
Interplanar spacing and ohmic contact metals used for some organic semiconductors

	PTCDA	NTCDA	CuPc	H_2Pc
Interplanar Spacing (Å)	3.21	3.51	3.38	3.40
Contact metal	In, Ti	In	Au	In

III. Fabrication of OI Heterostructures

Many molecular semiconductors such as PTCDA, 3,4,7,8 naphthalenetetracarboxylic dianhydride (NTCDA) and the phthalocyanines (Pc's)[3,10] have been used to form OI-HJ's with a variety of inorganic semiconductor substrates[15]. Here we give a brief outline of the fabrication procedures with additional detail given in the literature[2,3,9]. The first step in the fabrication of the OI heterostructure is wafer cleaning[11]. Organic solvents are used for degreasing, which is followed by native oxide etching in a dilute HF solution. For some III-V compounds such as InP and related materials, enhancement of the contact barrier can be achieved by oxidizing the samples in a solution such as HNO_3 and H_2O_2. Table II gives the cleaning sequence used to prepare several common inorganic semiconductors. The final step in surface preparation is a rinse in deionized water, followed by drying of the wafer with filtered nitrogen gas.

Table II
Cleaning Sequence For Some Semiconductors[a]

	1:4 $HF:H_2O$ (30s)	HNO_3 (conc.) (10s)	30% H_2O_2 (30s)
Si	X		
GaAs	X		X
InP	X	X	

[a]Surface treatments all follow a thorough organic solvent cleaning. Wafers should be rinsed in D.I. water for 5 min. after etching with acid.

Immediately after cleaning, the sample is loaded into a vacuum chamber which is pumped down to $< 10^{-6}$ torr. Next, 000-2000 Å of the organic material is vacuum sublimed onto the pre-cleaned top surface of the wafer. Organic materials generally have low sublimation temperature in the range between 100°C and 600°C. Good control of the deposition parameters can be achieved by using a two chamber source boat such as that employed for silicon monoxide deposition. Typical deposition rates for organic materials are 30-40 Å/s. Next, ohmic contact metal pads 2000-3000 Å thick are evaporated onto the organic film. The contact metals used for some organics are also listed in Table I. Finally, a full surface ohmic contact metal is evaporated onto the back side of the wafer.

It has been found that the microstructure[4] and surface morphology[5] of some aromatic compounds are very sensitive to both deposition rate and substrate temperature. For instance, thin films of PTCDA deposited at high deposition rates (50-100 Å/s) show strong preferred orientation. The crystalline perfection of films deposited at a high rate is demonstrated by the x-ray pole figure for the (102) interplanar diffraction peak as shown in Fig. 2(a). In sharp contrast, no preferred orientation is observed for films deposited slowly (2 Å/s), as shown in Fig. 2(b). It is noted that Kim et. al.[16] have observed that the surface morphology is better for organic films deposited at low substrate temperatures than those deposited at high temperatures. Therefore, substrate temperature also plays an important role in determining the microstructure of the organic film.

The effect that the microstructure of PTCDA has on electrical properties is apparent from Fig. 3. For films deposited at 100 Å/s, the carrier mobility can be as high as 1.4 cm^2/V-s, which is an order of magnitude larger than that for the films deposited at lower deposition rates. These results can be explained in view of the crystalline order of the films. A higher order implies fewer grain boundaries, and hence a reduced charge trapping at these imperfections. The existence of traps in the more disordered film is consistent with the hysteresis often observed in the current-voltage characteristics[4].

Fig. 3: Carrier mobility in PTCDA as a function of deposition rate.

IV. Measurement of Valence Band Discontinuity Energies

Knowledge of the band discontinuity energies is essential to the understanding of any semiconductor heterojunction. For the first time, we have measured[17] the energy band discontinuity of an OI-HJ. In this experiment, the sample was an isotype (p-P) PTCDA/p-Si heterojunction investigated using the temperature dependence of the I-V characteristics as well as internal photoemission spectroscopy.

It can be shown that the forward I-V characteristics are described[2,8,18] by

$$J = J_0 \exp(-q\phi_{Bp}/kT)[\exp(qV_D/kT)-1]$$
$$= J_s[\exp(qV_D/kT)-1] \qquad (1)$$

Here, k is the Boltzmann's constant, T is the temperature, q is the electronic charge, J_s is the saturation current and ϕ_{Bp} is the OI-HJ barrier potential. Also, V_D is the voltage drop across the depletion layer of the inorganic semiconductor which is taken to be positive under forward bias.

From Eq.(1), it is apparent that a measurement of the saturation current as a function of temperature will give its activation energy. A plot of $\log(J_s)$ as a function of 1/T is shown in Fig. 4. A schematic cross-sectional drawing of an organic-on-inorganic semiconductor heterojunction device is shown in the inset. A
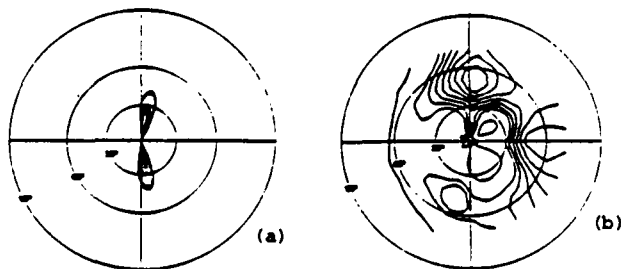

Fig. 2: X-ray pole figure of the (102) reflection intensity of PTCDA deposited at (a) >50Å/s and (b) approximately 2Å/s. Each contour represents a 10% and 2% change in peak intensity for (a) and (b) respectively.
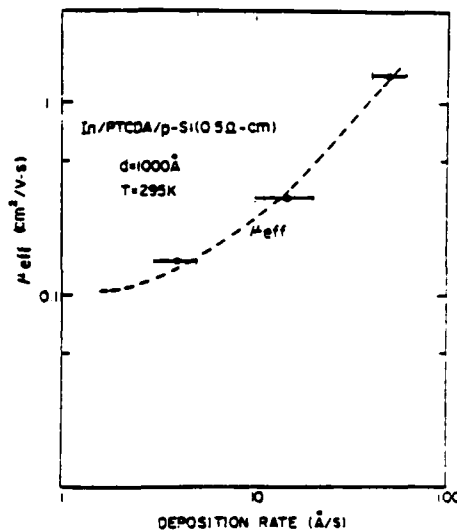
93

least square fit to the data, as indicated by the straight line, gives ϕ_{Bp} = 0.56 ± 0.02 eV. The valence band discontinuity energy, ΔE_v, for this isotype heterojunction is obtained from ϕ_{Bp} using[19]

$$\Delta E_v = q\phi_{Bp} + \delta_s - \delta_0 \qquad (2)$$

where δ_s and δ_0 are the differences between the Fermi-level and the valence band maximum in the inorganic and organic bulk semiconductors. Taking the p-Si hole concentration to be 5×10^{15} cm^{-3}, a hole concentration[3] of 5×10^{14} cm^{-3} for PTCDA, and assuming the effective hole mass (m*) in PTCDA is equal to the free electron mass, we obtain ΔE_v=(0.48±0.2)eV for a PTCDA/p-Si heterojunction. Note that the band gap of PTCDA is[3] 2.2eV. Therefore, $\Delta E_c = \Delta E_g - \Delta E_v$ = 0.6eV where ΔE_g is the difference in band gap energies between PTCDA and Si.

We have also measured ΔE_v directly by internal photoemission spectroscopy. In this experiment, a PTCDA/p-Si heterostructure was illuminated through the Si substrate using a chopped light source, such that light with energy greater than 1.1 eV is filtered by the substrate. Further attenuation of short wavelength light was achieved by inserting a second Si wafer between the sample and the light source. The short circuit photocurrent was then measured as a function of photon energy. Fig. 5(a) shows a photoemission spectrum where a peak is found at hν = 0.57eV. The results can be interpreted as follows: At hν<0.57eV, holes in the organic film are photo-excited, and subsequently emitted over the OI energy barrier. This photoemission current is expected to follow: $I_{ph} \propto (h\nu - \Delta E_v)^2$. Fig. 5(b) shows a plot of the square root of photocurrent versus hν for the data taken on the long wavelength side of the emission peak. A least squares fit to these data gives

ΔE_v=(0.50+0.1)eV-- a value which agrees with that obtained from the forward I-V characteristics.

Note that at hν >0.57eV, I_{ph} drops rapidly to zero. This can be understood using the band diagram shown in the inset of Fig. 5(a). Molecular semiconductors are characterized by narrow bandwidths, as indicated by the cross-hatched region in the figure. For PTCDA, the total bandwith (BW), which is the sum of highest occupied molecular orbital (HOMO) and lowest unoccupied molecular orbital (LUMO) bandwidths, is only 0.9 eV. Thus, transition "b" beyond the BW is forbidden, resulting in a drop in I_{ph} for high energy photons.
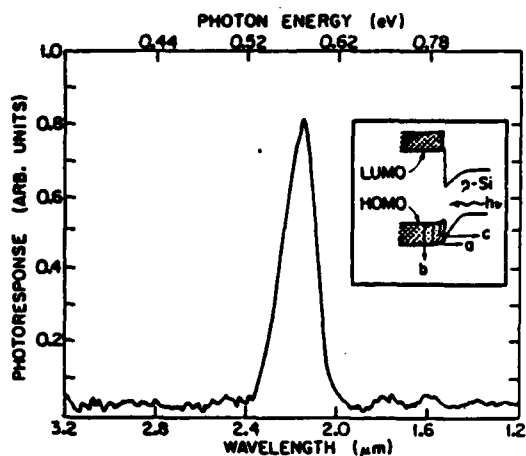

Fig. 5a: Photocurrent spectrum for an In/PTCDA/p-Si heterojunction illuminated via the p-Si substrate. The organic film thickness is 1000 Å.
Inset: Band diagram of a PTCDA/p-Si heterojunction showing allowed ("a" and "c") and forbidden ("b") photoemission transitions resulting in the spectrum shown.
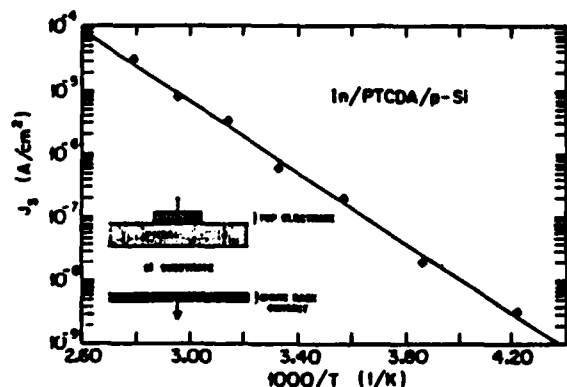

Fig. 4: Saturation current density (J_s) versus 1/T for an In/PTCDA/p-Si heterojunction. The solid line is a linear least squares fit to the data points.
Inset: Schematic view of an organic/inorganic semiconductor heterojunction device.
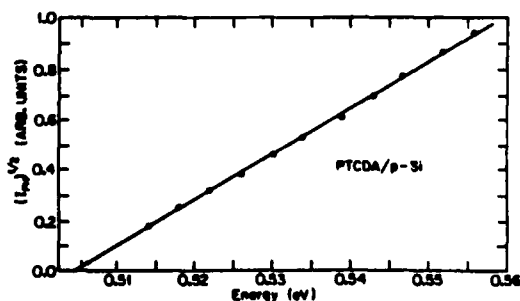

Fig. 5b: Square root of the photocurrent versus photon energy for the data on the long wavelength side of the peak shown in 5a. The solid line is a linear least squares fit to the data points.

IV. Effects of Interface Charge at the OI-HJ

Dianhydride containing compounds (such as PTCDA), have been used for semiconductor surface analysis[8,9] due to their inert nature when deposited onto inorganic semiconductor surfaces. In efforts to study the interactions between the substrate and the organic layer, we have investigated OI-HJs formed using NTCDA, PTCDA and two phthalocyanines (H_2Pc and CuPc) deposited on p-Si substrates. The interface state density as a function of surface potential was derived from the 1 MHz capacitance-voltage characteristics[10]. Figure 6 shows the interface state density (D_{ss}) at the Si surface for several OI-HJ's using these four organic semiconductors. It is apparent that the D_{ss} spectra for the PTCDA and NTCDA-containing diodes are qualitatively different from those for H_2Pc and CuPc. For example, D_{ss} for the former compounds are at a relatively low value of $10^{12} cm^{-2} eV^{-1}$, which is a typical value for silicon with a thin surface native oxide[20]. In contrast, CuPc, and to a lesser extent H_2Pc, show a pronounced peak at about 0.5 eV above the valence band edge. This peak is nearly two orders of magnitude higher than the background value of $10^{12} cm^{-2} eV^{-1}$. The existence of the high D_{ss} observed at the CuPc/p-Si interface can be explained in terms of the following mechanism: Water molecules can diffuse into the organic film in the laboratory environment and react with CuPc via:

$$H_2O + CuPc \longrightarrow H_2Pc + CuO \qquad (3)$$

The Gibbs free energy (ΔG^o) for this reaction is large and negative, implying the reaction is energetically favorable. The CuO molecules formed then diffuse through the surface native oxide layer and participate in the following reaction:

$$2CuO + Si \longrightarrow SiO_2 + 2Cu \qquad (4)$$

Once again, ΔG^o is negative, indicating the reaction is probable. It should be noted that the interface state density of the CuPc/p-Si heterostructure is peaked at 0.5eV above the valence band maximum, which corresponds[21] to one of the Cu deep acceptor levels of Si. This peak is likely to be due to the presence of free copper, or Cu-O-Si complexes at the Si surface. A similar reaction might occur at the H_2Pc/p-Si interface where H_2 molecules leave the organic molecules and form H-O-Si complexes, resulting in a high D_{ss} at about the mid-gap of Si. The existence of a high D_{ss} has the effect of pinning the surface Fermi level at the peak in charge density near $\phi_B = 0.5eV$.
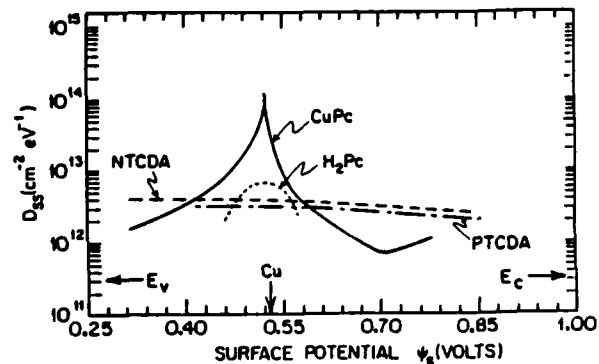

Fig. 6: Density of interface states (D_{ss}) as a function of surface potential in the Si band gap for four different organic/p-Si heterojunctions. The energy is with respect to the conduction (E_c) and valence (E_v) band edges of the Si substrate.

V. Conclusions

We have described the growth procedures for OI heterostructures. The microstructure and electrical properties of the organic films are very sensitive to the deposition conditions used. We have measured, for the first time, the valence band discontinuity energy for the PTCDA/p-Si heterojunction. This was accomplished using the forward I-V characteristics and internal photoemission spectroscopy data. Finally, we have analyzed the interface state densities of some organic-on-Si devices. In contrast to observations concerning dianhydride-based compounds which are relatively inert, CuPc has been found to react strongly with silicon, resulting in the presence of a high density of interface states which pin the Fermi level at the inorganic substrate surface.

References

1. F. Capasso and G. Margaritondo, Eds. Heterojunction Band Discontinuities: Physics and Device Application, North-Holland, Amsterdam, (1987).

2. S.R. Forrest, M.L. Kaplan, P.H. Schmidt, W.L. Feldmann, and E. Yanwoski, Appl. Phys. Lett., 41, 708 (1982).

3. S.R. Forrest, M.L. Kaplan, P.H. Schmidt, J. Appl. Phys., 55, 1492 (1984).

4. S.R. Forrest, M.L. Kaplan, P.H. Schmidt, J. Appl. Phys., 56, 543 (1984).

95

5. M. Ozaki, D. Peebles, B.R. Weinberger, A.J. Heeger, and A.G. MacDiarmid, J. Appl. Phys., 51, 4252 (1980).

6. F.F. So, S.R. Forrest, H.J. Garvin and D.L. Jackson, Integrated and Guided Wave Optics Tech. Dig., Santa Fe, 1988 (Optical Society of America, Washington, D.C., 1988).

7. C.-L. Cheng, S.R. Forrest, M.L. Kaplan, P.H. Schmidt, and B. Tell, Appl. Phys. Lett., 47, 1217 (1985).

8. S.R. Forrest and P.H. Schmidt, J. Appl. Phys., 59, 513 (1986).

9. S.R. Forrest, M. L. Kaplan, and P. H. Schmidt, J. Appl. Phys. 60, 2406 (1986).

10. F.F. So and S.R. Forrest, J. Appl. Phys. 61, 442 (1988).

11. S.R. Forrest, M.L. Kaplan, and P.H. Schmidt, Ann. Rev. Mater. Sci. 17, 189(1987).

12. Aldrich Chemical Co., Inc., Milwaukee, WI 53233.

13. F. Gutmann and L.E. Lyons, Organic Semiconductors (Wiley, New York, 1967).

14. A.J. Lovinger, S.R. Forrest, M.L. Kaplan, P.H. Schmidt, and T. Venkatesan, J. Appl. Phys., 55, 476 (1984).

15. P.H. Schmidt, S.R. Forrest, and M.L. Kaplan, J. Electrochem. Soc., 133, 769 (1986).

16. K.K. Kam, M.K. Debe, R.J. Poirier, and A.R. Drube, J. Vac. Sci. Technol., A5, 1914 (1987).

17. F.F. So and S.R. Forrest, Appl. Phys. Lett. 52, 1341 (1988).

18. S.R. Forrest and F.F. So, J. Appl. Phys., (June, 1988).

19. A.G. Milnes and D.L.Feucht, Heterojunctions and Metal-Semiconductor Junctions, Academic, N.Y. (1972).

20. J. Maserjian and N. Zamani, J. Appl. Phys. 51, 559 (1982).

21. A. G. Milnes, Deep Impurities in Semiconductors, Wiley, N.Y. (1973).

96